Synthesis of Silver decorated Graphene Based Materials for Antimicrobial Coatings

Kalotina M. Poulla

Candidate No. 21

Department of Electrical and Computer Engineering

Hellenic Mediterranean University

A Thesis submitted for the Master Degree of the Inter-institutional postgraduate program:

"*Nanotechnology for Energy Applications*"

Heraklion Crete, 2021

Hellenic Mediterranean University

Department of Electrical and Computer Engineering

This thesis was presented

By

Kalotina Poulla

It was defended on

February 13, 2021

and approved by

Professor Emmanuel Kymakis, Department of Electronic Engineering HMU

Professor Lazaros Tzounis, Associate Professor, Department of Mechanical Engineering HMU

Dr. Dimitra Vernardou, Assistant professor, Department of Electronic Engineering HMU

Preface

The presented Master Thesis was carried out in the laboratory of the Nanomaterials for Emerging Devices (Nano@HMU) group, a research unit within the Institute of Emerging Technologies, at the Department of Electrical and Computer Engineering, placed at Hellenic Mediterranean University (HMU) in Heraklion, under the supervision and guidance of Ms. Aikaterini Anagnostou and Prof. Emmanuel Kymakis. All experiments and material preparations were carried out on location at the laboratories of NANO Group with the exception of some measurements and characterizations which were performed at the Institute of Electronic Structure and laser (IESL) and the antimicrobial properties research under the supervision and guidance of Dr Areti Mourka and Dr Elena Deligianni in Institute of Molecular Biology and Biotechnology (IMBB) housed in the Foundation for Research & Technology-Hellas (FORTH).

Acknowledgements

I would like to thank Prof. Emmanuel Kymakis for giving me the opportunity to carry out my Master thesis at NANO@group laboratories and to work on cutting-edge techniques and technologies, thus broadening my horizons. A special thank you to the Foundation of Research and Technology Hellas (FORTH) and in particular Dr Elena Deligianni for our collaboration in antimicrobial assays and Dr. Areti Mourka for all the assistance and support she provided me during my very first steps in this project. Of the people of most importance during my Master thesis, Ms Aikaterini Anagnostou, who proved to be an excellent mentor and friend throughout this Master thesis, offering guidance, support and a solution to every single challenge I faced during my work. I also want to express my appreciation to my committee members; Professor Lazaros Tzounis, Professor Dimitra Vernardou, and Professor Emmanuel Kymakis for reading my thesis, listening to my presentation, and giving helpful suggestions. I would like to thank my parents (Michael Poullas and Irene Kougkra), my sister (Mary Poulla), my brother (Vasileios Lemonakis) and loved ones (Konstantinos, Manos and Dimitris), whose support and encouragement have been of the most important value to me throughout my academic progress. You are always there for me. Special thanks to Ms. Eleftheria Katachanaki and Mr. Konstantinos Kalbakis for their wise counsel, sympathetic ear and psychological support during my master. Finally, I would like to thank Nikolaos Tzoganakis and Konstantinos Chatzimanolis for their assistance during my characterization experiments, and of course all the members of NANO@group for our great collaboration on the projects, the team spirit and respect to each other.

Dedication

My master thesis is dedicated to my beloved Grandpa Pantelis, a victim of COVID-19 pandemic in 2021, who taught me that the road to success is not an easy one, but with hard work and faith, you can achieve anything.

Thank you Pappouli…

Abstract

The purpose of this Master thesis is the synthesis of antimicrobial coatings using graphene related materials and silver nanoparticles. More specifically, graphite was chemically modified by Hummer's method, and, through liquid phase exfoliation, graphene oxide (GO) was produced. GO was subsequently chemically reduced with Hydroiodic acid (HI) to obtain reduced graphene oxide (rGO). Besides GO and rGO, silver decorated graphene oxide (GO-Ag) was also produced using a variety of chemical synthesis protocols. All graphene related materials were evaluated in terms of their antimicrobial properties using bacteria (Escherichia Coli) and pseudomonas (Pseudomonas Aeruginosa). The aim of this work is to investigate the potential of these materials as antimicrobial coatings, to be used in in a wide variety of applications such as biomedical implants, sterilization of shared equipment, surfaces and public areas, laboratories, hospitals, and other medical services.

Περίληψη

Η παρούσα Μεταπτυχιακή εργασία περιγράφει την σύνθεση γραφενικών αντιμικροβιακών επιστρώσεων. Πιο συγκεκριμένα, χρησιμοποιήσαμε γραφίτη ο οποίος οξειδώνεται με τη μέθοδο Hummers από την οποία παράγεται το οξείδιο του γραφενίου, ένα υλικό που με τη σειρά του, μέσω αντιδράσεων αναγωγής και με την χρήση HI παράγει το τελικό προϊόν, το ανηγμένο οξείδιο του γραφενίου. Εκτός όμως από τα δύο προαναφερθέντα υλικά, το οξείδιο του γραφενίου και το ανηγμένο οξείδιο του γραφενίου, συνθέσαμε και Οξείδιο του γραφενίου διακοσμημένο με άργυρο. Οι αντιμικροβιακές ιδιότητες των τριών υλικών αυτών ελέγχθηκαν με το βακτήριο Escherichia Coli και την ψευδομονάδα Pseudomonas Aeruginosa. Σκοπός της εργασίας είναι η αξιολόγηση των αντιμικροβιακών ιδιοτήτων των παραγόμενων γραφενικών υλικών για την μελλοντική χρήση τους ως επιστρώσεις σε μία μεγάλη ποικιλία εφαρμογών, όπως στα εμφυτεύματα, στην αποστείρωση κοινόχρηστου εξοπλισμού, σε δημόσια μέρη, νοσοκομεία, εργαστήρια και ιατρικές υπηρεσίες.

Table of Contents

List of Abbreviations ***15***

Chapter 1: Carbon Chemistry ***18***

1.1 Carbon **18**

1.2 Allotropes of Carbon: **19**

1.3 Graphite: **19**

1.4 Graphene: **20**

1.5 Fullerene: **22**

1.6 Carbon Nanotubes: **23**

Chapter 2: Graphene **24**

2.1 Structure: **24**

2.1 Properties of Graphene: **26**

2.2 Properties of Single- and Bi-layer Graphene **26**

2.3 Disorders in graphene structure: **30**

2.3.1 Corrugations: **30**

2.3.2 Topological defects: **31**

2.3.3 Vacancies, adatoms and sp^3-defects: **32**

2.4 Synthesis of Graphene: **33**

2.4.1 Top-down preparation: **33**

2.4.1.1 Exfoliation and Cleavage: **33**

2.4.2 Bottom-up preparation: **34**

2.4.2.1 Chemical Vapor Deposition: **34**

2.4.2.2 Epitaxial growth: **35**

2.4.3 Other Graphene preparation routes: **35**

2.5 Graphene Oxide **36**

2.6 Graphene Oxide structure and Synthesis **38**

2.7 Graphite Oxide to Graphene Oxide **41**

2.8 Graphene Related Materials Applications **42**

2.8.1 Biomedical applications **42**

2.8.1.1 Biosensing: **42**

2.8.1.2 Drug Delivery Systems: **44**

2.8.1.3 Tissue engineering:	*46*
2.8.1.4 Antimicrobial Properties of Graphene Oxide	*48*
2.9 Reduced Graphene Oxide	*49*
Chemical Reduction	*50*
Green Chemical Reduction	*52*
Biological Reduction	*52*
Photoreduction	*53*
2.10 Reduced Graphene Oxide Applications	*53*
Chapter 3: Antimicrobial Activity of Materials	*55*
3.1. Antimicrobial Activity of Graphene Oxide:	*55*
3.2. Antimicrobial Activity of Reduced Graphene Oxide:	*58*
3.3. Antimicrobial Activity of Silver:	*59*
3.4. Antimicrobial Activity of Ag-GO:	*62*
Chapter 4: Experimental Section	*0*
4.1 Hummer's method	*1*
4.2 Reduction of Graphene Oxide	*10*
4.3 Preparation of Silver Decorated Graphene Oxide	*13*
4.3.1 Silver decoration of GO via Method 1	*13*
4.3.2 Silver decoration of GO via Method 2	*14*
4.3.3 Silver decoration of GO via Method 3	*16*
4.3.4 Silver decoration of GO via Method 4	*17*
4.3.5 Silver decoration of GO via Method 5	*18*
4.3.6 Silver decoration of rGO via Method 6	*20*
4.3.7 Silver decoration of rGO via Method 7	*21*
4.3.8 Final Experimental Procedure for Silver Decoration	*22*
4.4 Preparation of Bucky Papers	*25*
4.5 Dispersions	*28*
4.6 Thin film preparation	*31*

4.7 Alkaline Piranha Solution Preparation for glass substrates cleaning **33**

4.8 Thin film Preparation of the Materials using Spray Gun **34**

Drop casting **37**

4.9 Antimicrobial Protocol **38**

Chapter 5: Characterizations, Results and Discussion **45**

5.1 UV-Vis Absorption Measurements **45**

5.2 Sheet-Resistance, Resistivity, Conductivity **50**

5.3 Contact Angle (CA): **51**

5.4 X-ray Powder Diffraction (XRD) **53**

5.5 FT-IR Spectroscopy: **55**

5.6 Raman Spectroscopy **58**

5.6.1. Raman Spectroscopy for Graphene: **58**

5.6.2. Raman Spectroscopy for Graphite/Graphene Oxide: **60**

5.6.3. Raman Spectroscopy for Graphene Reduced Graphite/ Graphene Oxide: **61**

5.6.4. Raman Spectroscopy for Silver decorated Graphene oxide (GO-Ag): **63**

5.7 Atomic Force Microscopy: AFM **64**

5.10 Antimicrobial assays **67**

Imaging **67**

5.10.1 Pseudomonas Aeruginosa qualitative antimicrobial assays **67**

5.10.2 Escherichia Coli qualitative antimicrobial assays **69**

5.11 Pseudomonas Aeruginosa quantitative antimicrobial assays **72**

5.12 Escherichia Coli quantitative antimicrobial assays **73**

5.13 Discussion of Antimicrobial mechanisms **74**

6.0 Conclusions **75**

7.0 Future Work **76**

References **78**

List of Abbreviations

The list below includes all of the abbreviations featured in this Master Thesis.

Abbreviation	Definition	Abbreviation	Definition
AC-TEM	Aberration corrected Transmission Electron Microscopy	**ITO**	Indium Tin Oxide
AFM	Atomic Force Microscopy	**LED**	Light Emitting Diode
CNTs	Carbon Nano Tubes	**MWNTs**	Multi Wall Nano Tubes
CVD	Chemical Vapor Deposition	**PEG**	Polyethylene Glycol
DDS	Drug Delivery System	**RGO**	Reduced Graphene Oxide
DLS	Dynamic Light Scattering	**SEM**	Scanning Electron Microscopy
E_F	Fermi level	**SV**	Single Vacancy
FET	Field-Effect transistor	**SWNTs**	Single Wall Nano Tubes
FRET	Fluorescence-Resonance-Energy Transfer	**TEM**	Transmission Electron Microscopy
FT-IR	Fourier-Transform Infrared Spectroscopy	**XPS**	X-ray Photoelectron Microscopy

GO	Graphene Oxide	**ΔE_F**	Fermi level shift
HP	Hildebrand Parameter	**AgNPs**	Silver Nanoparticles
HSP	Hansen Solubility Parameters		

Chapter 1: Carbon Chemistry

1.1 Carbon

Carbon is a non-metal element of the 4th periodic table group. It has four valance electrons which are capable of forming four covalent chemical bonds. The electronic structure of this atom in the ground state is: $1s^2 2s^2 2p_x^1 2p_y^1$. In order for the carbon atom to form four covalent bonds, four unpaired electrons are needed. These unpaired electrons are made available when one electron is transferred from the 2s, to the $2p_z$ orbital creating the electronic structure: $1s^2\ 2s^1 2p_x^1\ 2p_y^1 2p_z^1$. The carbon atom 2s and 2p orbitals hybridize forming sp^x hybridized orbital.

Carbon can form single, double or triple bonds, depending on the number of atoms connected to main carbon atom. If carbon bonded to four are atoms, then the hybridization is sp^3 and the arrangement is tetrahedral. A carbon atom bound to three atoms (two single bonds, one double bond) is sp^2 hybridized and forms a flat trigonal or triangular arrangement with 120° angles between bonds. The third possible arrangement for carbon is sp hybridization which occurs when carbon is bound to two other atoms (two double bonds or one single and one triple bond). This way carbon forms a linear arrangement and carbon atoms have an angle of 180° between bonds (1).

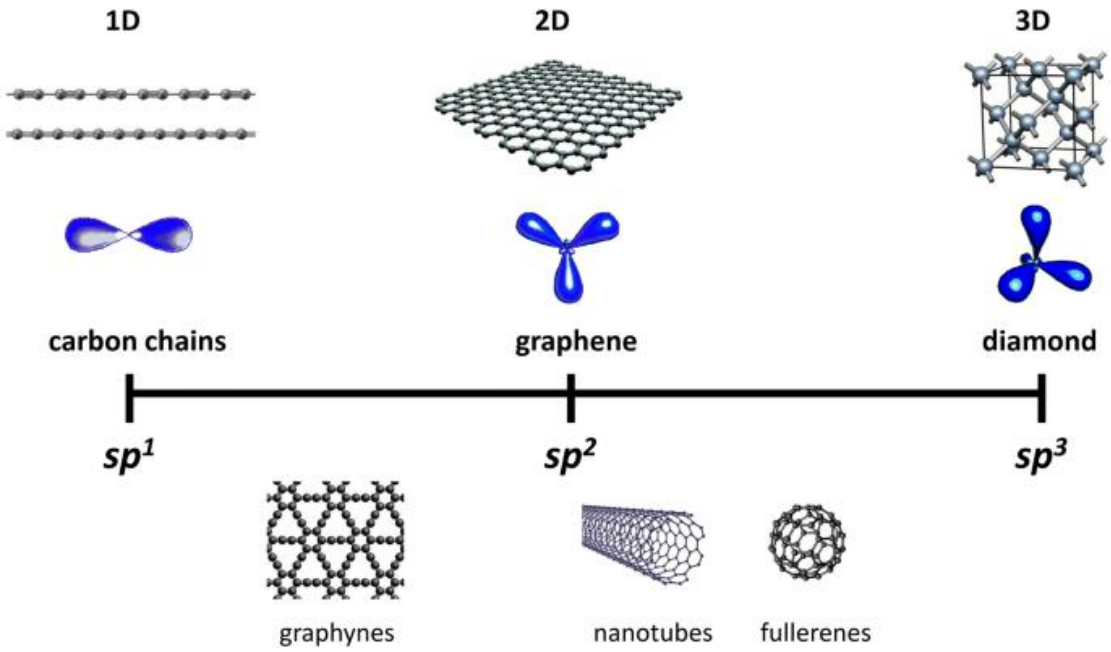


Figure 1 Hybridization of s and p orbitals of carbon atom and geometry of hybridized orbitals (2)

Carbon forms covalent bonds and shares electrons with atoms valence of 4. This happens because carbon is bonded to atoms with similar electronegativity. In this way carbon can easily bond with other carbon atoms to form long chains or rings. The bonds that carbon forms with other carbon atoms are very strong because two identical species are involved. Usually, carbon's double and triple bonds are commonly found in nature and animals.

1.2 Allotropes of Carbon:

Due to its valency, carbon can form various allotropes such as graphite, diamond, graphene and fullerene. Graphene and its derivatives are of great importance within this diploma thesis and in Perovskite Solar Cells development.

1.3 Graphite:

Graphite is an allotrope of carbon, in which multiple sp^2 hybridized carbon atoms are linked together. Each carbon atom connects via single bonds with three neighboring carbon atoms creating a 2-D hexagonal pattern. These

structures are stacked on top of each other and each sheet is known as *Graphene*.

Graphite consists of multiple graphene sheets which are held together via weak Van der Waals forces forming a layered, planar structure. Graphite is an electrical conducting material due to the dislocation of the π-electrons. The three sp^2 electrons of each carbon atom is used in three σ-bonds with neighboring carbon atoms. The fourth electron is located in the p_z orbital. Each p_z orbital is perpendicular to the plane defined by the σ-bonds and overlaps sideways with the p_z orbital of the neighboring atoms, thus creating a system of π-molecular orbitals.

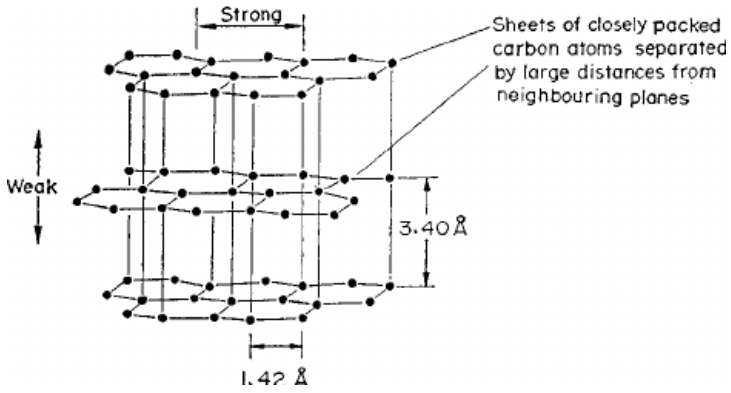


Figure 2 Chemical structure of graphite. It consists of single layers of a carbon-based lattice in which the carbon atoms form hexagonal rings. The sheets in graphite are held together via Van der Waals forces (3)

1.4 Graphene:

As mentioned previously, graphene is a planar allotropic structure of carbon. It is a 2-D material with high crystallinity, a thickness of only one carbon atom and is a crucial component of other allotropic carbon structures. A structure of over 10 stacked layers of graphene is considered a 3D material (graphite). Graphene can also be swaddled to form fullerene, a 0-D material or rolled to form carbon nanotubes, a 1-D material, as shown in Figure 4. Graphene will be discussed further in Chapter 2: Graphene.

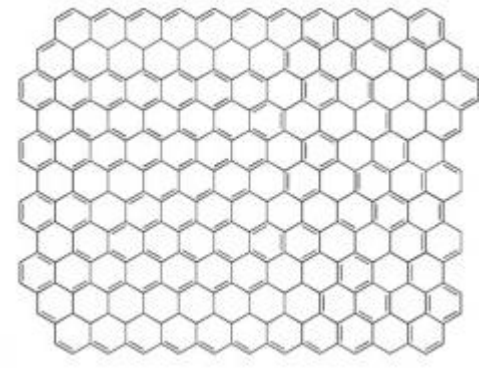


Figure 3 Graphene layer-the individual layer found in graphite (4)

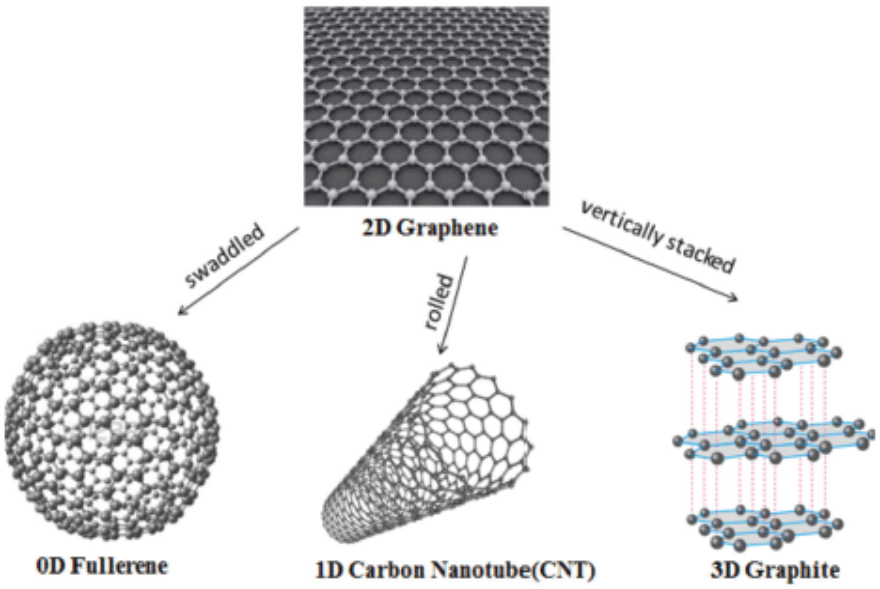


Figure 4 Allotropic structures of carbon (5)

1.5 Fullerene:

In 1966 David Jones suggested that if pentagonal ring were to be inserted between the hexagonal rings of graphene, then the material would bend resulting in a closed, spherical structure (6). This theory was proven correct in 1985 when Harold W. Kroto, Robert F. Curl and Richard E. Smalley discovered a new allotrope of carbon, in which the atoms are arranged in closed shells.

The new form, which consisted of 60 carbon atoms, was found to have the structure of a truncated icosahedron, and was named Buckminsterfullerene (Bucky ball). The definition of fullerenes typically refers to a compound which consists exclusively of an even number of carbon atoms that form a polycyclic, cage shaped structure of 12 five-membered rings and 20 six-membered rings. Each carbon atom is connected to three neighboring carbon atoms creating a uniform spherical grid which consists of alternating single and double bonds.

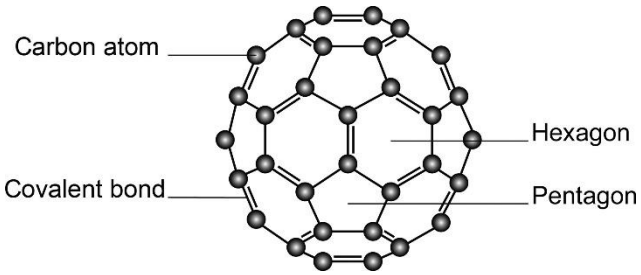


Figure 5 Fullerene C60 structure consisted from hexagons and inserted pentagons (7)

Fullerenes can be used as electron acceptors in OPVs in the active layer, since they obtain high electron affinity. This property leads to their use as electron transfer complexes alongside weak electron donors, such as conjugated polymers, in organic photovoltaics. The unique physical and electronic properties of fullerenes can be enhanced with the insertion of additional groups via chemical tuning.

1.6 Carbon Nanotubes:

Carbon Nanotubes (CNTs) are made up from rolled Graphene sheets, creating a 2-D material in which carbon atoms are arranged in the hexagonal lattice. CNTs are an intermediate between plain Graphene and Fullerene and can be categorized in single wall carbon nanotubes, double wall carbon nanotubes and multi-wall carbon nanotubes, depending on the number of graphene sheets, which are weakly bound together by Van der Waals interactions. (8) CNTs can either exhibit satisfying electrical conductivity or be semi-conductors. Besides electrical conductivity, they have exceptional tensile strength and thermal conductivity and can be chemically modified making them precious in upcoming technologies for electronics, optics, nanotechnology, energy and materials. CNTs have been also incorporated in the active layer of organic solar cells (OSCs), to improve short circuit current, flexibility and fabrication (9). (8)

However, on November 2019, CNTs became the first nanomaterial to be added to the SIN (‘substitute It Now’) List by the ChemSec non-profit organization. SIN list suggests that CNTs should be banned or restricted in the EU, due to their carcinogenicity, reproductive toxicity and persistency. (10) Scientific community disputed the The International Chemical Secretariat claiming that banning carbon nanotubes would be scientifcally unjustifed and damaging to innovation. (11)

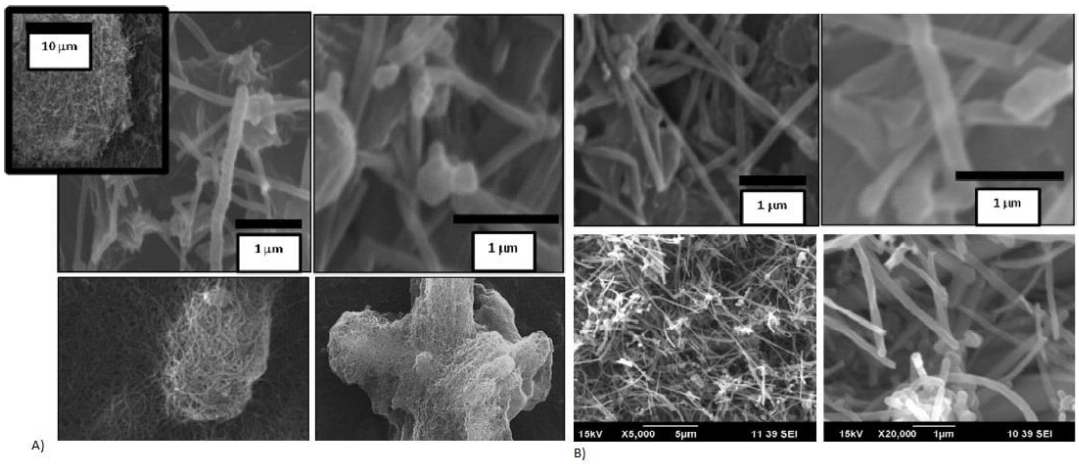


Figure 6 SEM images of MWNTs dispersions in different solvents A) ethanol B) in a surfactant solution of Triton X-100

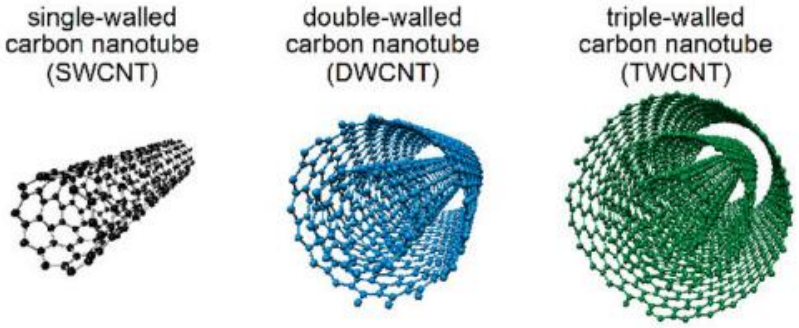


Figure 7 Single, double, multi walled carbon nanotubes (9)

Chapter 2: Graphene

2.1 Structure:

As early as 1947, Wallace used the 'tight binding' approximation to investigate the electronic energy bands in crystalline graphite and to obtain monolayer Graphene. They achieved reduction of the thickness of Graphite films to 30nm, inspiring the scientific community. (12)

In 2004, Novoselov et al. (13) Isolated Graphene from Graphite using a micro-computer peeling method. The structure of graphene is shown in Figure 1, which is composed of a layer of independent sp^2 hybrid carbon atoms, creating a 2-D material. Until today, graphene is the strongest nanomaterial, having remaining p electrons to form bonds perpendicular to the graphene plane and creating a very stable structure. There is no rearrangement or misalignment in Graphene and this is attributed to the stability of the structure. Electrons in Graphene can move in internal orbit in order to avoid scattering phenomenon when they interfere with other atoms or lattice defects. (14) (15) This unique lattice structure gives graphene various excellent properties.

The carbon-carbon length is about 0.142 nm and consists of σ-bonds in hexagonal structure with strong connections between atoms. The π-bond located vertically to the lattice plane, gives graphene its unique conductivity. π-bonds hybridize to form π-π* bonds which are responsible for electronic properties of graphene through their half-filled band that hosts the moving electrons.

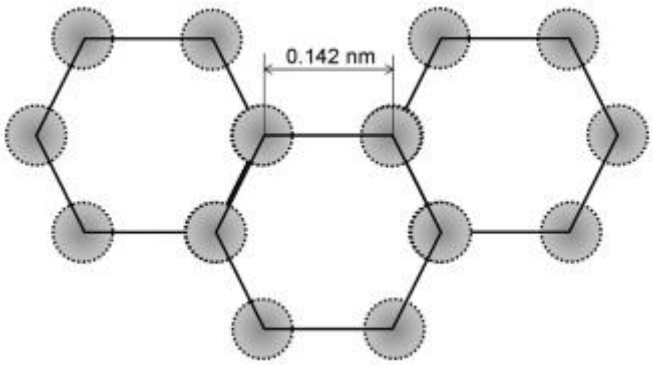


Figure 8 Hexagonal Structure of Graphene and Carbon-Carbon length between atoms (16)

The thickness of Graphene is 0.35nm and creates a stable structure because the covalent bonds between carbon atoms are strong enough to endure external force by twisting lattice plane to avoid the reconfiguration of atoms. Graphene can exist as nanoribbons with tunable width which controls the energy barrier allowing it to be used in graphene-based energy devices. (17)

The edges of Graphene can be classified as “zigzag” or “armchair” depending on the different carbon chains, as seen in Figure 9, which leads to different conducting behaviours, meaning that a graphene nanoribbon with zigzag edge usually behaves as a metal while a nanoribbon with an armchair edge conduct electricity and act as a metal or semi-conductor.

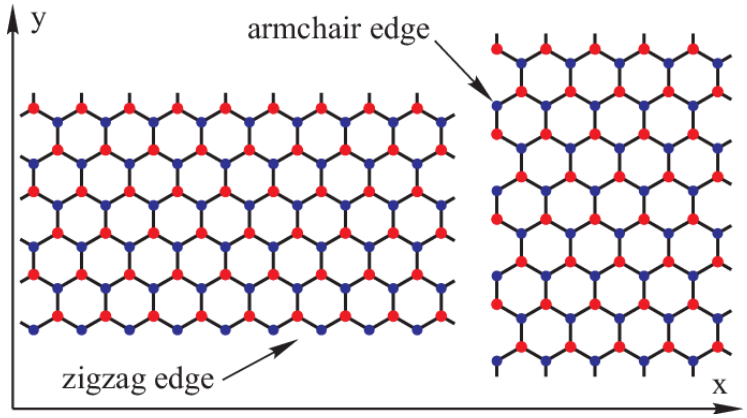


Figure 9 Graphene Nanoribbon (18)

2.1 Properties of Graphene:

Graphene gained much interest due to its unique properties and its involvement in electronics and sensing applications. However, Graphene can also be manufactured into sheets, flakes or pills and be used in many biomedical applications such as drug delivery systems, biosensors or as a potential antibacterial agent, which will be extensively discussed below.

2.2 Properties of Single- and Bi-layer Graphene

As mentioned before, a single layer graphene is defined as a two-dimensional sheet of carbon atoms arranged in hexagons. Bi-layer and few-layer Graphene has 2 or more layers (up to 10) of these two-dimensional sheets and are of great interest in scientific community.

In bi and few layer Graphene, carbon atoms are arranged and stacked in several ways, creating hexagonal, AA stacking, Bernal or AB stacking and rhombohedral or ABC stacking Figure 11. Graphene has sp2 hybridization and holds three in-plane σ-bonds per atom which are strong bonds and work as the rigid backbone of the hexagonal structure and π-orbitals perpendicular to the plane which control interactions between Graphene layers (19).

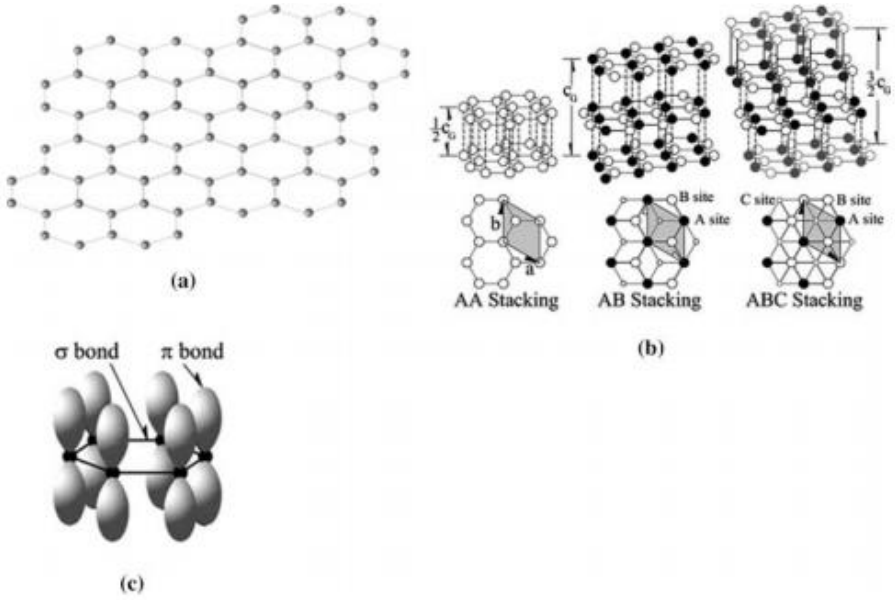


Figure 10 a) Graphene structure of single two-dimensional hexagonal sheet of carbon atoms, (b) three most common structures and stacking sequences of graphene and (c) Schematic of the in-plane σ bonds and the π orbitals perpendicular to the plane of the graphene sheets (19)

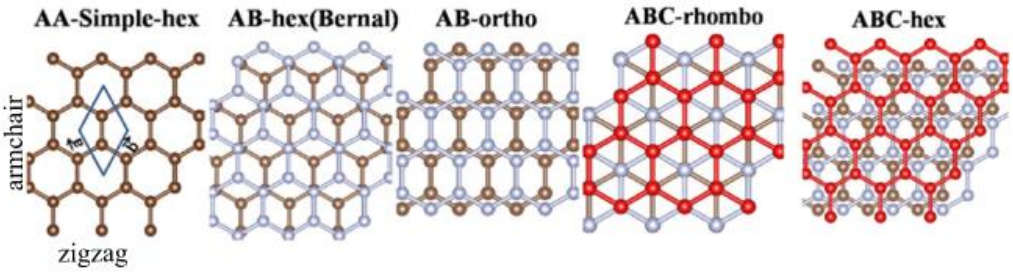


Figure 11 Top-down view of various layer stackings (20)

Graphene has a planar density of 0.77 mg/m^2 and a hexagonal area of 0.052nm^2. (21) The hexagonal ring of Graphene consists of two carbon atoms, since each atom at vertex is shared by three-unit rings. Graphene has one atomic layer of carbon atoms, making it ultralight and super thin, with a

transparency of 97.7%. It absorbs only 2.3% of visible light and this transparency of graphene becomes an indication of the number of layers of Graphene because the difference of transparency between a substrate and single layer graphene, as well as single layer and double layer graphene are 2.3% too. (21) This claim is also confirmed by Dirac fermion theory.

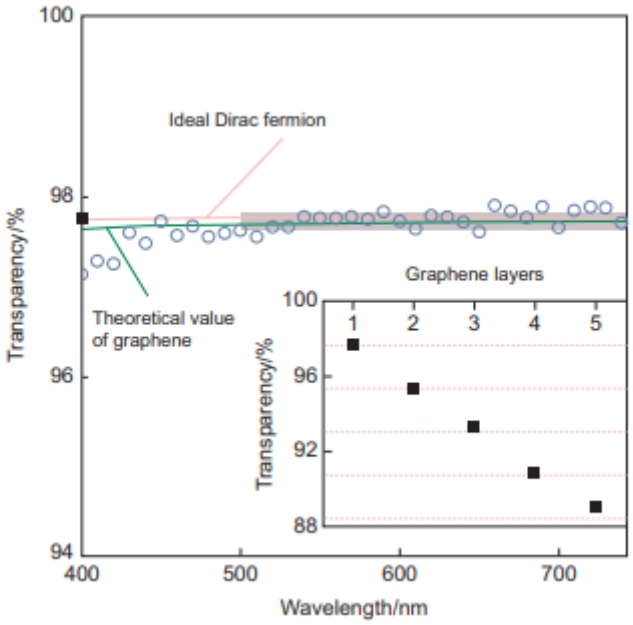


Figure 12 Theoretical transparence of graphene

The thickness of Graphene could also affect its theoretical and experimental optical properties and exhibit high conductivity. What is of great importance is the fact that Graphene can be used to solve problems of fragility, pollution, and material resources, to replace traditional membranes such as indium tin oxide (ITO), fluorine doped tin oxide (FTO).

Graphene-based materials can be synthesized to create Solar Cells and LEDs for window barriers, as well as in optoelectronic devices as an electrode in supercapacitors. Moreover, the absorption of light in graphene would reach saturation if the intensity of light exceeds a certain critical value. This kind of saturated absorption in graphene occurs at the near-infrared region due to a

wide absorption range and zero band gap of graphene. This characteristic could be utilized in ultrafast photonics such as fiber lasers. (22)

Another important characteristic of Graphene is the electron mobility. Until now, graphene holds the record of the most conductive material, at room temperature, with a conductivity of 10^6 S/m and a sheet resistance of 31 Ω/sq. (23). This happens because it has the very high electron mobility of $2x10^5$ cm^2/Vs, 140 times the electron mobility of silicon.The π-electrons are free to move with little interference at room temperature and, besides this, graphene is semimetal with small overlap between valence and conduction band and thus, electrons can flow with lower energy from the top of the valence band to the bottom of the conduction band without any heat stimulation. The unique characteristic of Graphene is that at zero temperature a certain concentration of electrons can move to the conduction band and a certain number of holes, to the valence band. Conduction and valence band in graphene meet at the Dirac Point, as is illustrated in Figure 13.

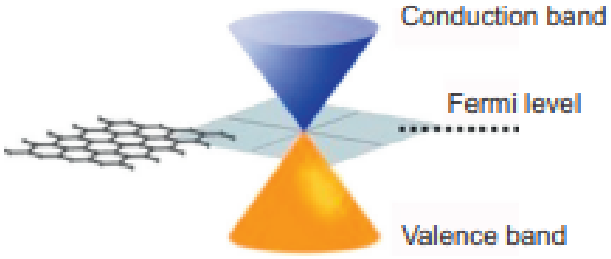


Figure 13 Energy bands of Graphene (24)

The conductivity of graphene can be tuned by inserting different elements in its lattice while preserving its hexagonal form. For example, hydrogen atoms could be inserted to the lattice to make graphene an insulator. If vertical electric field is applied to bilayer graphene, the in-plane movement of the electrons is inhibited and a great deal of resistance is created. (25) (26)

Lastly, thermal conductivity of Graphene at 25ºC reaches $5x10^3$ W/mK and the surface area of graphene is about 2630 m^2/g, a property that finds application in microdetectors, in order to follow the change in resistance induced by adsorption and desorption of gas molecules. (27) (28) (29)

All varieties of Graphene, single-, bi- and few-layer, have found potential applications in electronics, memory, batteries, energy, biotechnology, sensing etc.

2.3 Disorders in graphene structure:

Due to the regular arrangement of graphene atoms, monolayer Graphene exhibits extraordinary properties. However, in ordere to be used in specific applications, disorder needs to be induced.Also, disorder could also assist in understanding of graphene defects. Some properties of graphene might be enhanced by assembling process, but large disorder is introduced to the graphene crystal by this synthesis process. Disorders in graphene can be categorized as a) Corrugations b) Topological defects c) Adatoms d) Vacancies e) sp^3-defects.

2.3.1 Corrugations:

Ultra-thin films with dozens of layers seem to be more thermodynamically unstable, unless they inherently constitute a part of 3-D structures. For this reason, tuning the thermal fluctuations onto different materials can form different structures in graphene sheets, proven by TEM images. These structures are known as ripples, wrinkles and crumples depending on the substrate used in each case. (30)

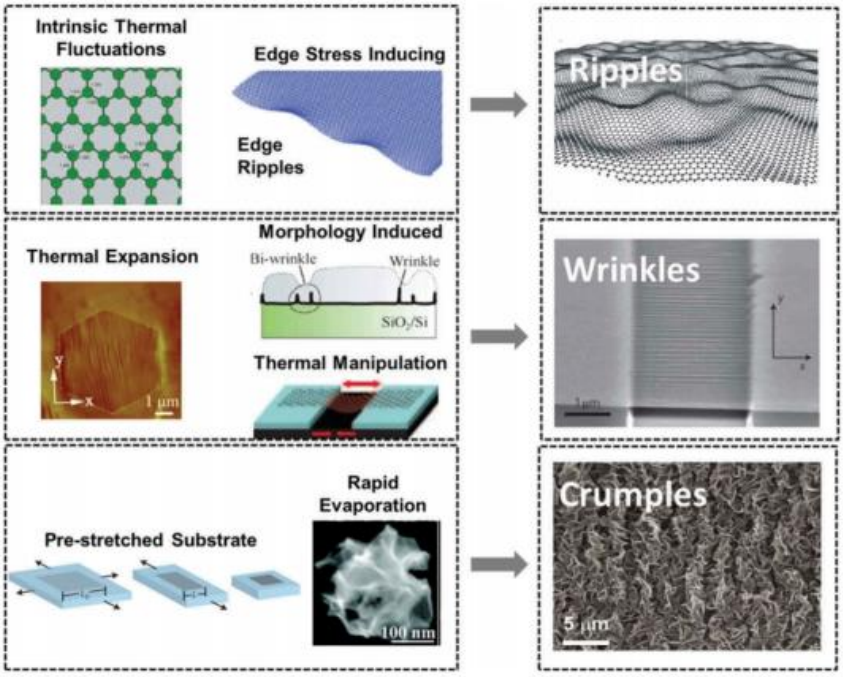


Figure 14 A summary illustration of three types of corrugations (i.e. ripples, wrinkles and crumples) (31)

2.3.2 Topological defects:

Chemical Vapor Deposition (CVD) is a commonly used method to produce polycrystalline Graphene, but leads to many topological defects such as disclinations, dislocations and line defects separating graphene grains (crystallites/domains) with different crystal lattice orientations, which can alter the orientation of Graphene. An intriguing feature of these topological defects is that they can exist in graphene without introducing local disorder into the crystalline lattice and can lead to the addition or removal of semi-infinite wedges.

As presented in Figure 15, the s = 60° angle allows a pentagon to be embedded into the lattice of graphene while the s = −60° angle creates a heptagon in the graphene lattice. This isolated non-hexagonal rings result in non-planar structures. (32)

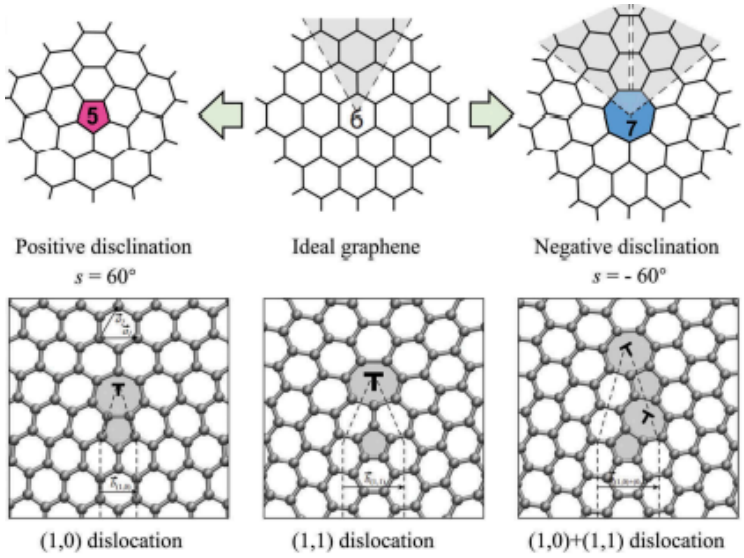


Figure 15 Configurations of disclinations (up) and dislocations in graphene lattice (down) (32)

2.3.3 Vacancies, adatoms and sp^3-defects:

A vacancy is a gap in the lattice of Graphene, because there is one missing carbon atom in the structure. This missing atom can be observed by TEM. Two single vacancies can form a double vacancy. Transition metal atoms can be easily adsorbed in the hexagonal structure of Graphene, they exhibit low migration barriers (0.2-0.8 eV) and these adatoms can move at room temperature on singles vacancies of graphene as seen in Figure 16. (33) sp^3 defects can be observed in chlorinated, fluorinated, hydrogenated and oxidized graphene. Shown in Figure 16d, are sp^3 defects, caused by chlorination of graphene (34), where Cl atoms form covalent bonds with carbon atoms located on the graphene sheets after a 5 min reaction. Furthermore, sp^3 defects usually appear in form of dimers or clusters rather than being isolated. (35)

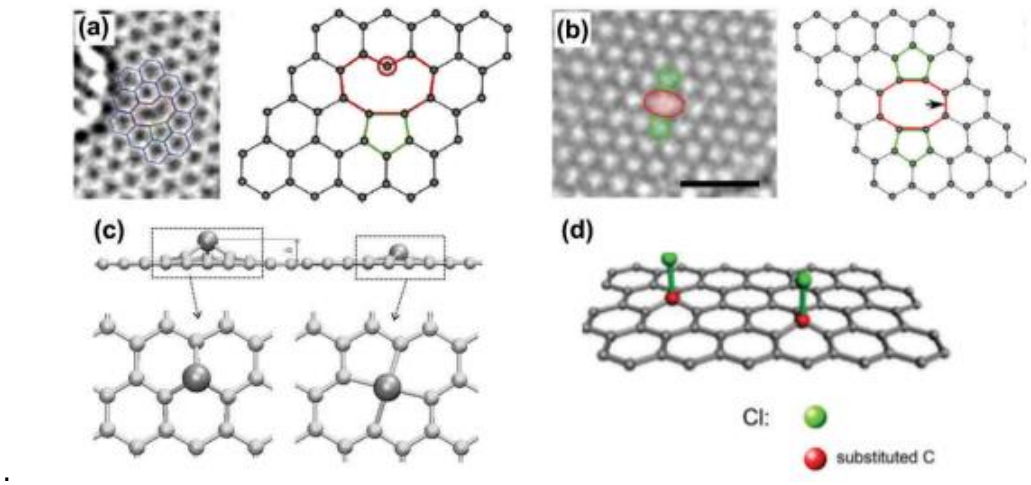


Figure 16 . Configurations of (a) Single Vacancy (5–9) (36), (b) double vacancy (36), (c) transition metal atoms adsorbed on single and double vacancies in a graphene sheet (37) and (d) sp^3 defects

2.4 Synthesis of Graphene:

Preparation methods of Graphene are divided into two different categories: bottom-up and top-down. Bottom-up techniques are mainly Chemical Vapor Deposition (CVD) and epitaxial growth. Top-down techniques focus on the exfoliation of Graphene with physical methods (mechanical exfoliation, liquid phase exfoliation, reduction of Graphene Oxide via irradiation etc.) and Chemical methods (exfoliation and cleavage). These methods are shortly listed and summarized in the following paragraphs.

2.4.1 Top-down preparation:

2.4.1.1 Exfoliation and Cleavage:

As mentioned before, Graphite consists of many Graphene sheets stacked together with weak van der Waals forces. If these interactions are overcome, then high purity graphene can be obtained. Exfoliation and Cleavage use chemical energy or mechanical properties to break these forces and isolate graphene. Viculis et al., inserted potassium metal to graphite sheets and then exfoliated them with ethanol to create a dispersion with sonication and obtain

nano-scrolls. (38) However, the desirable few layer Graphene or single layer Graphene was not produced until 2004 (39), when Novoselov managed to mechanically exfoliate single layer Graphene flakes using Scotch® tape to peel them from the bulk graphite. Exfoliation is a repeated peeling process and helps in synthesis of large-scale graphene. In another report, few layered graphene was produced with borosilicate glass, wherebulk graphite is secured to the glass substrate and then exfoliated to graphene sheets. (40) Stankovich et al., proposed a liquid phase exfoliation in order to obtain GO and then exfoliate GO nanosheets by ultrasonication and heating. In this way, partially reduced exfoliated graphite oxide is produced. (41)

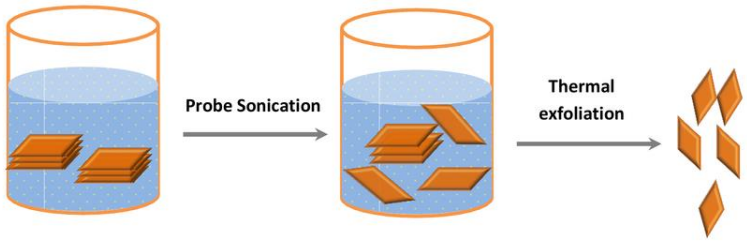


Figure 17 Exfoliation through probe sonication- An illustration of Graphite in solution (42)

2.4.2 Bottom-up preparation:

2.4.2.1 Chemical Vapor Deposition:

In this method, thin films can be formed on the surface of substrates when exposing the sample to one or more gaseous compounds, which contain the elements of the thin film. The by-products are then removed through evaporation (43). For graphene, single and few layer graphene can be synthesized on Ni foil, by exposing the Ni substrate to a gas mixture of H_2, CH_4 and Ar at 900^{o}C in a quartz tubular furnace under 750 Torr pressure. Another existing method for the growth of graphene, is CVD in atmospheric pressure, but in this method the produced graphene is of lower quality since it consists of a defective layer (44).

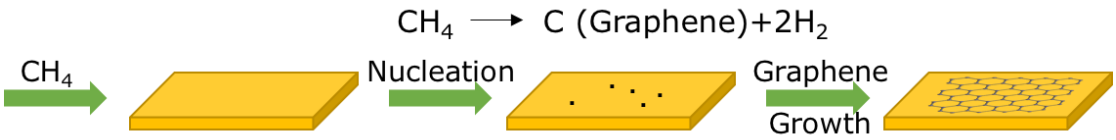


Figure 18 Chemical Vapor Deposition Technique illustration by ACS suppliers (45).

2.4.2.2 Epitaxial growth:

Epitaxial growth is method to grow monolayers of carbon on a surface of C-doped nickel single crystals. Single or few-layer graphene can also be grown on C-doped metals such as Fe, Pt, Pd, and Co. With epitaxial growth can also be used to produce large-scale few-layer graphene on silicon carbide. (46)

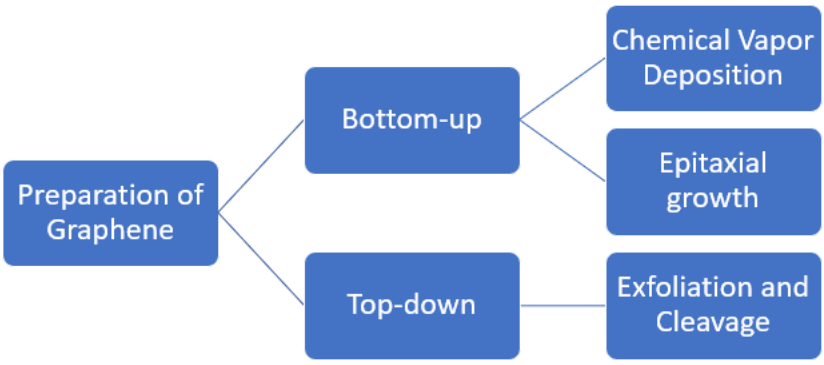


Figure 19 A summarized diagram for the preparation of graphene.

2.4.3 Other Graphene preparation routes:

Besides the commonly used techniques to produce high quality Graphene, CVD, epitaxial growth etc. as mentioned above, there are several chemical methods which can extract Graphene films from Graphite, without the exfoliation step.

There is a report about using sulfuric and nitric acid which were intercalated between the Graphite layers, while rapidly heated at 1000^{o}C. In this way, the Graphite sheets are produced through an explosive evaporation of the acid molecules (47). Tetrabutylammonium hydroxide and oleum may also be intercalated into Graphite sheets in order to produce single and few layer Graphene through sonication in a surfactant solution. The intercalation process aims to achieve the minimum damage of the sp^2 network in the Graphene for the production of high-quality material.

Another popular Graphene preparation technique is thermal decomposition of Silicon on the (0001) surface plane of single crystal of 6H-SiC (48). Graphene sheets (1-3 layers) were formed when a H_2-etched surface of 6H-SiC was heated to temperatures of 1250 to 1450◦C, for a short time (1 to 20 minutes). It was reported that the number of layers is dependent on the composition temperature.

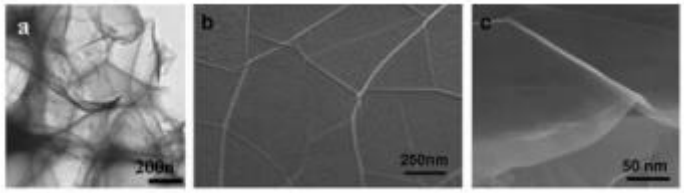


Figure 20 (a) TEM image of agglomerated graphene sheets produced by chemical route (b), (c) SEM images of the graphene sheets epitaxially grown on SiC (0001) surface (annealed for 4 h in vacuum at 1900◦C); fracture surface in (c) shows that bright lines in (b) are wrinkles in graphite (49) (50)

2.5 Graphene Oxide

Graphene Oxide (GO) gained interest and was studied after graphene was first isolated. It was initially hoped that GO might be a synthetic precursor to graphene. It is a single monomolecular layer of graphite containing oxygen groups, namely epoxide, carbonyl, carboxyl and hydroxyl groups.

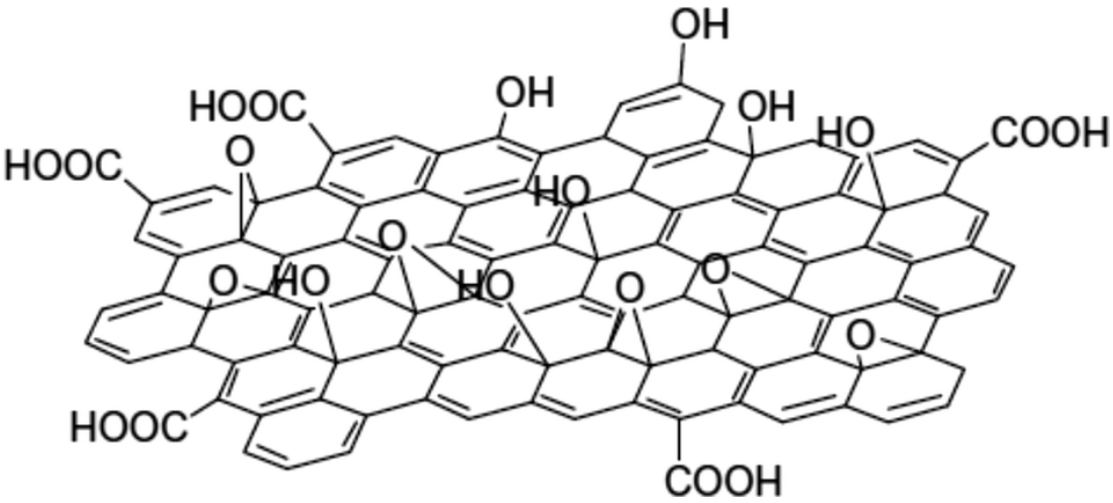


Figure 21 Chemical structure of graphene oxide (51)

Graphene oxide (GO) can be easily synthesized via the Hummers' method for graphite oxidation (graphite oxide) and its subsequent exfoliation using ultra-sonication (graphene oxide). GO acts as a precursor to synthesis rGO or Graphene Nano Sheets (GNS). It is produced from graphite flakes by oxidative reaction. (52) (53)

During oxidation, graphene is transformed to graphene oxide. The lattice of the graphene introduces oxygen-containing functional groups into the planar structure. Carboxyl groups mainly occupy the edges of the GO sheet, whereas epoxy and hydroxyl groups are introduced onto the basal plane. Since polar groups are presented in GO, it is more readily dispersed in polar solvents. Every different functional group can be identified with Fourier transform infrared (FTIR) spectroscopy. In addition, some groups e.g., C=O or conjugated carbon−carbon double bonds absorb light in the ultraviolet (UV) range. In comparison with graphite, graphene oxide can be dispersible in water, a property that occurs due to the functional groups mentioned above, whereas graphite is non-dispersible in water as shown below:

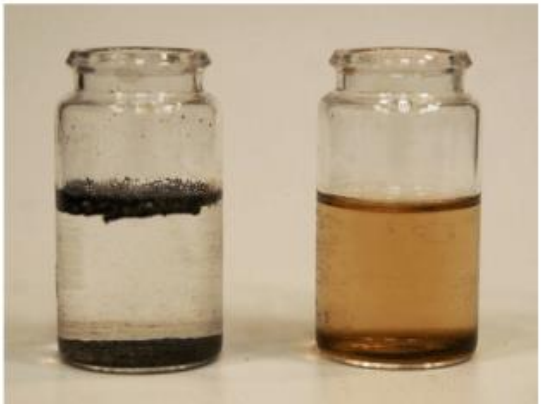


Figure 22 (Left) Graphite not dispersible in water (Right) Graphene oxide interacts with water forming dispersion.

Graphene holds great promise as a film electrode for various devices, as it possesses high electrical conductivity, transparency, flexibility, and stability against chemical environments. Surface functionalization has shown great potential, in order to tune the optical and electrical properties of graphene. . A matter of great importance is that graphene can transition from a conductor to a semiconductor and even to an insulator and its optical transmittance and surface chemistry can be modified simultaneously. Surface oxidation is of particular interest since it is a relatively simple and low-cost process compared with other methods involving the use of fluorine- and chlorine-containing reagents.

2.6 Graphene Oxide structure and Synthesis

To produce Graphene Oxide, a two-step procedure is carried out, including oxidant intercalation and sheet peeling. The first person to produce graphite oxide was B.C. Brodie 150 years ago, using sodium chlorate in nitric acid. The developed techniques for the preparation of graphene oxide can be seen in the Table 1. . Each different method has advantages and disadvantages. At the very first stages, nitric acid and $KClO_3$ were used, but harmful gases such as ClO_2, NO_2 and N_2O_4 were generated during the reaction. Alternatively, The Hummers' method was used widely, but this method produces NO_2, $N2O_4$ and

heavy metal pollution. Also, the products contained Na^+ and NO_3^- ions, which were difficult to remove.

The oxidizing agent ($NaNO_3/KMnO_4$) had strong oxidizing properties in concentrated sulfuric acid, and there was a high risk of explosion when Mn_2O_7 contacted with organic matter at 55°C. The preparation method used for the purposes of the present thesis was the Modified Hummers method, the schematic synthesis of which is shown in Figure 23.

Scientists	Reagent	Reaction time	Reaction Temp	Characteristics
Brodie (54)	$KClO_3$, HNO_3	3-4h	60°C	First synthesis
Staudenmaier	$KClO_3$, HNO_3, H_2SO_4	96h	RT	
Hummers (55)	HNO_3	20h	RT	Only using HNO_3
David (56)	$KMnO_4$, $NaNO_3$, H_2SO_4	<2h	35°C	Short reaction time
Eigler (57)	$KMnO_4$, $NaNO_3$, H_2SO_4	16h	10°C	High quality RGO
Shen (58)	Benzoyl peroxide	10min	110 °C	No liquid

Table 1 Graphene Oxide Preparation methods

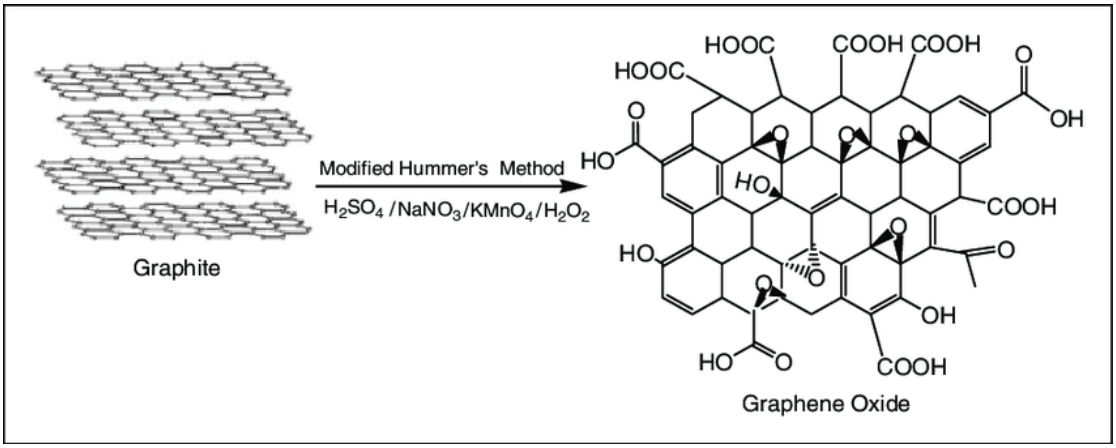


Figure 23 Graphene Oxide preparation using modified Hummer's method (59)

Currently, the feasibility of the industrial preparation of graphene with graphene oxide as the precursor is high, but the existing graphene oxide preparation methods generally have technical problems such as complicated purification steps and many defects in the resulting product. Therefore, compared with mechanically exfoliated high-quality graphene, the prepared reduced graphene oxide is inferior in structure and properties.

The structure of Graphene Oxide can be seen through direct imaging of the atomic structure using aberration-corrected transmission electron microscopy (AC-TEM). In the structure of GO, 20-30% oxygen functionalization on the basal plane is reported, limiting its electrical and thermal transport and thus its widespread use in electronics and optical applications. As mentioned above, multiple models for the structure of GO have been proposed, but the most widely accepted was Lerf−Klinowski model, which reports the decoration of the carbon basal plane with epoxides and hydroxyls, with sheet edges terminated by carboxylic acid functional groups. The oxygen-containing functionalization disrupts the sp^2 order of the graphene backbone such that regions of sp^2 (ordered) are interrupted by the sp^3 (disordered) in the carbon basal plane.

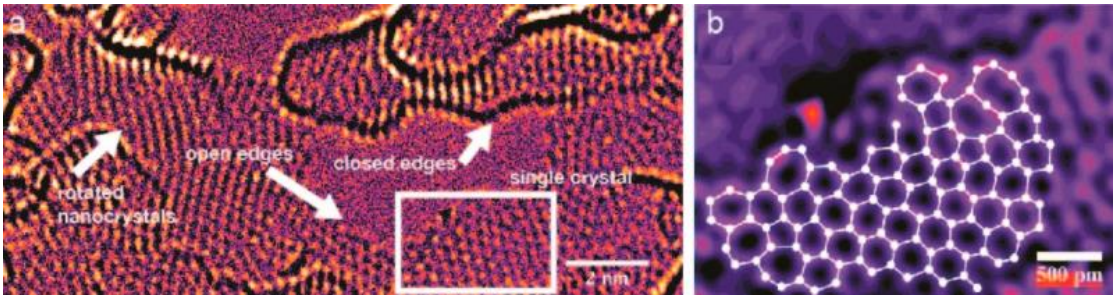


Figure 24 Atomic structure can be resolved using in situ heating with AC-TEM at 700 °C with features shown in (a). Sufficient resolution is achieved to identify defects in the bond structure (b). In (b), not all of the atomic structure could be accurately resolved, likely due to structural changes occurring during image acquisition, and only the directly resolved atomic structure is indicated by white dots and lines. (60)

2.7 Graphite Oxide to Graphene Oxide

Usually, when producing graphene oxide by oxidizing graphite, obtain graphite oxide is obtained. In order to turn graphite oxide to graphene oxide, the sample needs to undergo sonication, stirring or both. As a result, this could cause damage to the graphene layers. The process to obtain graphite oxide is still damaging to the graphene structure by changing the excellent electronic properties and reducing the initial size of the material. However, this could help the interspersed Graphene to be soluble in water solvents. (There happens surface modification)

An extremely successful technique to exfoliate graphite oxide, is sonication which can consume less time and produce high quality graphene oxide. However, this method heavily damages the graphene flakes by reducing the size from micrometres to nanometres and producing many different sizes of the graphene platelets, leading to anhomomorphic structures.

.

2.8 Graphene Related Materials Applications

Graphene Oxide shows great promise in many applications, from photonics and flat optics, to coatings, biomedical treatments, and tissue regeneration.

GO has heterogeneous atomic structure, exhibiting a series of distinctive material properties. Compared to graphene, which consists entirely of sp^2 - hybridized carbon atoms, GO is a 2D network consisting of variable sp^2 and sp^3 concentrations, thus enabling interesting and tuneable electrical, chemical, and optical properties.

To be more precise, GO has excellent field emission properties, which are promising for field-effect transistors (FETs). (61) The high flexibility in tuning its conductivity and pseudo-capacitance also makes GO a good candidate for high performance transparent conductive electrodes (TCOs) and supercapacitors. (62) In addition, owing to its large surface area, GO can bind various catalysts or active materials to its lattice for hydrogen storage and generation. (63) In tissue regeneration, GO can play a crucial role when binding metals on its surface, creating a new material with the desired properties e.g., magnesium has bone-like mechanical properties making it an ideal candidate for many biomedical applications. GO can reduce or block the formation of porosity and lead to formation of more compact and thicker coatings. (64)

2.8.1 Biomedical applications

2.8.1.1 Biosensing:

Graphene has been utilised in biosensors for the detection of nucleic acids, small molecules, ions, proteins, and cells (65). To gain insight into how biosensors operate, they generally consist of two elements: a receptor and a transducer Figure 25.. The receptor is an organic or inorganic material that interacts selectively with the target molecule (analyte), which can be an organic or inorganic molecule or even whole cells. The transducer is the component of the sensor, which, after interacting with the analyte, converts chemical

information into detectable measurements. Graphene and graphene-based nanomaterials are used as transducers in biosensors due to their large surface area, electrical conductivity, and their ability to attach various molecules via EDC/NHS chemistry or physisorption (Figure 25b).

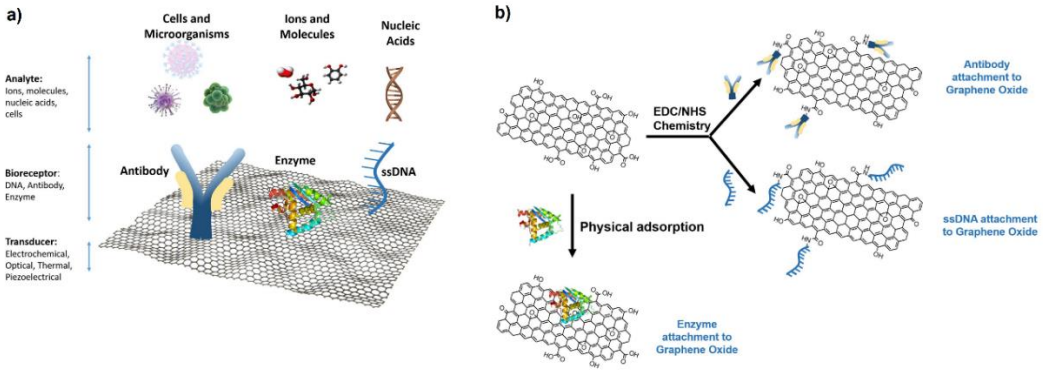


Figure 25 a) Examples of biosensors and components on a graphene platform. Shown: different analytes and the bioreceptor that they bind to. b) Processes in which different types of bioreceptors attach to the graphene platform. Image taken from reference (64)

Graphene and graphene-based nanomaterials have been used in fluorescence-resonance-energy transfer (FRET) biosensor development (66). FRET function is based on the transfer of energy from a donor fluorophore to an acceptor fluorophore and is one of the advanced tools available for measuring nanometre-scale distance and changes, both in vivo and in vitro. (67) Briefly, the principles of operation of graphene-based FRETs, which is represented schematically in Figure 26, is as follows: ssDNA, aptamers or molecular beacons which act as probes are adsorbed onto the planar graphene surface. Fluorophore labels on the ends of these probes are quenched rapidly when adsorbed onto the graphene surface. When analytes (complementary DNA (cDNA), thrombin and a designed complementary ssDNA or functional nucleic acids like surviving mRNA) are introduced to the graphene-probe system and bind their probes (ssDNA, aptamer, and molecular beacons, respectively), the probe fluorescence is recovered, allowing detection and measurement of the analyte (68).

Compared with organic quenchers, graphene has been shown to offer advantages in this role such as superior quenching efficiency various fluorophores, a low background and high signal-to-noise ratio as well as structural advantages such as resistance to enzymatic cleavage. (66) Furthermore, graphene and GO have been reported to interact strongly with nucleic acids through π-π stacking between the ring structures in the nucleic acid bases and the hexagonal rings of graphene and GO.

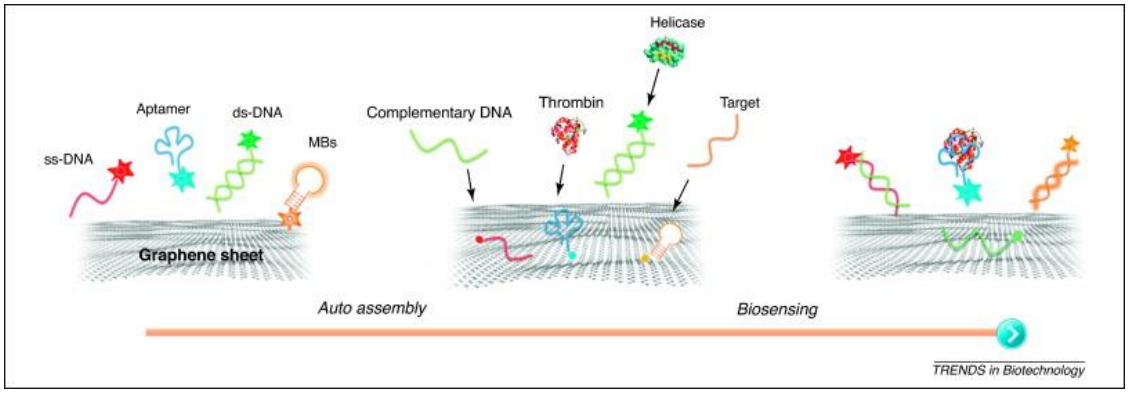


Figure 26 Schematic representation of graphene-based FRET. The fluorophore probe adsorbs to the graphene sheet which causes quenching. The respective analyte interacts with the probe which leads to recovery of fluorescence. Image taken from reference (69)

2.8.1.2 Drug Delivery Systems:

One of the key factors in constructing drug delivery systems is the selection of an appropriate carrier. For years there has been advancements in the development of drug delivery systems (DDSs) with the aid of graphene-based nanomaterials and now they have been considered one of the optimal choices, which can be engineered to integrate multiple functions in a single system. The innovative efforts to incorporate graphene into DDSs began with Liu et al. at Stanford University when they functionalised nanoscale GO (NGO) with biocompatible branched polyethylene glycol (PEG) to design a water-soluble carrier for SN38, an insoluble camptothecin (CPT) analogue which acts as an anti-cancer drug (70). The chemical structure of the NGO-PEG-SN38 complex

can be seen in Figure 27. Since then, graphene-based DDSs are being intensively explored by many research groups. Many promising results have been produced and efforts have been made to overcome challenges such as the nonbiodegradable nature of graphene and its potential long-term toxicity. (71)

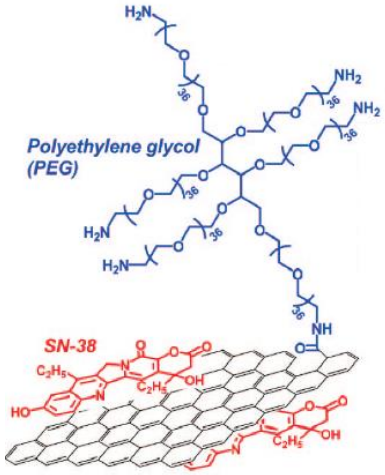


Figure 27 Chemical structure of PEGylated GO nanosheet; a water-soluble carrier for the anticancer drug SN38. Image taken from reference (69).

Many recent advances have been made in graphene-based drug carriers for anticancer drugs such as doxorubicin (DOX) (72). When considering cancer therapy, it is extremely important to specifically target tumour cells while leaving healthy cells and tissues intact. This makes accurate targeting a crucial factor in anticancer drug development. There are two methods of tumour cell targeting design to achieve this goal: active targeting and passive targeting. In passive targeting, the carrier reaches the target administration site without the aid of conjugated target-specific ligands to serve as homing devices. A disadvantage of this targeting mechanism is that low drug concentrations ultimately reach the target cell due to leakage, inactivation of drug and encounter of obstacles during the prolonged circulation. Moreover, the ionic interaction of the electronegative cell membrane and the electropositive nanoparticles could cause toxicity and off-target side-effects (73). In contrast, active targeting is a mechanism in which the surface of the carrier is functionalised with ligands designed to act as homing devices by recognising and binding to specific administration sites. This could achieve enhanced therapeutic effects and

reduced side effects by the interactions between ligand and corresponding targeted cell.

2.8.1.3 Tissue engineering:

Tissue engineering is a branch of the medical field which embraces the potential of repairing and regenerating damaged tissues and replacing defective body parts or organs that have been affected by disease and trauma. Being potentially biocompatible with striking chemical, biological and optical properties, graphene-based materials have been employed to further the advancement of tissue engineering.

Functionalised graphene has been used to generate 2D and 3D scaffolds which are necessary for tissue regeneration in a cell culture. (74) Biopolymers such as chitin and gelatine have been used to create scaffolds for human osteosarcoma cells and human embryonic stem cell growth, respectively (75) (76). Other polymers have similarly been utilized. Since then, graphene and graphene-based materials have been proven very promising in generating improved scaffolds for engineering various types of cells and tissues, such as bone tissue muscle tissue and cardiac tissue. A recent example is the work of B. Nyambat et al. who developed a sponge-scaffold for skin tissue engineering by generating a nanocomposite comprising of GO and genipin-crosslinked ECM (cell-derived extracellular matrix) taken from rabbit adipose derived stem cells. (77)

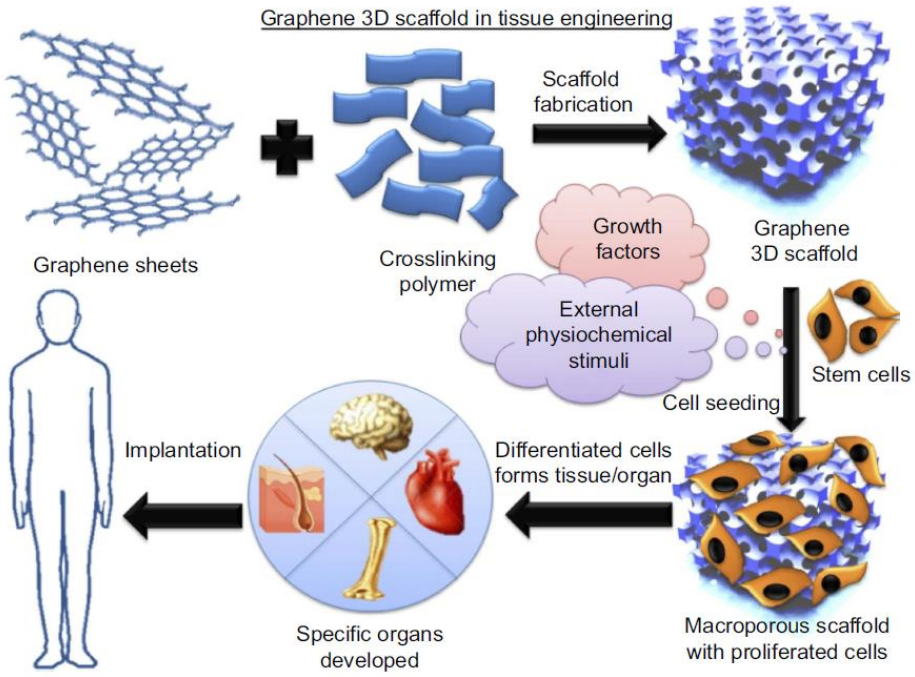


Figure 28 Schematic showing the utilisation of graphene in the engineering of 3D scaffolds for tissue regeneration. Image taken from reference (78).

Graphene-based materials have also been used or tissue engineering in the dental field (79). A strong example of graphene in dental tissue engineering is the proliferation and differentiation of dental pulp stem cells. According to work carried out by Gronthos et al., these cells have the ability to differentiate into odontoblasts/osteoblasts, adipocytes and neural-like cells (80). They also express genes that are linked to initiating mineralisation and bone homeostasis, which is essentially bone remodelling i.e., removing old bone tissue and replacing it with new bone tissue (81). Graphene-based scaffolds have been made to produce dental pulp stem cells. Although there was no difference in proliferation to be seen when compared to a reference glass substrate, the graphene-based scaffold proved to promote mRNA expression resulting in higher gene expression.

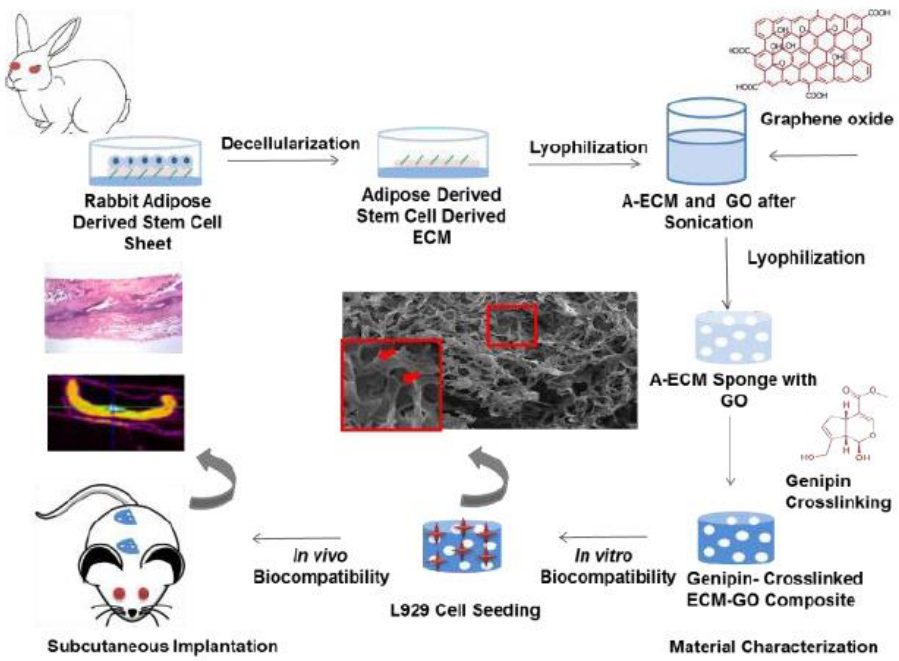


Figure 29 Step-by-step process for developing Genipin crosslinked ECM-GO sponges for skin tissue engineering. Image taken from reference (81).

2.8.1.4 Antimicrobial Properties of Graphene Oxide

Graphene Oxide seems to hold great interest in antimicrobial material applications, as it has high-efficient antibacterial activity to diverse pathogenic bacteria. However, the detailed antibacterial mechanism of GO is not fully clear. As Meizhen Wanga et al., mention, GO can be the perfect candidate for use against model Gram-positive (Gram+) bacteria (Staphylococcus aureus and Staphylococcus epidermidis) and Gram-negative bacteria (Gram−) (Pseudomonas aeruginosa and Escherichia coli) (82). GO, has also been used against COVID-19, by stopping the viral replication. GO showed high antiviral activity at room temperature. GO is used with Dialdehyde cellulose (DAC), which is one of the most widely used and highly reactive cellulose derivative. By this method aldehyde groups are introduced into polysaccharides and serve as useful material that can be used in different applications such as adsorption of heavy metal, separation of protein and drug carriers (83).

2.9 Reduced Graphene Oxide

Reduced Graphene Oxide (rGO) is produced by the reduction of Graphene oxide. Although graphene holds great interest in the scientific community, there is no inexpensive way to produce it. For this reason, rGO is popular, attractive, and inexpensive and there are several methods of reduction.

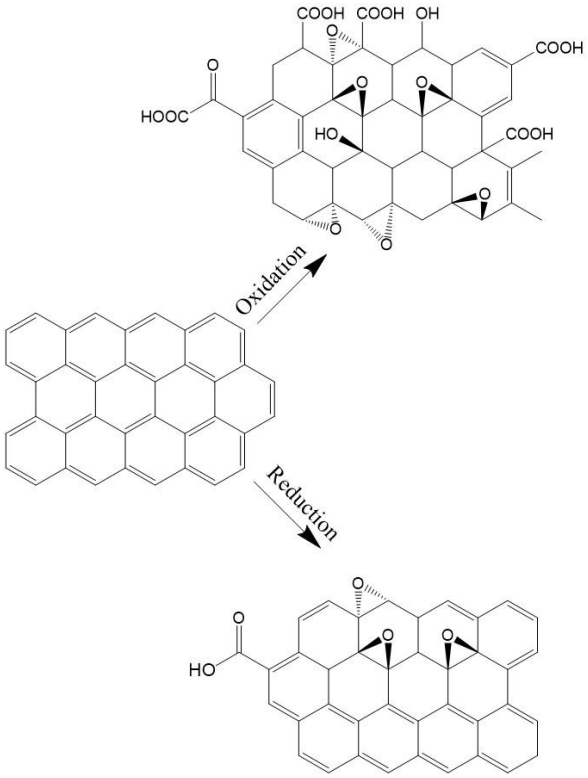


Figure 30 Graphene to 1) Graphene Oxide (Oxidation route) 2) reduced Graphene Oxide (Reduction route) designed in ChemDraw

2.9.1. Reduced Graphene Oxide Synthesis-Reduction Methods

There are several existing reduction strategies in order to produce rGO depending on the application in which it will be used. More particularly, there are chemical, thermal, biological and photochemical methods in order to obtain high quality rGO. All the previously mentioned categories will be discussed in detail in the sections to follow, mentioning the reaction conditions and the properties of each produced material in order to assess the effectiveness of each method.

Chemical Reduction

To the best of our knowledge, hydrazine reduction, firstly used in 2007 by Stankovich el al (84), is the most widely used chemical reduction including hydrazine monohydrate ($N_2H_4*H_2O$) for obtaining a closely related to graphene material in terms of electronic and structural properties. In their attempt, Stankovich's group, observed in the rGO structure a C/N ratio of 16.1 and an electrical conductivity of ~2×10^2 S/m. To complete this study, Ren et al carried-out experiments changing temperature conditions and reaction times (85). Results showed that reduction at 95◦C for 3 h yielded the highest C/O ratio of 15.1 compared to 3.1 of GO along with a significant increase in electrical conductivity from 1.5×10^{-6} (GO) to 5 S cm^{-1} (rGO) under these conditions.

In their publication, Ren et al, suggested that carboxyl groups of GO could react with hydrazine in a second reaction to produce hydrazole type bonding (-C=N-N=C-) as shown in Figure 31.

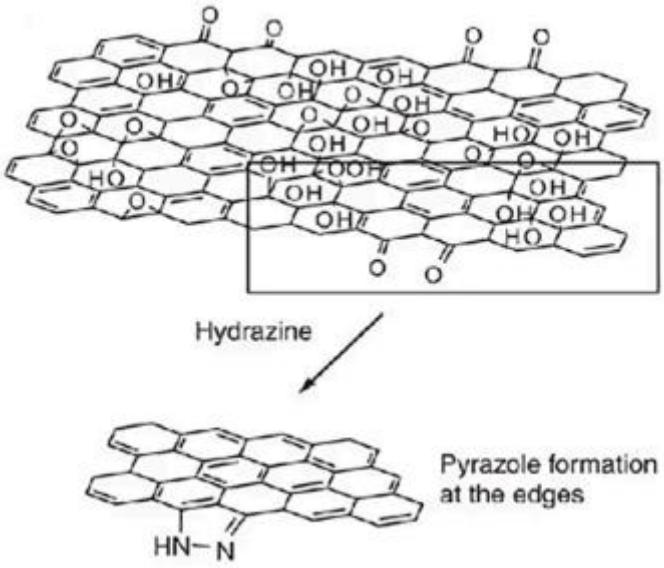


Figure 31 Pyrazole Formation on GO edges (85)

Reduction is used as a process to form carbon-carbon double bonds upon the loss of oxygen groups, however there is still doubt about the pyrazole group and how they undergo full reduction in order to achieve a conjugated C=C bond to account for this increase in electrical conductivity. It is obvious that the resulting rGO will not have the pristine graphene structure and concomitant nitrogen doping of rGO cannot be avoided.

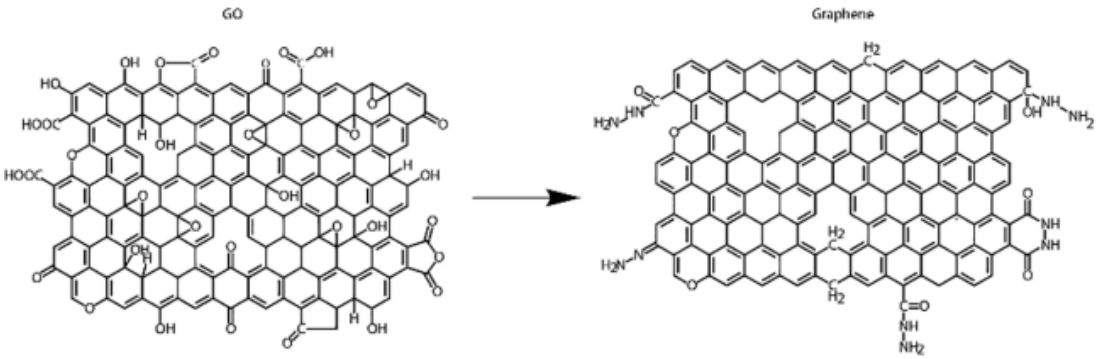


Figure 32 Structure of GO (left) and nitrogen-doped GO (right) (85)

Green Chemical Reduction

As years go by, the need of replacing hazardous chemicals with green substitutes is of vital importance, since a green planet is a clean planet. For this reason, green chemistry is being used more and more over the decades, in order to cut down on emissions, reduce pollution and help our planet.

In this concept, green reduction of graphene oxide has been developed, using eco-friendly materials such as Ascorbic acid, Amino acids, plant extracts, coffee extracts, metal powders, antioxidants even water, which show competitive results, have sufficiently lower cost, and form stable dispersions in a number of solvents, such as alcohol, H_2O, etc.

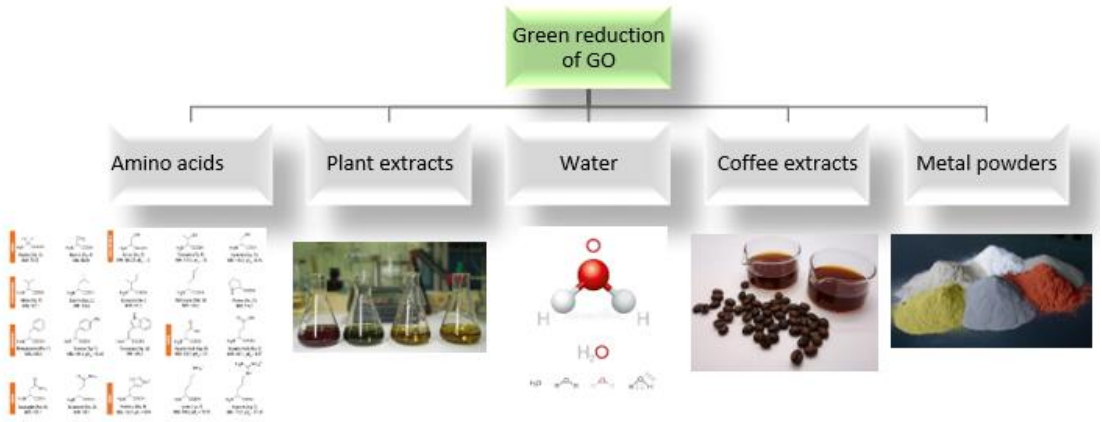


Figure 33 Summary of green reduction methods Schematic illustration by. Kalotina Poulla.

Biological Reduction

A different type of green reduction, biological reduction, gained much interest due to its novel use in aerobic and anaerobic conditions with the assistance of different types of pathogen microorganisms and yeast. An example of microorganism used is Shewanella, which has been shown to effectively reduce GO under both aerobic and anerobic conditions. Unlike the hydrazine reduction

method, Shewanella reduces hydroxyl moieties and not (carboxyl and carbonyl groups mainly due to the higher bond energy of C=O compared to C-OH (86).

Photoreduction

Another chemical free method to produce fast, low cost and high-quality reduced graphene oxide, is photoreduction of GO usually done by short laser pulses, plasma, camera flash or photothermally. These methods can be used alone or in combination with catalysts or other organic and inorganic compounds. Short laser pulses include short, high-energy pulses which localize heat on a certain area in order to decompose oxygen-containing functional groups and consequently lead to the reduction of GO. (87)

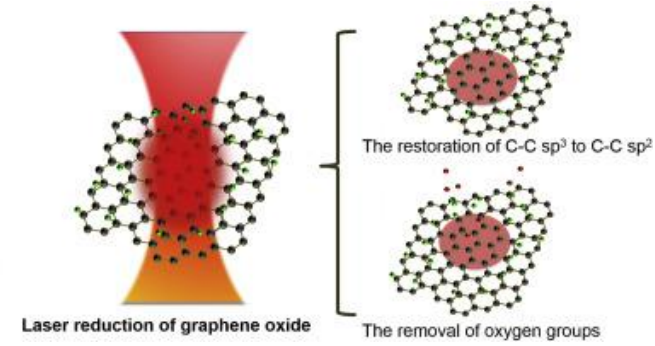


Figure 34 Reduction of GO using pulsed laser source- Removal of oxygen containing groups and restoration of C-C sp^3 to C-C sp^2 hybridization (88)

2.10 Reduced Graphene Oxide Applications

rGO can be used in electronics and be used as a field effect transistor, in chemical sensors and biosensors. In biosensors, it can be used to detect hormonal catecholamine molecules, avidin and DNA. Dopamine is one of the most important catecholamine neurotransmitters since it is involved in many

functions of the human central nervous system, including motor control, reward, or reinforcement. It is of utmost importance to quantify the amount of dopamine since abnormal levels can cause a variety of medical and behavioral problems. rGO-based composite was utilized to cultivate neuroblastoma cells and to quantify the amount of dopamine released from the living cells, thus demonstrating its biocompatibility.

rGO is also used in light emitting diodes (LEDs) and solar cell devices. For these applications, having transparent electrode is important and rGO is a convenient for these devices. rGO can be used in nanocomposites of rGO, and especially for lithium-ion batteries. In these batteries, nanoparticles of insulating metal oxide are absorbed onto rGO which enhances the performance of these materials in lithium-ion batteries. It is also used in many composite materials and printable graphene electronics.

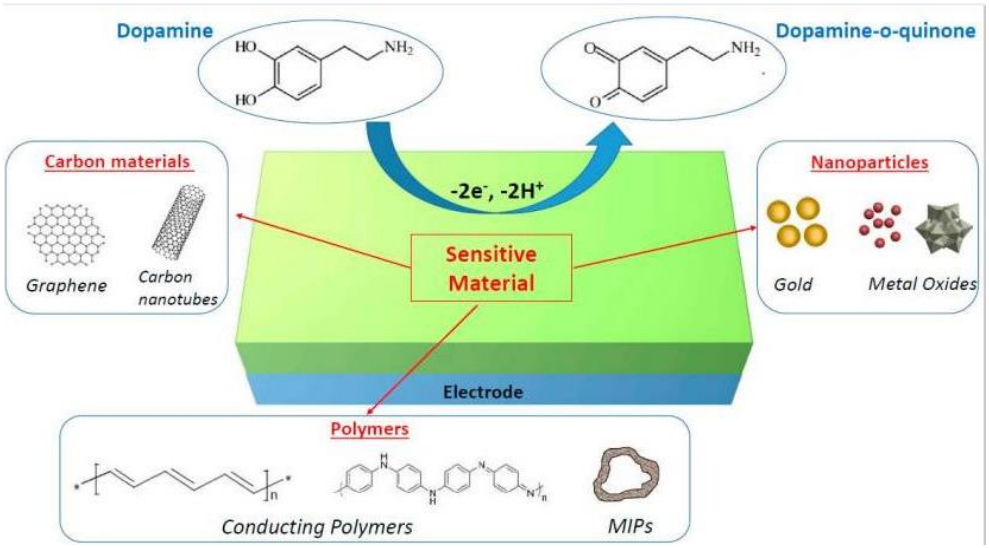


Figure 35 Schematic illustration of nanomaterial-modified electrodes for electrochemical biosensing of dopamine (89).

Chapter 3: Antimicrobial Activity of Materials

3.1. Antimicrobial Activity of Graphene Oxide:

In recent years, overpopulation of our planet has led to undesirable phenomena such as and extensive environmental pollution, and easily spreadable diseases, such as the coronavirus outbreak in 2019. Thus, new, innovative, and eco-friendly materials need to be researched and evaluated in order to inhibit the growth of hazardous microorganisms on surfaces.

Antimicrobial surfaces, contain antimicrobial agents, which can act in several ways, such as preventing microorganisms from growing on them, or killing them. They can be functionalized using a variety of processes, for example using chemical agents or laser modification of the surface making them toxic to the microorganism. This could happen either because the material itself has a certain morphology which, for example, causes cellular membrane damage, or it has some antimicrobial agent attached, e.g., Ag, Au, Cu etc., which could act synergistically and target certain parts of the microorganism leading to cell death.

These antimicrobial surfaces could prove valuable as antimicrobial coatings on important healthcare equipment, medical services, implants, hospitals, public places, laboratories etc. to provide a safe environment by eliminating bacteria, fungi, viruses which can be transmitted to humans and lead to spread of infectious diseases. The materials of interest in this thesis are Graphene oxide (GO), reduced Graphene Oxide (rGO) and Silver (Ag) decorated Graphene Oxide (GO-Ag) as will be analyzed below.

Graphene Oxide has already exhibited antimicrobial activity. According to recent research, GO's physical and chemical mechanisms have shown effective antibiotic properties because it can wrap the microorganism's membrane and cause oxidative stress leading to damage of the cellular membrane. (90) Bacteria's membranes can be oxidized by GO and produce glutathione a precious cellular antioxidant. (91)

According to Francois Perreault et al., size of graphene oxide nanosheet maters, due to graphene oxide's contact-based antimicrobial activity. The smaller GO sheets are, the higher the antimicrobial effect is, mainly due to oxidative mechanisms associated with the higher defect density of smaller sheets. The antimicrobial effect of GO increased with increasing the sheet area and inactivation observed for 0.65μm2 sheets after 3 h exposure. (92)

In another study, Hina Naeem et al., proposed that graphene oxide–silver nanocomposite can be used for decontamination of water from multiple pollutants. In the specific study, GO-Ag composite can provide a triplicate benefit in wastewater treatment by removing dyes, aromatic compounds and destroying harmful microorganisms. The composite, exhibit better adsorption capacity against aromatic and organic pollutants and better antibacterial performance, while being also an environmentally friendly material. (93)

GO-Ag composite has been used together with copper oxide nanoparticles, to enhance the antibacterial activity. The produced nanocomposite, showed a band gap of 4.43 eV, compared to the 3.95 eV when decorated with just silver nanoparticles and bacterial cell apoptosis compared to standard sample, went down by 85.6%. Enhancing antibacterial activity by introducing metallic and metallic oxide nanoparticles across GO nanosheets could well recommend these bio-composite materials are customized to suit clinical applications. (94)

G.S.Lekshmi et al., proposed that reduced graphene oxide-silver-silver oxide nanocomposite show strong photocatalytic, antioxidant and antibacterial activity for environmental remediation. The flame reduced graphene oxide (FRGO) is synthesized from edible sunflower oil via a simple flame synthesis method. Next, silver nanoparticles (Ag/AgO/Ag2O) are produced by

phytochemical reduction of AgNO3 using a reducing agent based on flavonoids from Coleus aromaticus (Mexican mint), also used in food industry. FRGO-Ag/AgO/Ag2O composites show strong antioxidant activity, with improved radical inhibition as well as dye degradation properties when compared to pristine flame reduced graphene oxide (95).

GO-Ag has been used together with nickel-titanium alloy as a anti-biofilm on medical devices. Material was prepared using electrophoretic deposition using various deposition-coating times and anti-bacterial effect was tested on Streptococcus mutans, measuring the biofilm mass and the number of viable cells. NiTi alloy surface modification showed that it can be a promising coating to reduce consequences of biofilm formation.

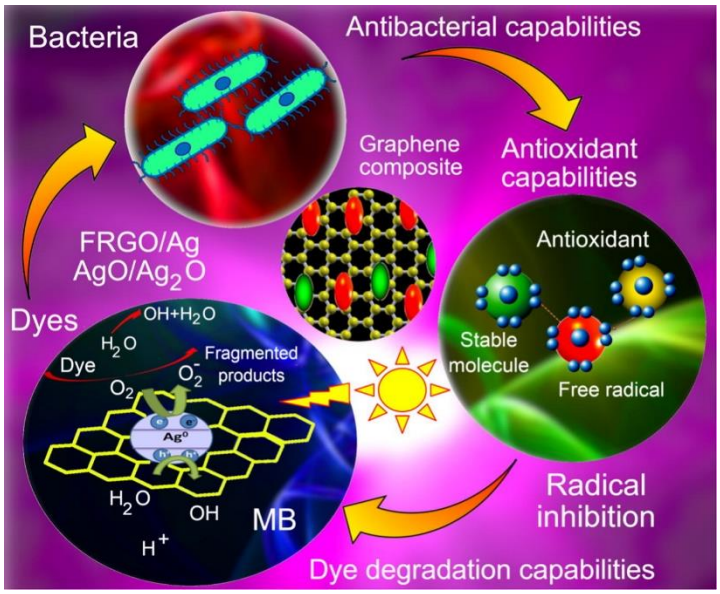


Figure 36 Schematic representation of techniques used for the fabrication of flame-synthesized reduced graphene oxide (FRGO) and FRGO/Ag/AgO/Ag2O nanocomposites. (a) Preparation of soot containing reduced graphene oxide by burning sunflower oil, is deposited onto

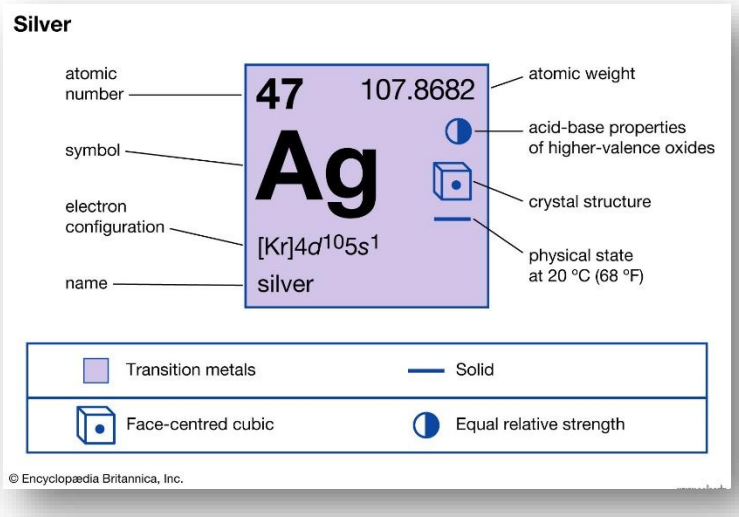
3.2. Antimicrobial Activity of Reduced Graphene Oxide:

Besides GO, reduced graphene oxide has proven to be an ideal candidate for use in antimicrobial coatings. More particularly, rGO demonstrated excellent antibacterial activity compared to GO against E.coli bacteria. After binding on the cell wall rGO could penetrate the cells and cause damage to the intracellular organelles apart from physical disruption of the cell wall. Intracellular ROS production assay confirmed that ROS played a significant role in oxidative damage of the bacterial cells, while the contact angle study demonstrated good hydrophobic behavior of the rGO-coated surface, which prevented the bacterial adhesion on the surface. (96)

Reduced graphene oxide has been used as antibiofilm for pathogenic bacteria. The synthesized rGO could manage the extension of biofilm at its adhesion strength, which is the initial start in the antimicrobial means. Consequently, rGO can be applied as an antimicrobial agent in the biomedical for limited purposes, since the toxicity level must be examined, such as face masks, cosmetics, and dressing (97).

Reduced graphene oxide has been used in photoactive antimicrobial coatings, together with metals in order to create a stable and potentially photoactive biocide surfaces. The prepared reduced graphene oxide has been prepared by the sol-gel technique to create photocatalytic surfaces using spin coating. The prepared material caused damage and intracellular oxidative stress produced by the photogenerated reactive-oxygen species. Metal, such as Zinc, have been used to enhance the performance of rGO, by increasing the photocatalytic performance of rGO (98).

3.3. Antimicrobial Activity of Silver:



Silver is a chemical element located in Group 11 or Ib and 5th period of Periodic Table of the elements. It is a metal known for its exceptional electrical conductivity and chemical and physical properties. It belongs to the list of the precious metals since besides science, it can be used for decorative purposes. In chemistry, silver can be used as catalyst to convert ethylene to ethylene oxide which is an important precursor in organic chemistry. Its chemical symbol is Ag and atomic number 47. The atomic weight of the element is 107,87 respectively and it is solid at room temperature. Another reported property of significant value is that silver, exhibit great antimicrobial properties alone or synergistically with other materials and thus used in many applications around the world. In this thesis silver nanoparticles (AgNPs) will be used to produce the final material as described below. (99)

Silver nanoparticles (Ag NPs) have been recognized as potential candidates for the generation of novel antimicrobial agents. For this reason, silver has been used as antimicrobial agent for treatments and equipment to avoid infectious diseases. Silver can also play important role in the inactivation of the microorganisms, by inhibiting the growth of microbial species.

Firstly, there is the modification stabilization of Ag NPs surface according to microbial environment via various process dissolution, aggregation, photo redox reaction and releasement of Ag NPs. Then, interaction of Ag cations-Ag NPs with the cell walls of bacteria occurs, resulting in inhibition of the functions of bacterial proteins, which avoids the microbial growth and leads to bacteria cell death. The activity of Ag NPs also depends on the size distribution, morphology, physicochemical properties, environment, and concentration of Ag NPs.

In order to create effective nanoparticles, their structure needs to include three layers: 1) core, 2) shell, 3) surface. The core can be synthesized using various methods, conditions, and precursors. Shell could be added if necessary but in order to prepare 1-D nanoparticle from single salt, the shell is mostly composed of the identical material with the core. And lastly, surface must be functionalized depending upon the project. This includes, either agglomeration or to give specific functions to nanoparticles. The surface functionalization of nanoparticles is due to transient van der Waals interactions of used compounds with the nanoparticle surface.

According to Enoch et al., silver can exhibit exceptional anti-fungal properties, against various fungal species. More particularly, he studied antifungal activities on C.albicans and Trichophyton mentagrophytes and it was noticed that the nano-size Ag NPs exhibited same antifungal activity as amphotericin B (medicine). The size also showed that there was lower hemolytic activity. (100)

Another study suggested that Ag NPs, show antiviral activity on various viral species such as hepatitis b, human immunodeficiency virus, respiratory syncytial virus and can be used in various antiviral therapies. Authors noticed that fabricated Ag NPs showed high binding affinity towards viruses DNA, inhibiting the production of extracellular virions (101).

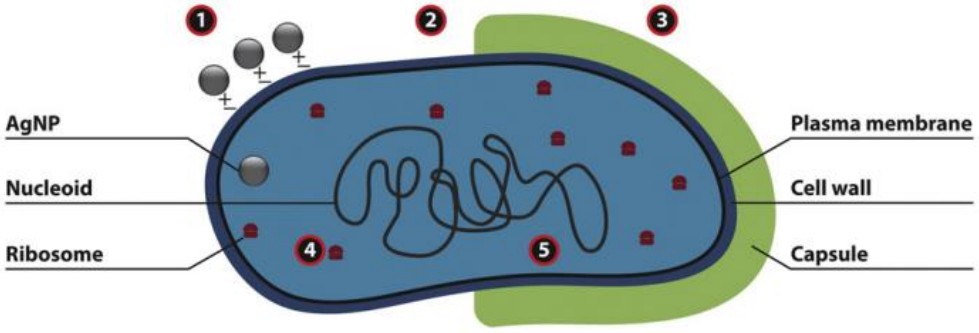


Figure 37 Proposed mechanism of antibacterial action of silver nanoparticles: 1—electrostatic attraction, 2—production of free radicals, changes in permeability, disturbance of respiration, leakage of intracellular content, 3—modulation of phosphotyrosine profiles of proteins, involved in the cell cycle progression and in the synthesis of capsular polysaccharides, 4—interaction with SH-groups; inhibition of protein synthesis and function, 5—interaction with phosphorus-containing molecules (DNA) (102)

Rai et al conducted an important retrospective analysis of the role of silver ions, ROS production and morphological modifications after silver nanoparticles act on bacterial cells, as well as the factors influencing the antibacterial properties of nanoparticles, such as chemical composition, concentration, size, and shape (Figure 37).

Silver has been also used together with chitosan, to treat H1N1 influenza A virus. In this study, the antiviral activity was enhanced with the control and increased quantity of Ag NPs releasement on the surface. Also, the smaller size of Ag NPs showed higher antiviral activity compared to larger parts and can be used for treatment and coating to avoid various viral infections (103).

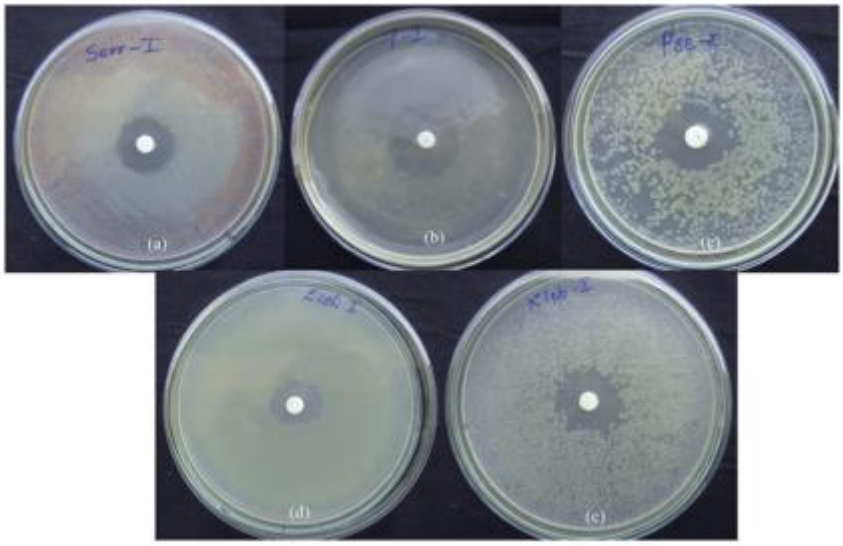


Figure 38 Examination of antibacterial properties of BSA Ag NPs on various bacterial species (A) S. aureus, (B) S. marcescens, (C) P. aeruginosa, (D) E. coli, and (E) K. pneumoniae. (103)

3.4. Antimicrobial Activity of Ag-GO:

Silver nanoparticles can bind to GO to produce a material which is hydrophilic, chemical stable and with exceptional antimicrobial activity, due to the toxicity of silver which leads to cell-death and the wrap-mechanism of GO that causes the oxidative stress of microorganisms' cellular membrane and wall.

Also, as stated in another study (104), bacteria are less prone to develop resistance in silver than in conventional antibiotics so the combination of the two above materials can create an antibiotic of high standards. In the following chapters we will discuss the synthesis of Silver decorated Graphene Oxide, the characterization of the material and its antimicrobial activity tested on 2 different microorganisms, Escherichia Coli and Pseudomonas Aeruginosa.

According to a study GO, silver nanoparticles, ceria nanoparticles and composites of these materials have been studied and tested for inactivation of Escherichia coli and Salmonella Typhimurium. Several concentrations and ratio between GO and silver have been tried in order to find the perfect match for the antimicrobial assays. Also, different exposure times have been examined in order to determine the inactivation of the bacteria. When GO coupled to silver, antimicrobial activity was boosted in order to achieve full inactivation of the pathogens. In this way, this material can be used to develop water systems to avoid the growth of coliforms that can cause borne diseases. (105)

GO-Ag can be used in medical equipment since it exhibits low toxicity and can be easily used in sprayable antimicrobial coatings. Depending on the synthesis method GO-Ag could exhibit different properties and antimicrobial mechanisms. Ex-situ preparation method exhibited the greatest antimicrobial activity against K. Rhizophila, P. aeruginosa and B. cereus and results showed that GO-Ag can be used as additive in paints and coatings to diminish the development of biofilms (106).

Composite GO-Ag has also been prepared through exposing the aqueous solutions of GO to garlic extract in the presence of Silver Nitrate in order to

achieve the GO decoration with silver ions. The prepared material tested for its antibacterial properties and proven to be an excellent candidate for eliminating the surface E. Coli bacteria (107).

Chapter 4: Experimental Section

For the purpose of the present diploma thesis several materials were used as listed in

Table 2.

Reagent:	Purchased from: :
Graphite powder (<20 μm)	SIGMA-ALDRICH
Sulfuric acid (H_2SO_4, 95-97%)	HONEYWELL
Sodium nitrate ($NaNO_3$)	SIGMA-ALDRICH
Potassium permanganate ($KMnO_4$)	SIGMA-ALDRICH
Hydrogen peroxide (H_2O_2, 30%)	SIGMA-ALDRICH
Hydroiodic acid (HI, 55%)	SIGMA-ALDRICH
Glacial Acetic acid (CH_3COOH or AcOH, 100%)	MERCK
Sodium bicarbonate ($NaHCO_3$)	SIGMA-ALDRICH
Acetone (CH_3COCH_3, 99%)	SIGMA-ALDRICH
Silver Nitrate	SIGMA-ALDRICH
Ammonia Solution >99%	SIGMA-ALDRICH
Sodium Hydroxide pellets	SIGMA-ALDRICH

Table 2 Materials used for the purpose of this diploma thesis

Equipment

Centrifugations were carried out using a Beckman Coulter Allegra X-22 Centrifuge and Universal 320 Hettich. Dispersions of GO and RGO were prepared using a Hielscher UP200Ht ultrasonic probe. All UV-Vis absorption measurements were performed with a Shimadzu UV-2401 PC Recording Spectrophotometer

4.1 Hummer's method

For the production of graphene oxide, a modified Hummer's method was performed. The Hummer's method is an experiment carried out in two days



Figure 39 Hummer's method preparation

Day 1-Steps:

1. In a 600 ml beaker add 1g of graphite and 46ml of sulfuric acid (95-98%).
2. Beaker should be placed in a plastic container which provides the ice bath for 20 minutes.
3. Then we slowly add (exothermic reaction) 1g of $NaNO_3$ which works as an oxidizing reagent.
4. Stir for 1h.
5. Add 6g of $KMNO_4$ add very slowly (add for about 20 minutes) because the reaction is violent. With the addition of $KMNO_4$ a green color is observed.
6. The reaction is left stirring overnight.

Graphite oxide was chemically synthesized from graphite using a modified Hummer's method. More specifically, 1 g of graphite powder is added to a 600 ml beaker containing a large stirring magnet followed by 46 ml of sulfuric acid (H_2SO_4,95-98%). The beaker is placed in an ice bath and the mixture is left stirring for 20 min. Then, 1 g of sodium nitrate ($NaNO_3$) is added slowly and small amounts at a time as the reaction is exothermic. The mixture is left stirring for 1 h. The reaction that takes place is

$$\mathbf{2\ NaNO_{3\ (aq)} + H_2SO_{4\ (aq)} \rightarrow 2\ HNO_{3\ (aq)} + Na_2SO_{4\ (aq)}}$$

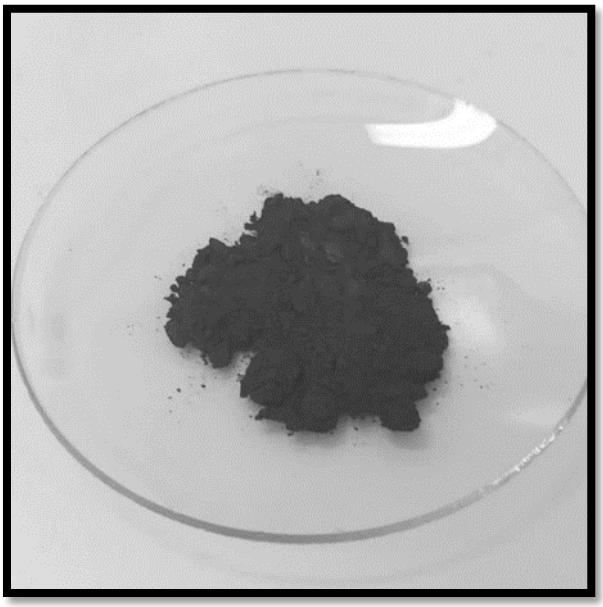


Figure 40 1g of graphite powder used to chemically synthesise graphite oxide via modified Hummer's method.

Day 2-Steps:

1. Heat solution at 35^{o}C for 1h and 40 minutes with stirring.
2. Turn up heat to 90 ^{o}C and add 80ml DH_2O slowly.
3. Leave stirring at 90 ^{o}C for 4o minutes. The reaction turns brown.
4. Turn off heat.
5. Add 200ml of DH_2O and 20ml H_2O_2 30%. Bubbling and a green-brown color observed.
6. Leave stirring till it reaches room temperature.
7. Centrifugation of the entire amount of the solution at 4200rpm for 20 minutes at a time.
8. Heat 200ml DH_2O to 65 ^{o}C for washing.
9. Washing of sediment & centrifugation with 200ml warm DH_2O (100ml for each vial).
10. Washing sediment & centrifugation with cold DH_2O until pH=7. Use pH strips.

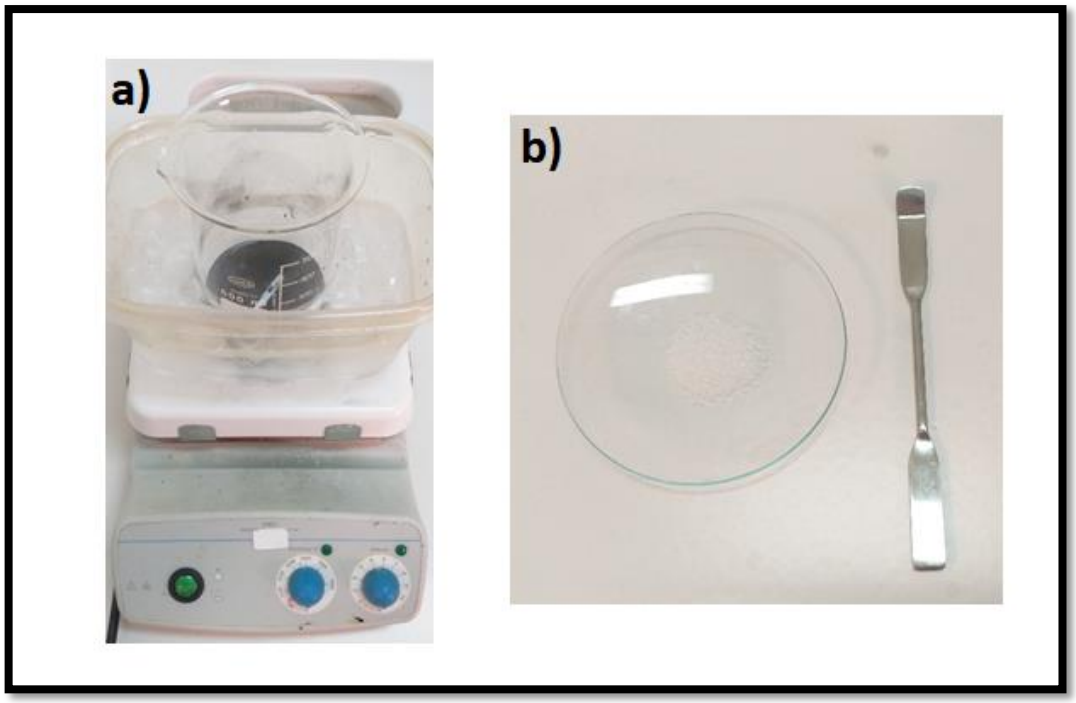


Figure 41a) The graphite-H_2SO_4 mixture is placed in an ice bath as the reaction that are about to occur are highly exothermic. b) 1g of NaNO3 is then added

$NaNO_3$ acts as an oxidising agent. The intercalation of graphite by H_2SO_4 cannot take place without an oxidizing agent. This is HNO_3 which is produced from the reaction of $NaNO_3$ with H_2SO_4. That way $NaNO_3$ enhances oxidation on the basal planes of graphite. This was proven with UV-Vis absorption measurements, in which graphite oxide with the addition of $NaNO_3$ had a higher absorption peak that graphite oxide without the addition of $NaNO_3$. It has also been shown that $NaNO_3$ increases the distance between the graphene layers and results in GO with smaller crystallite size.

When the hour is up, 6 g of potassium permanganate ($KMnO_4$) is added very slowly and in small amounts as the reaction that takes place is violently exothermic. Although the Hummers method is generally not considered hazardous, the addition of $KMnO_4$ must be performed with care, as the reaction between H_2SO_4 and $KMnO_4$ forms dimanganese heptoxide (Mn_2O_7), a highly reactive species Mn_2O_7 is known to detonate at temperatures higher than 55^{o}C.

With the addition of $KMnO_4$ a thick, green solution is observed. $KMnO_4$ is a strong oxidising agent. When it is added to the H_2SO_4 solution the following reactions occur:

$$KMnO_{4\,(aq)} + 3\,H_2SO_{4\,(aq)} \rightarrow K^+_{(aq)} + MnO_3^+{}_{(aq)} + H_3O^+_{(aq)} + 3\,HSO_4^-{}_{(aq)}$$

$$KMnO_{4\,(aq)} \rightarrow K^+_{(aq)} + MnO_4^-{}_{(aq)}$$

$$MnO_3^+{}_{(aq)} + MnO_4^-{}_{(aq)} \rightarrow Mn_2O_{7\,(aq)}$$

$$GIC_{(s)} + Mn_2O_{7\,(aq)} \rightarrow \text{Graphite Oxide}_{(s)} + \text{by-products}_{\,(aq)}$$

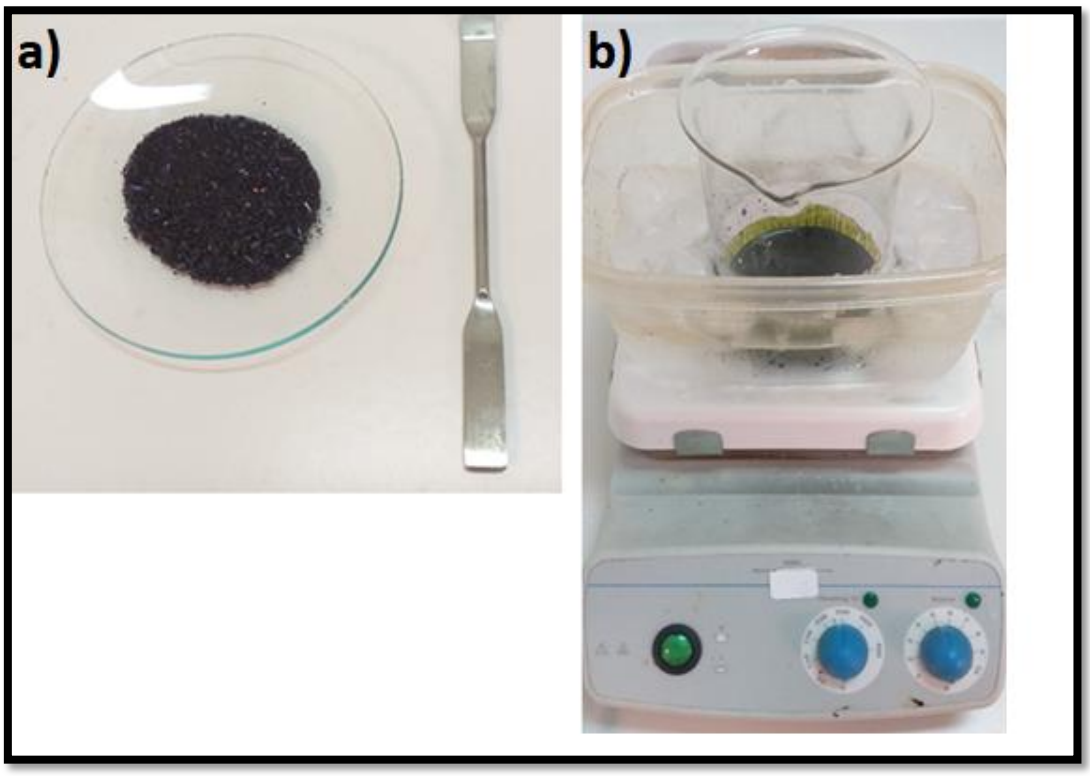


Figure 42a) KMnO4 crystals used as strong oxidising agent. b) With the addition of KMnO4, the solution turns green

At this stage, the graphite is in the form of the graphite intercalation compound (GIC). This is essentially graphite with H_2SO_4 molecules occupying the space between the graphene sheets. When KMnO4 is added, the oxidising agent manganese (III) oxide ($MnO3^+$) is formed according to reaction equation. This is what gives the solution its green colour. The oxidising agent manganese (VII) oxide (Mn_2O_7) is also generated according to reaction equations above.

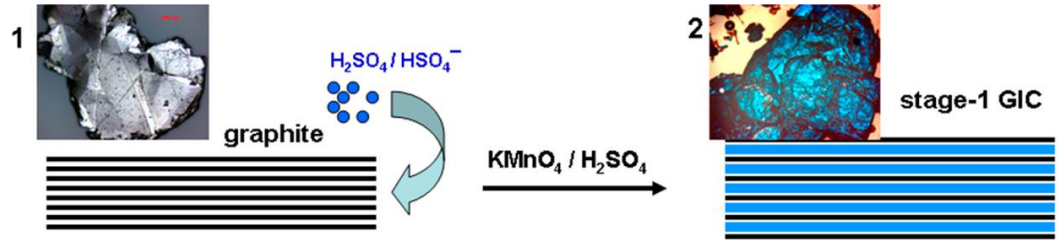


Figure 43 Schematic representation of H_2SO_4 intercalation between the graphene layers of graphite. The black lines represent the graphene layers, and the blue lines represent the H_2SO4/ HSO_4- intercalant

.

After the addition of $KMnO_4$ the solution is left stirring for 24 h. The next day, the solution is then stirred at 35^{o}C for 1h and 40 min. The colour of the mixture is now a dark brown (Figure 44). The heat is turned up to 90^{o}C and 80 ml of deionised water (DI H2O) are added very slowly. The reaction is left stirring at 90oC for 40 min. After 40 min the reaction is removed from the hotplate and 200 ml of DI water are added followed by 20 ml hydrogen peroxide solution (H_2O_2, 30%) which is added slowly and carefully. The additional water further exfoliates the graphite planes while H_2O_2 is added to stop the oxidation reaction and additionally remove any traces of excess $KMnO_4$



Figure 44 After 24 hours, the mixture has turned a dark brown colour.

Although H_2O_2 itself is an oxidising agent, in this reaction it has reducing properties. In acidic condition, such as in the presence of H_2SO_4 solution, H_2O_2 reduces Mn^{7+} cations to colourless Mn^{2+} cations while H_2O_2 itself is oxidised releasing oxygen gas, as seen in reaction equation (8). This prevents further oxidation of the GOC by MnO_4^- ions. The reactions that take place with the addition of H_2O_2 are:

$$\mathbf{5\ H_2O_{2\,(aq)} + 2\ KMnO_{4\,(aq)} + 3\ H_2SO_{4\,(aq)} + \text{-> } 5\ O_{2\,(g)} + MnSO_{4\,(aq)} + K_2SO_{4\,(aq)} + 8\ H_2O_{(l)}}$$

$$\mathbf{H_2O_{2\,(aq)} + HNO_{3\,(aq)} \text{-> } HNO_{4\,(aq)} + H_2O_{(l)}}$$

$$\mathbf{H_2O_{2\,(aq)} + MnO_4^{-}{}_{(aq)} + H^{+}{}_{(aq)} \text{-> } 2\ Mn^{2+}{}_{(aq)} + 8\ H_2O_{(l)} + 5\ O_{2\,(g)}}$$

With the addition of H_2O_2, bubbling is observed due to the generation of O_2 gas, and the solution turns a green-brown colour, as seen in Figure 45. The reaction is then left stirring until it reaches room temperature. The final colour of the reaction should be green-brown, confirming successful oxidation of the graphite flakes.

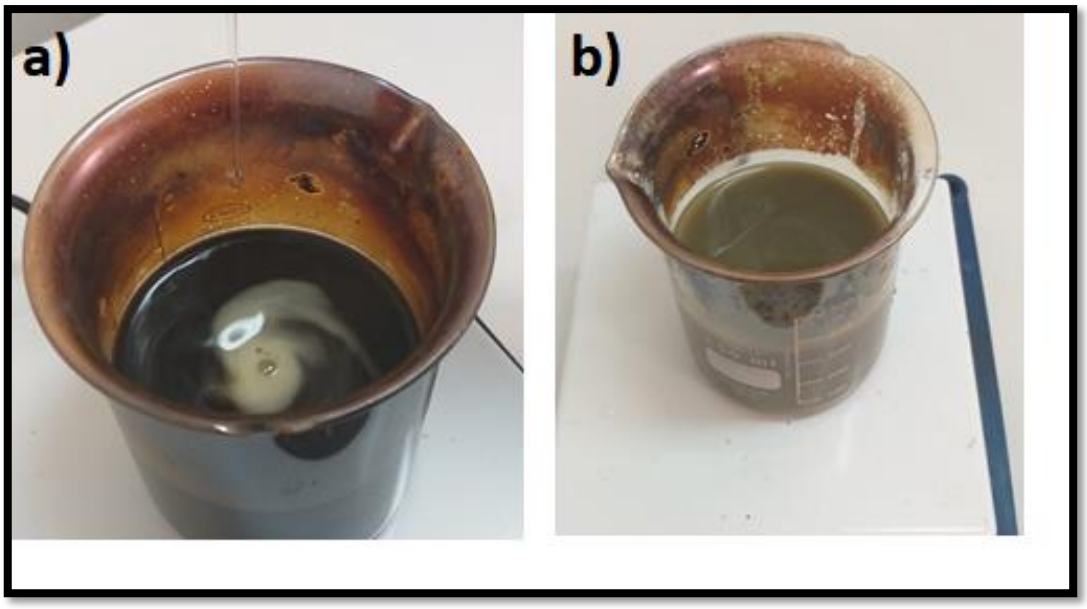


Figure 45 a) With the addition of H_2O_2 bubbling is observed due to O_2 gas being generated. b) After the H_2O_2 has been added, the mixture turns a green-brown colour.

The entire solution is then centrifugated at 4200 rpm for 20 min to isolate the solid graphite oxide in the form of a sediment. The sediment is washed with 200 ml of warm DI H2O which has been previously heated to about 65oC. The sediment is then washed with DI H2O at room temperature until the supernatant reaches neutral pH. Lastly, the sediment, which is now clean graphite oxide, is left to dry in an oven at 60oC for several days.

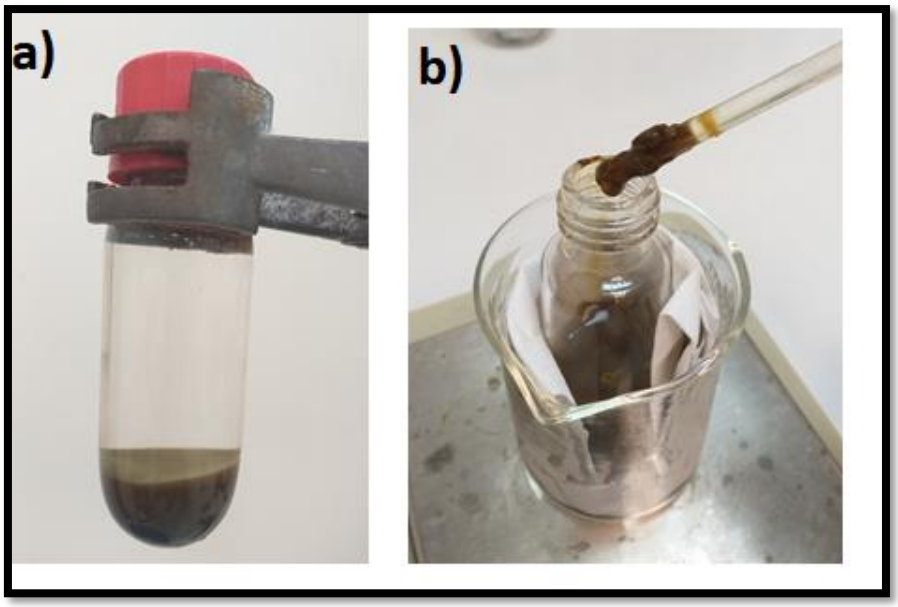


Figure 46 a) When the solution is centrifuged, graphite oxide and biproducts of the reaction are isolated in the form of a sediment. The graphite oxide must be thoroughly washed of the biproducts. b) During the washing process, the mixture has a gel-like form.



Figure 47 The washed graphite oxide is left to dry in an oven at 55^{o}C for several days until it is completely dry.

Once the graphite oxide is dried, it is pulverised using a pestle and mortar until it is in the form of a fine powder (Figure 48).



Figure 48 When graphite oxide has fully dried, it is transferred to a mortar to be pulverised with a pestle into a fine powder.

As approaching to step 7 of day 2, a certain process needs to be followed as mentioned above. To be more specific: The liquid product is separated in two Centrifuge glass tubes of same weight and placed in a Centrifuge Allegra X-22 BECKMAN COULTER 4000 rpm for 30 minutes. When centrifugation ends, precipitate is keeped and supernatant is rejected. Both tubes are fullfiled with warm deionized water and balanced for the 20-minute centrifugation under same circumstances. This procedure is repeated with cold water too, until pH reaches a value of 7,0-7,5. Then it sets to dry for 3-4 days in the oven at 55 ^{o}C.

Then, the produced GO is drained andpowdered using mortar and pestle. The GO is now ready for storage in a 40 ml vial for further use.

4.2 Reduction of Graphene Oxide

Reduced graphite oxide was prepared from graphite oxide synthesised previously via modified Hummer's method, using chemical reducing agents, namely hydroiodic acid (HI), a strong reductant and acetic acid (CH_3COOH or AcOH), a mild reductant. The reducing process can be described briefly by the following steps:

1. Addition of glacial AcOH (37 ml) to graphite oxide (1g). Ultrasonication bath.
2. Addition of HI 55% (2 ml). Ultrasonication bath.
3. Heat in oil bath at 60ºC for 48 h.
4. Centrifugation at 4200 rpm for 20 min.
5. Washing of sediment with $NaHCO_3$.
6. Washing of sediment with acetone.
7. Drying of sediment.

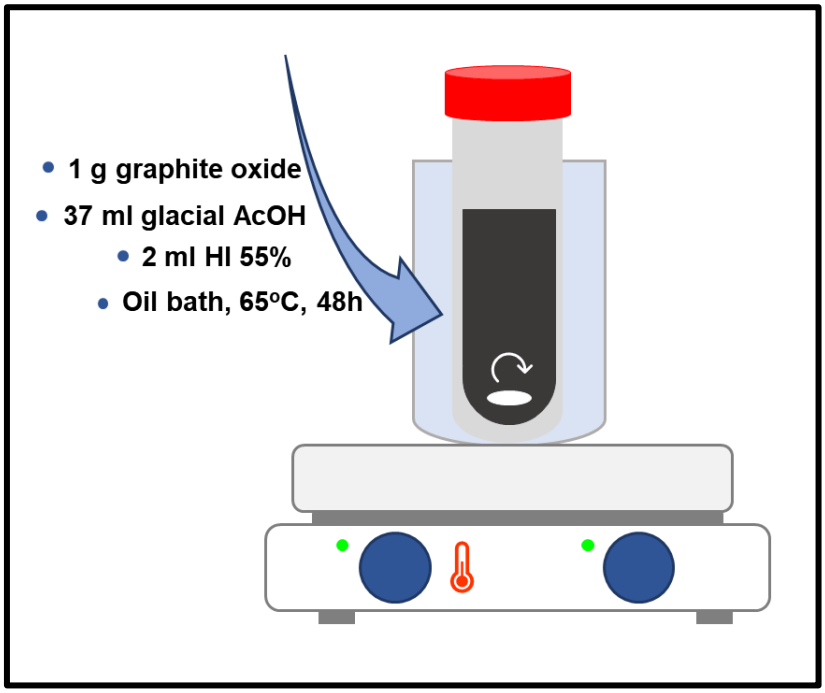


Figure 49 Reagents required for the reduction of graphite oxide (108).

Firstly, graphite oxide (1g) is added to a centrifugation tube followed by glacial AcOH (37 ml). The solution is placed in an ultrasonication bath at room temperature for 10 min to achieve uniformity. HI 55% (2 ml) is then added followed by another 5 min of ultrasonication. The centrifugation vial is then placed in a silicone bath at 60ºC, and the solution is left stirring for 48h. When 48h have passed, the solution is centrifugated at 4200 rpm for 20 min. The supernatant, which contains the majority of excess HI, is disposed of. The

sediment is then washed 5 times with a saturated sodium hydrogen carbonate ($NaHCO_3$) solution to neutralise the excess HI. The reactions that take place are:

$$\mathbf{HI + NaHCO_3 \rightarrow CO_2 + H_2O + NaI}$$

$$\mathbf{HI + NaHCO_3 \rightarrow H_2CO_3 + NaI}$$

$$\mathbf{NaI \rightarrow Na^+ + I^-}$$

The sediment is then washed with acetone until the yellow colour of the supernatant has completely disappeared, showing that there are no traces of excess HI. The sediment is then placed in an oven at 60oC to dry overnight.

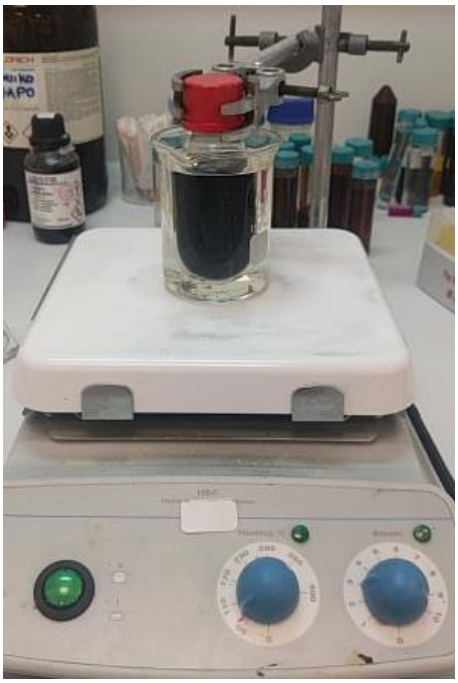


Figure 50 Graphite oxide reduction reaction left in a silicone bath at 60°C for 48h.

The chemically prepared graphite oxide and reduced graphite oxide were characterised via FT-IR and Raman spectroscopy to ensure the successful oxidation of graphite and the subsequent reduction of graphite oxide.

4.3 Preparation of Silver Decorated Graphene Oxide

For the preparation of silver decorated Graphene Oxide, 6 different synthesis methods were followed in order to end up with the most efficient, low cost and suitable one.

4.3.1 Silver decoration of GO via Method 1

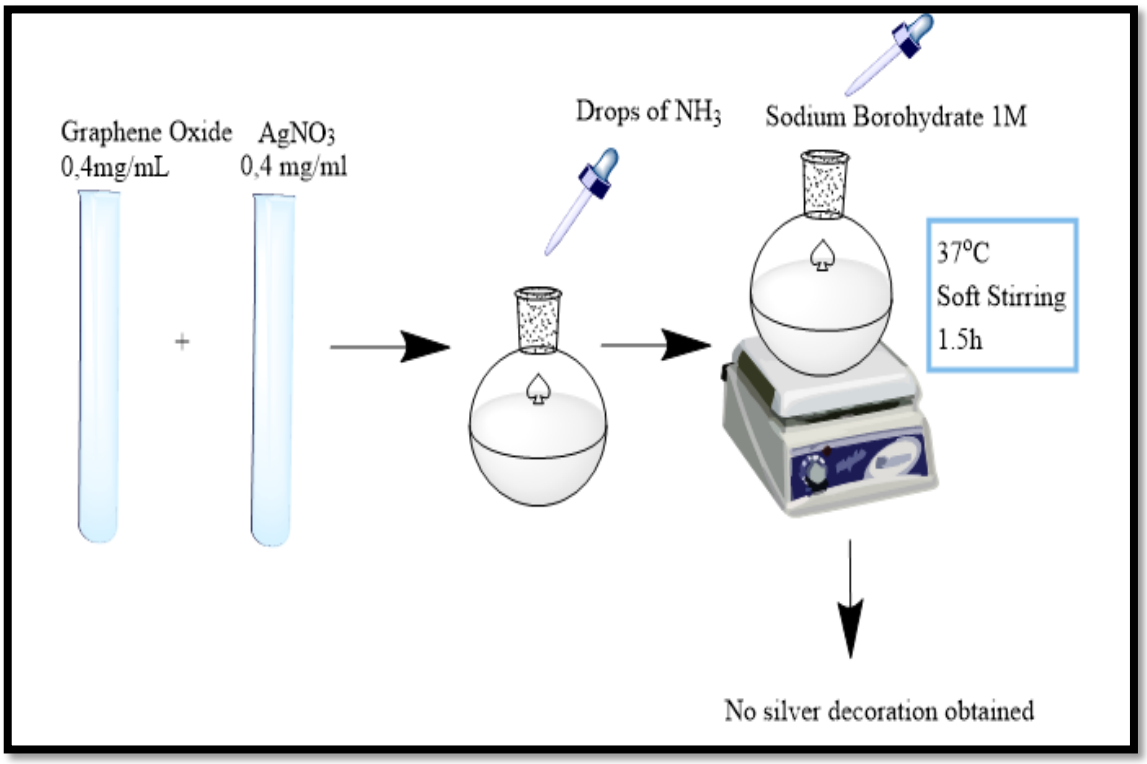


Figure 51 Silver Decoration method 1. All illustrations were designed in ChemDraw 2015.

Synthesis Protocol:

1. Add in a vial 40 ml of GO dispersion in ultrapure H_2O (0.4 mg/ml) which was prepared via ultrasonic probe (see dispersion chapter).

2. Add 40ml Silver Nitrate ($AgNO_3$) in ultrapure water (0.4 mg/ml).
3. Add drops of ammonia solution
4. Let it be mild stirred for 1.5h at 37ºC
5. Centrifugation at 9000 rpm/30min

4.3.2 Silver decoration of GO via Method 2

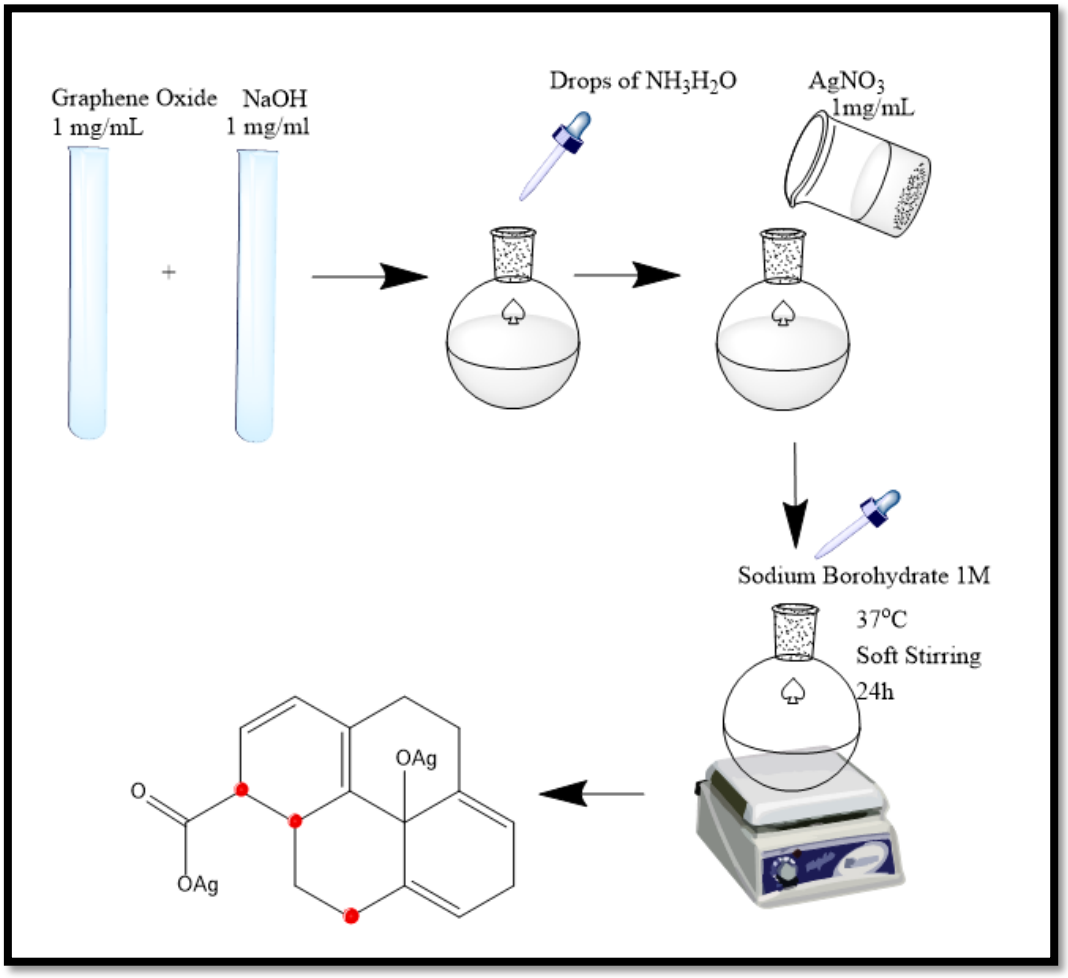


Figure 52 Silver Decoration method 2. All illustrations were designed in ChemDraw 2015.

Synthesis Protocol

1. Add in a vial 40 ml of GO dispersion in ultrapure H_2O (1 mg/ml) which was prepared via ultrasonic probe (see dispersion chapter).
2. Add in a vial 40 ml of NaOH dispersed in ultrapure H_2O (1 mg/ml) which was prepared via ultrasonication probe.
3. Add 40ml Silver Nitrate ($AgNO_3$) in ultrapure water (1 mg/ml).
4. Add drops of ammonia solution
5. Let it be mild stirred for 24h at 37^oC
6. Centrifugation at 9000 rpm/30min

4.3.3 Silver decoration of GO via Method 3

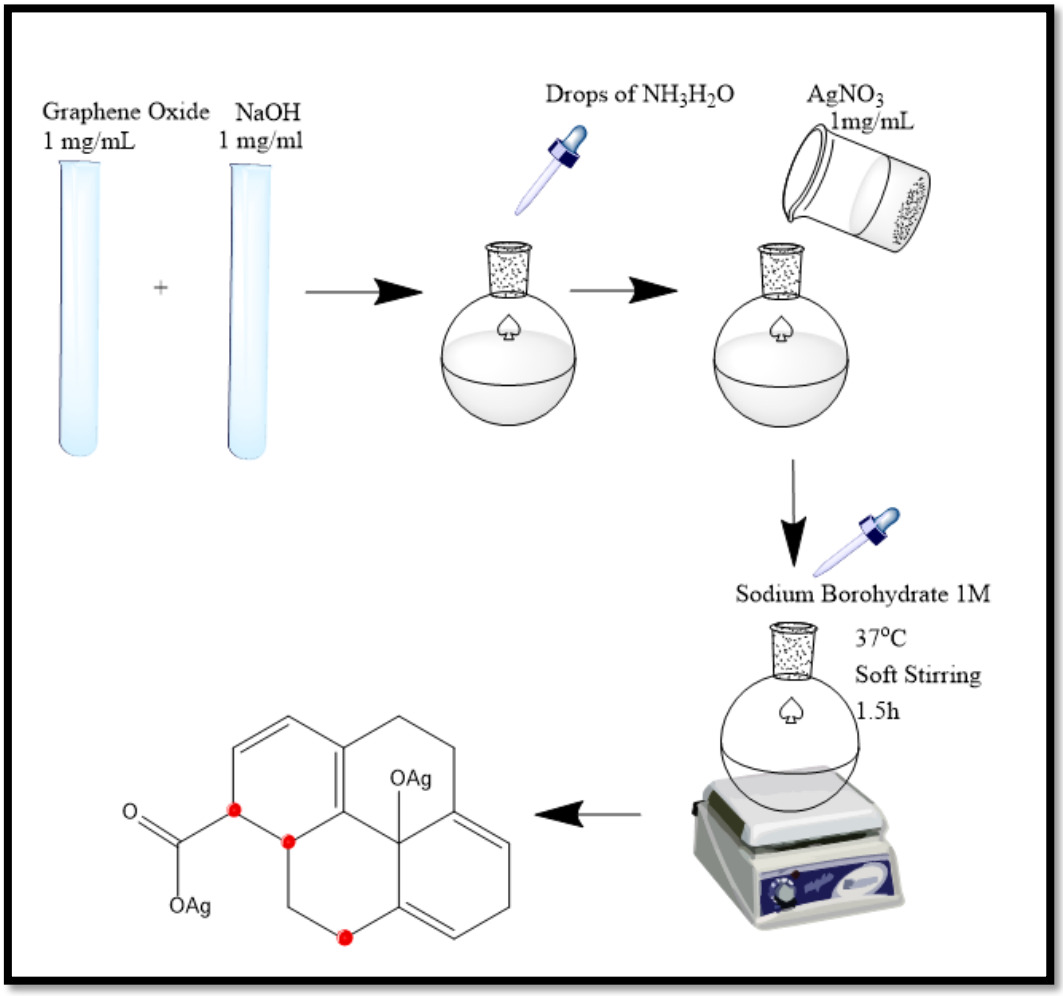


Figure 53 Silver Decoration method 3. All illustrations were designed in ChemDraw 2015.

Synthesis Protocol

1. Add in a vial 40 ml of GO dispersion in ultrapure H_2O (1 mg/ml) which was prepared via ultrasonic probe (see dispersion chapter).
2. Add in a vial 40 ml of NaOH dispersed in ultrapure H_2O (1 mg/ml) which was prepared via ultrasonication probe.
3. Add 40ml Silver Nitrate ($AgNO_3$) in ultrapure water (1 mg/ml).
4. Add drops of ammonia solution
5. Let it be mild stirred for 1.5h at 37°C
6. Centrifugation at 9000 rpm/30min

4.3.4 Silver decoration of GO via Method 4

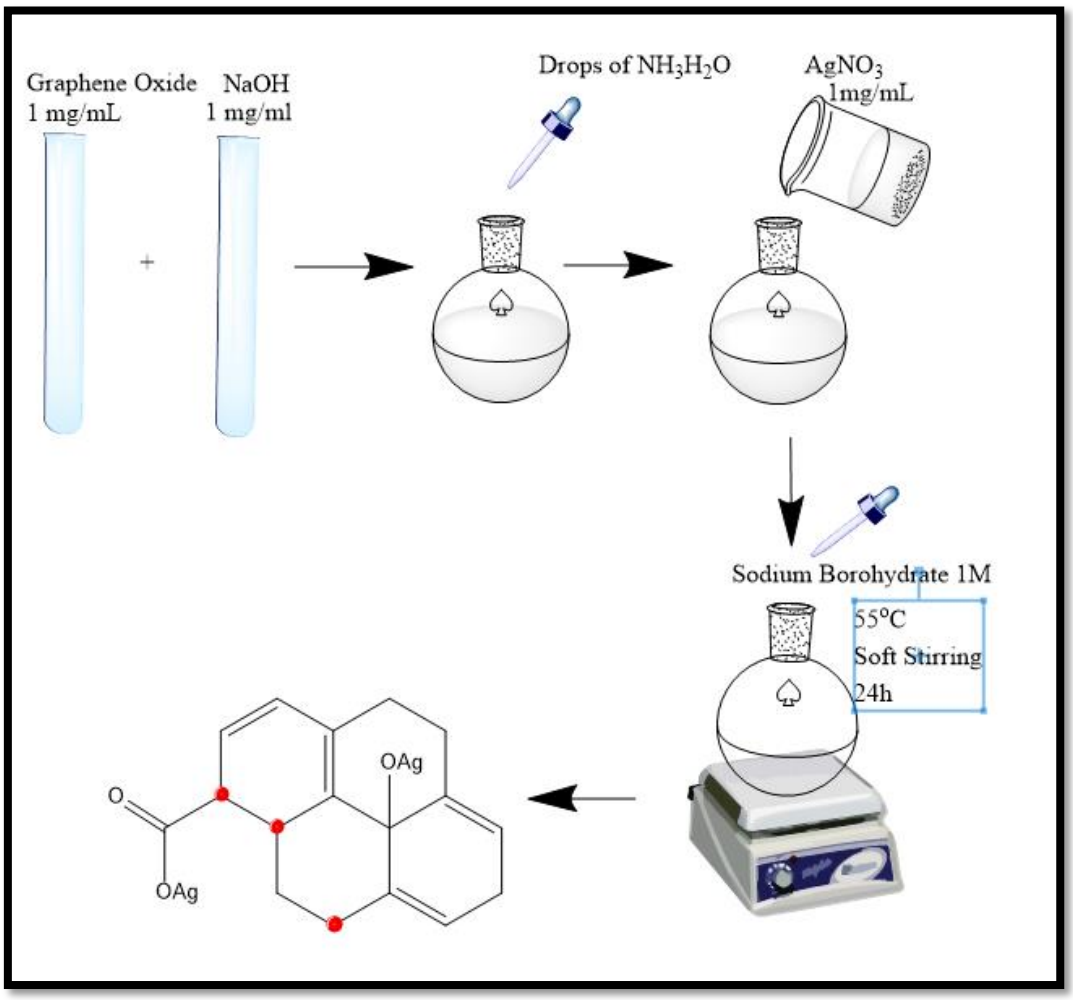


Figure 54 Silver Decoration method 4. All illustrations were designed in ChemDraw 2015.

Synthesis Protocol

1. Add in a vial 40 ml of GO dispersion in ultrapure H_2O (1 mg/ml) which was prepared via ultrasonic probe (see dispersion chapter).
2. Add in a vial 40 ml of NaOH dispersed in ultrapure H_2O (1 mg/ml) which was prepared via ultrasonication probe.
3. Add 40ml Silver Nitrate ($AgNO_3$) in ultrapure water (1 mg/ml).

4. Add drops of ammonia solution
5. Let it be mild stirred for 24h at 55ºC
6. Centrifugation at 9000 rpm/30min

4.3.5 Silver decoration of GO via Method 5

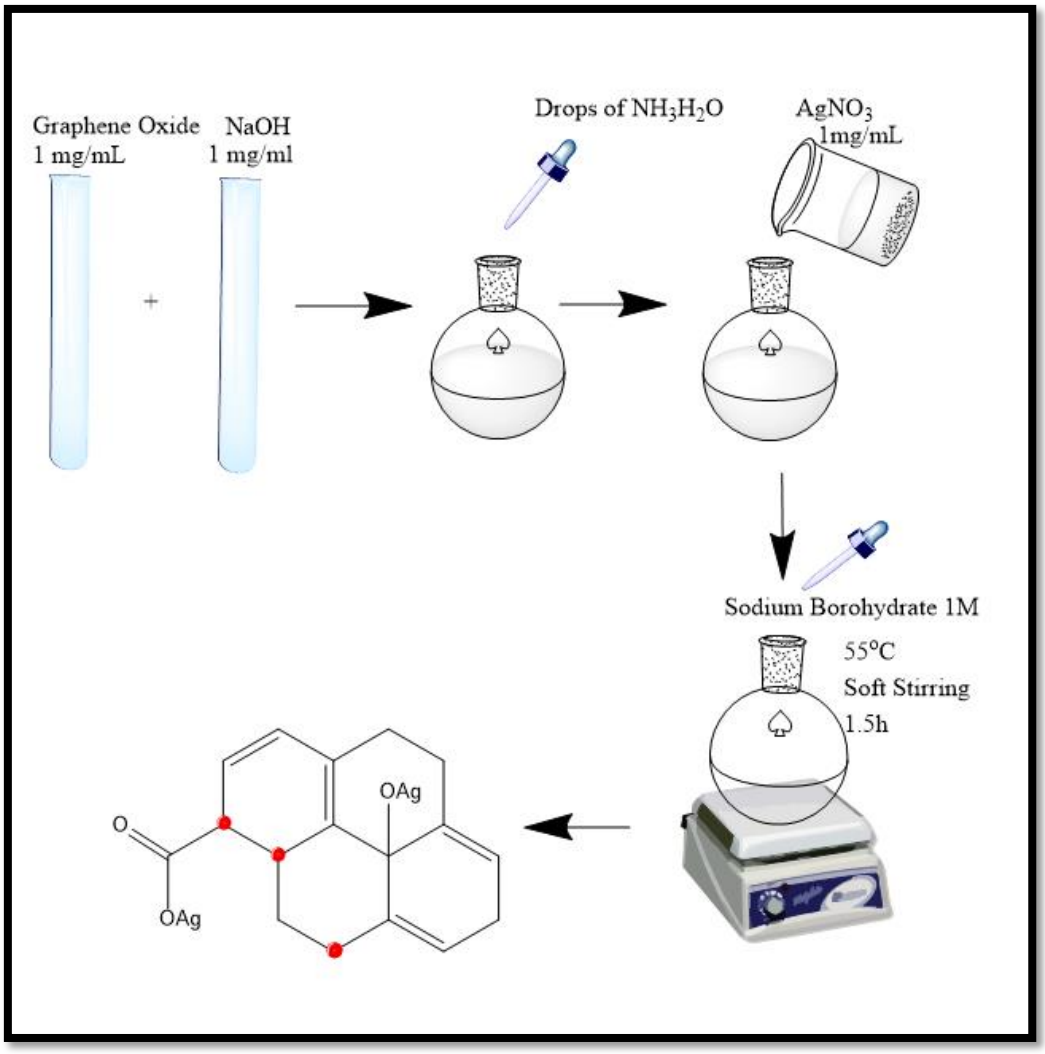


Figure 55 Silver Decoration method 5. All illustrations were designed in ChemDraw 2015.

Synthesis Protocol

1. Add in a vial 40 ml of GO dispersion in ultrapure H_2O (1 mg/ml) which was prepared via ultrasonic probe (see dispersion chapter).
2. Add in a vial 40 ml of NaOH dispersed in ultrapure H_2O (1 mg/ml) which was prepared via ultrasonication probe.
3. Add 40ml Silver Nitrate ($AgNO_3$) in ultrapure water (1 mg/ml).
4. Add drops of ammonia solution
5. Let it be mild stirred for 1.5h at 55^oC
6. Centrifugation at 9000 rpm/30min

4.3.6 Silver decoration of rGO via Method 6

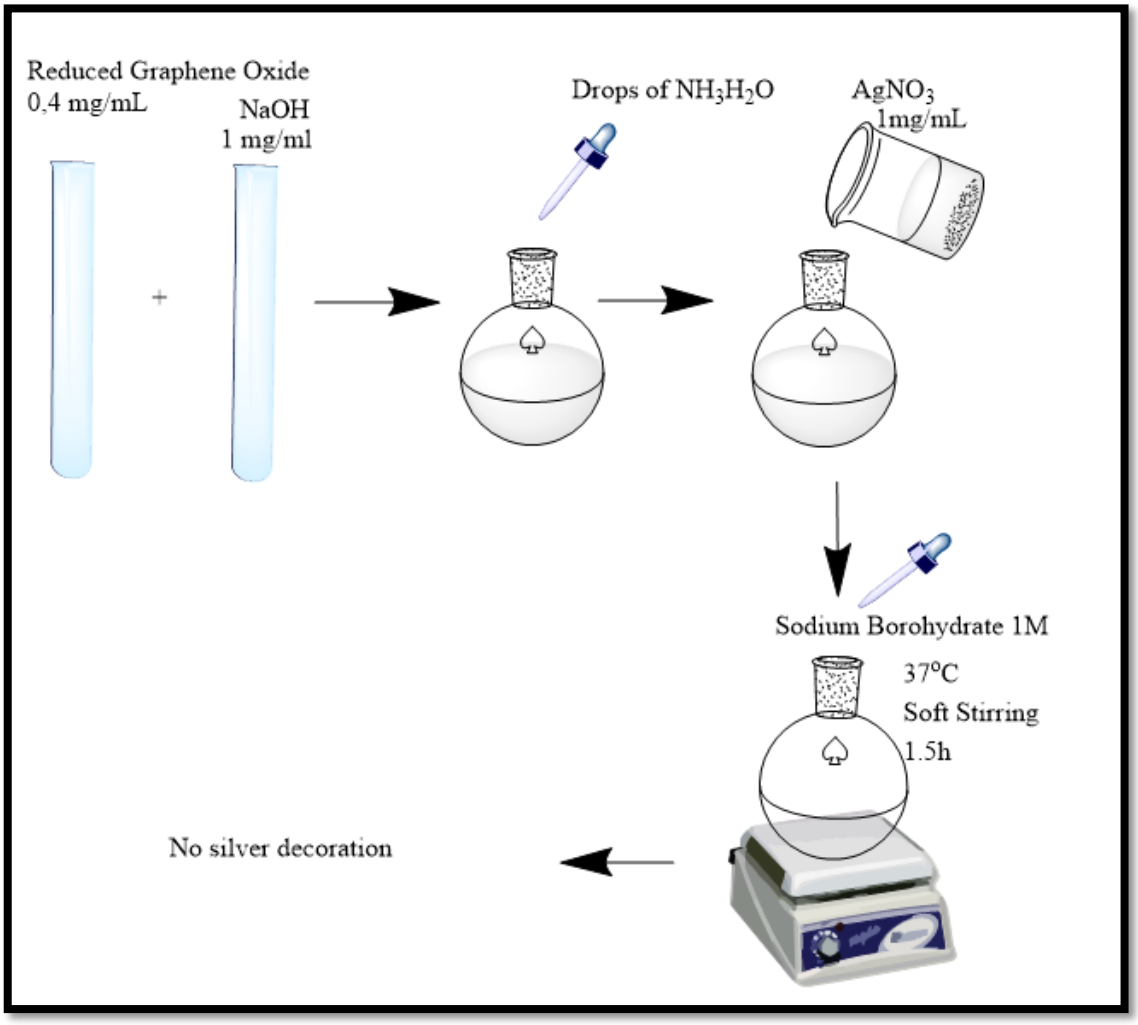


Figure 56 Silver Decoration method 6. All illustrations were designed in ChemDraw 2015.

Synthesis Protocol

1. Add in a vial 40 ml of rGO dispersion in ultrapure H_2O (0.4 mg/ml) which was prepared via ultrasonic probe (see dispersion chapter).
2. Add in a vial 40 ml of NaOH dispersed in ultrapure H_2O (0.4 mg/ml) which was prepared via ultrasonication probe.
3. Add 40ml Silver Nitrate ($AgNO_3$) in ultrapure water (1 mg/ml).
4. Add drops of ammonia solution
5. Let it be mild stirred for 1.5h at 37°C
6. Centrifugation at 9000 rpm/30min

4.3.7 Silver decoration of rGO via Method 7

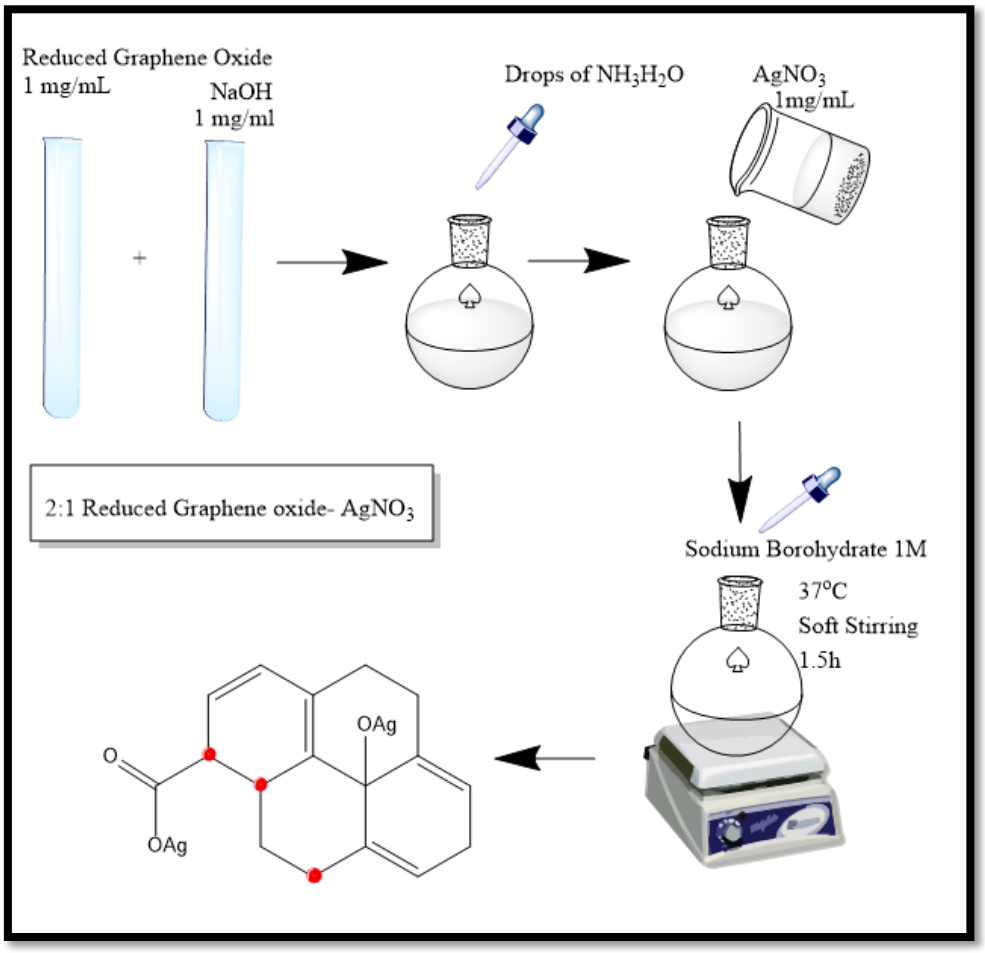


Figure 57 Silver Decoration method 7. All illustrations were designed in ChemDraw 2015

Synthesis Protocol

1. Add in a vial 40 ml of rGO dispersion in ultrapure H_2O (1 mg/ml) which was prepared via ultrasonic probe (see dispersion chapter).
2. Add in a vial 40 ml of NaOH dispersed in ultrapure H_2O (1 mg/ml) which was prepared via ultrasonication probe.
3. Add 40ml Silver Nitrate ($AgNO_3$) in ultrapure water (1 mg/ml).

4. Add drops of ammonia solution
5. Let it be mild stirred for 1.5h at 37^{o}C
6. Centrifugation at 9000 rpm/30min

4.3.8 Final Experimental Procedure for Silver Decoration

Silver decorated graphene oxide was prepared from graphite oxide synthesized previously via modified Hummer's method, using chemical reducing agents, namely sodium borohydride, a strong reductant and sodium Hydroxide (NaOH) and ammonia solution (NH_4OH). The decoration process can be described briefly by the following steps:

1. 100mg GO in H_2O (1mg/ml) in a vial. Sonication bath.
2. 100mg NaOH in H_2O (1mg/ml) in a vial. Sonication bath.
3. Addition of NaOH (100ml) to GO (100ml) in a flask.
4. Addition of 100mg $AgNO_3$ in the flask.
5. Addition of ammonia solution 25% (drops until transparent).
6. Addition of fresh-cool $NaBH_4$ 20mg (1M)
7. Heat in oil bath at 37^{o}C for 1.5 h.
8. Centrifugation at 9000rpm for 40 min.
9. Washing of sediment with ultrapure water (x3).
10. Drying of sediment.

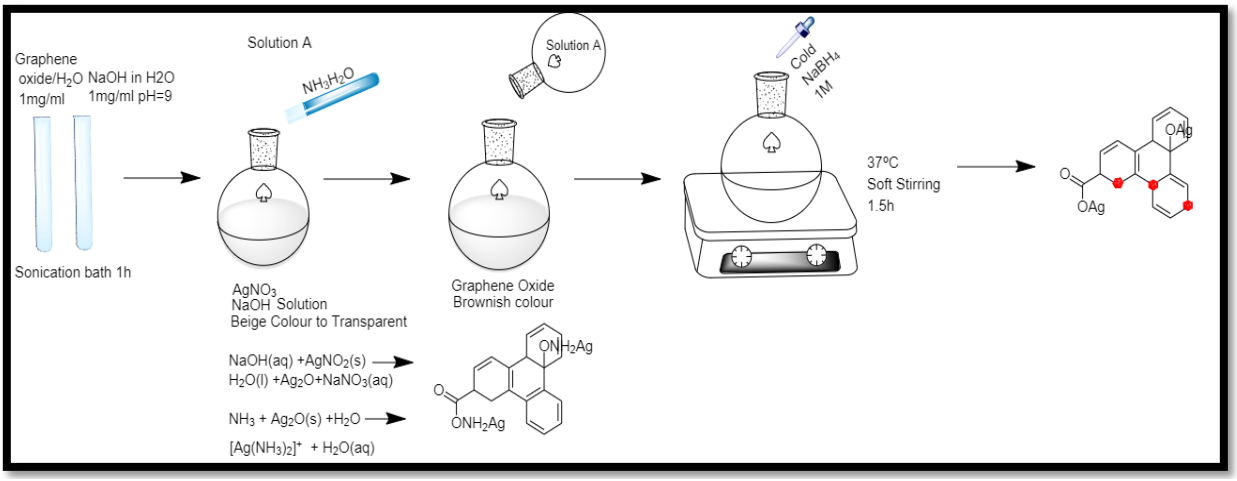


Figure 58 Schematic illustration of the silver decoration of GO.

Firstly, 100mg GO 1mg/ml and 100mg NaOH 1mg/ml are added to two separate vials followed by sonication bath for 1h. NaOH solution was then added to the GO solution, placed in a flask in an oil bath. Then 100mg of $AgNO_3$ are added to the flask together with drops of ammonia solution 25% and left to be stirred. In the meanwhile, 20mg of sodium borohydride 1M left in an ice bath to cool for 10minutes and added to the solution to form the final reaction. The flask is then placed in a silicone bath at 37°C, and the solution is left stirring for 1.5h. When 1.5h have passed, the solution is centrifugated at 9000 rpm for 40 min. The supernatant, which contains the majority of excess $AgNO_3$, is disposed of. The sediment is then washed 3 times with ultrapure water to remove all the by-products. The sediment is then placed in an oven at 60°C to dry overnight.

The reactions that take place are:

$NaOH\ (aq) + AgNO_2\ (s) \rightarrow H_2O\ (l) + Ag_2O\ (s) + 2NaNO_3\ (aq)$

$NH_3\ (aq) + Ag_2O\ (s) + H_2O \rightarrow [Ag(NH_3)_2]^+ + H_2O\ (aq)$

$Graphene\ Oxide + [Ag(NH_3)_2]^+ \rightarrow Ag@Graphene\ Oxide + H_2O\ (aq)$



Figure 59 Silver decoration of Graphene oxide.



Figure 60 GO-Ag powder

4.4 Preparation of Bucky Papers

For the characterization of the synthesized materials, GO, rGO and GO-Ag bucky papers were prepared using vacuum filtration. Vacuum filtration is a technique used to separate the components of a solution to obtain the solid material. The steps followed to obtain the final solid material are described below:

1. GO-Ag redispersed in ultra-pure water for 1.5h.
2. Set-up of the vacuum filtration equipment.
3. Set the suitable membrane for each sample (47mm hydrophilic).
4. Deposit the dispersion slowly under vacuum.
5. Let it dry in open air for 10min under vacuum.
6. Let it dry in the oven at 60 ^{o}C for 20min.

After drying, the obtained bucky papers were chopped into smaller circles using hole punch as shown in Figure 65.

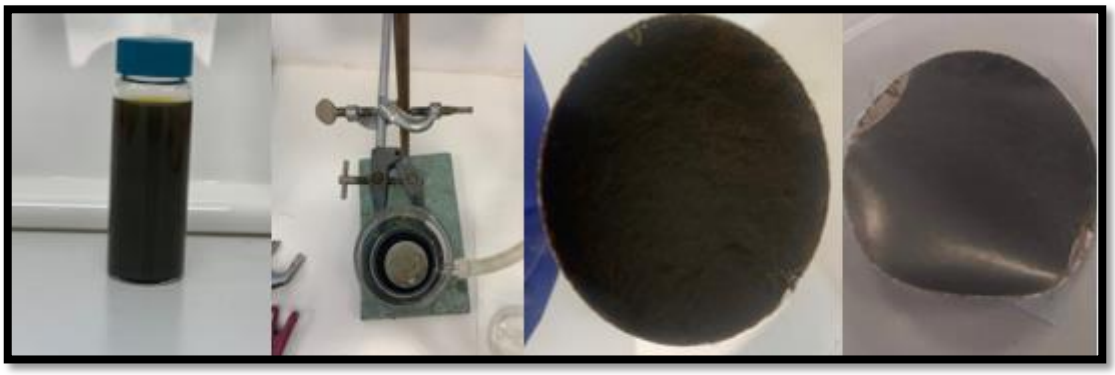


Figure 61 Bucky paper synthesis using vacuum filtration beginning from GO-Ag dispersion on the left, followed by vacuum filtration set-up, ending to bucky papers wet and dry on the right.

.



Figure 62 GO/H_2O bucky paper 1mg/ml-light brown

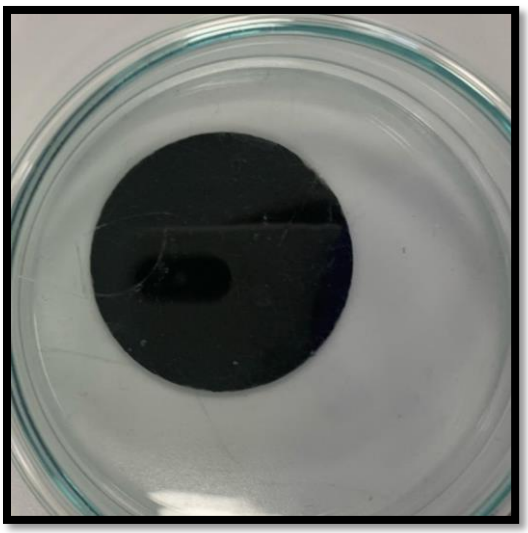


Figure 63 rGO/H_2O bucky paper 1mg/ml-black

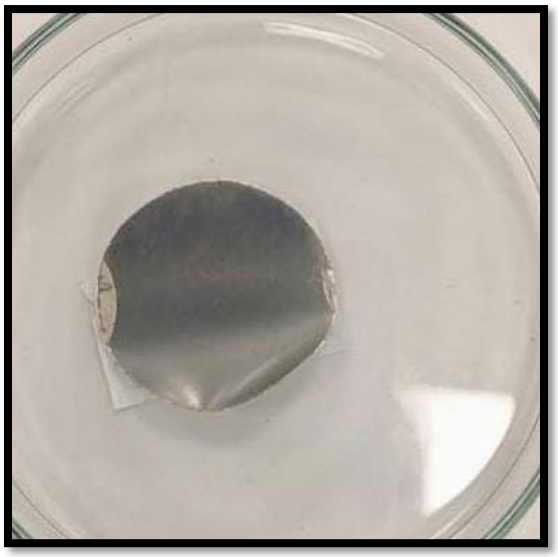


Figure 64 GO-Ag/H2O bucky paper 1mg/ml-silver



Figure 65 Hole punch and bucky papers chopped into smaller circles

4.5 Dispersions



Figure 66 Sonication Probe

For the experiments GO dispersions in de-ionized water were prepared with a concentration of 1mg/ml. GO and rGO dispersions were prepared from graphite oxide and reduced graphite oxide. This was achieved with ultrasonic exfoliation using a Hielscher UP200Ht ultrasonic probe. Each sample was prepared by firstly weighing graphite oxide and placing it in a 40 ml glass vial. The sample is ultrasonicated for 1.5 h at 26 KHz. The ultrasonication set-up has an adjustable shelf which allows for control over how deeply into the mixture the probe is immersed. The procedure described in steps can be found below.

1. 38ml of ultra-pure water were mixed with 38 mg of GO in a 40 ml vial.
2. The vial is placed in Styrofoam holders to keep it in place during the ultrasonication process and avoid tipping or spinning.
3. The vial-Styrofoam set-up is then placed in an ice bath to avoid over heating during ultrasonication.

4. Removed the vial lid and place the Styrofoam holders accordingly so that the vial doesn't tip or spin.
5. The vial lid is removed, and the set-up is placed on the shelf which is lifted to a suitable height self so that the probe is submerged in the dispersion.
6. The tip of the probe should be about 0.5 cm from the bottom of the vial. Probe should not be in contact with the bottom of the vial. Ultrasonic frequencies will break the glass.
7. A piece of paper should be placed under the beaker to avoid the slip of the shelf.
8. Ultra-sonication for 1h and 30 minutes by changing the ice-bath every 15 minutes to avoid over-heating.

By using the ultra-sonication probe, we exfoliate graphite oxide, and graphene oxide was produced by dissolving it in water solution.

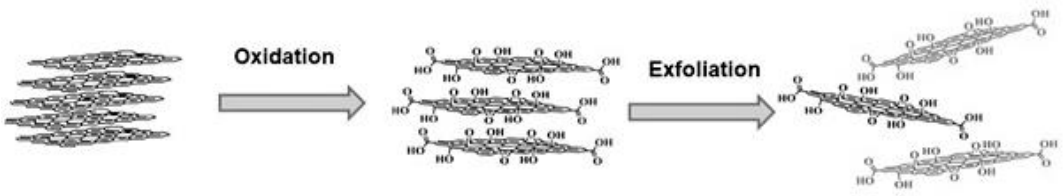


Figure 67 Exfoliation of Graphite oxide to produce graphene oxide

When sonication ends, Centrifuge with Allegra X-22 BECKMAN COULTER 9000 rpm for 20 minutes was used. When centrifugation ends, supernatant is keeped and stored it in a clean 40 ml vial.

It was observed that the relation between dispersability and the ultra-sonication time for GO dispersions is represented by a Gaussian plot line, with an optimum ultra-sonication time of 1.5h. Dispersability shown to drop after 1.5h of sonication.

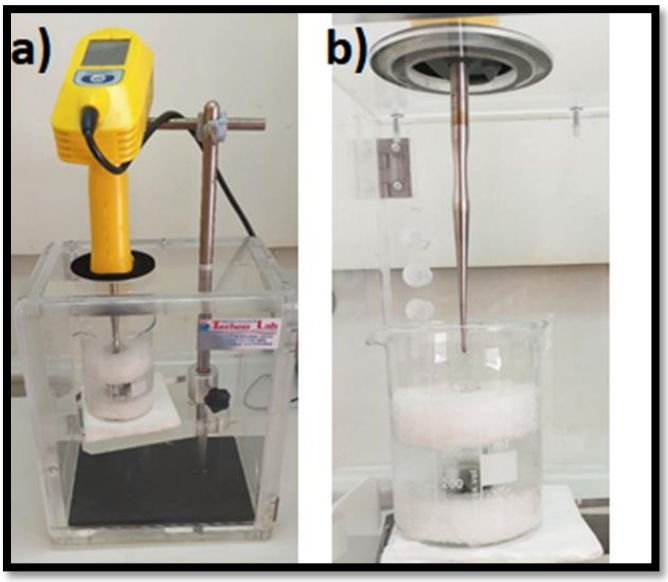


Figure 68a) Mechanical exfoliation of graphite oxide in ultra pure water via ultrasonication to create GO dispersion. b) Ultrasonic probe before it is inserted into the aqueous mixture of graphite oxide.

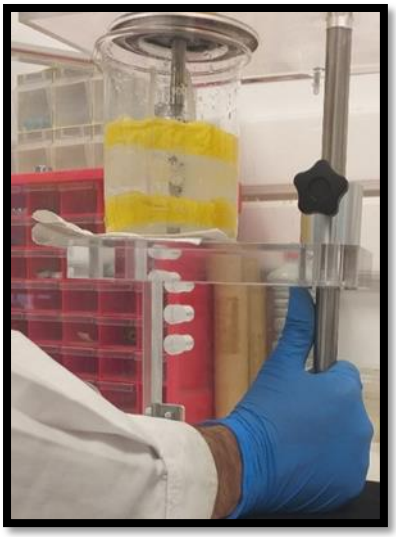


Figure 69The ice bath sis on a shelf whose height can be adjusted to control how deep the ultrasonic probe is immersed.

4.6 Thin film preparation

Besides bucky papers, think films were also produced to use them in various characterizations, namely sheet resistance, absorbance, contact angle. The substrate used was borosilicate glass and the deposition methods were spray coating and drop casting of GO, rGO and GO-Ag dispersions. Before deposition, substrates were cleaned using base piranha solution, the protocol of its synthesis is described below.

Borosilicate glasses should be thoroughly cleaned before applying the product. We use a four-step cleaning method:

- First step: The substrates are first inserted into a holder with the glass-coated side facing in the same direction. The holder is then submerged into soap water (deionized water to be exact) inside a 1000ml beaker. The beaker is then put into an ultrasonic bath at room temperature for 10 minutes. The substrates are then thoroughly rinsed with deionized water as to remove all traces of soap.

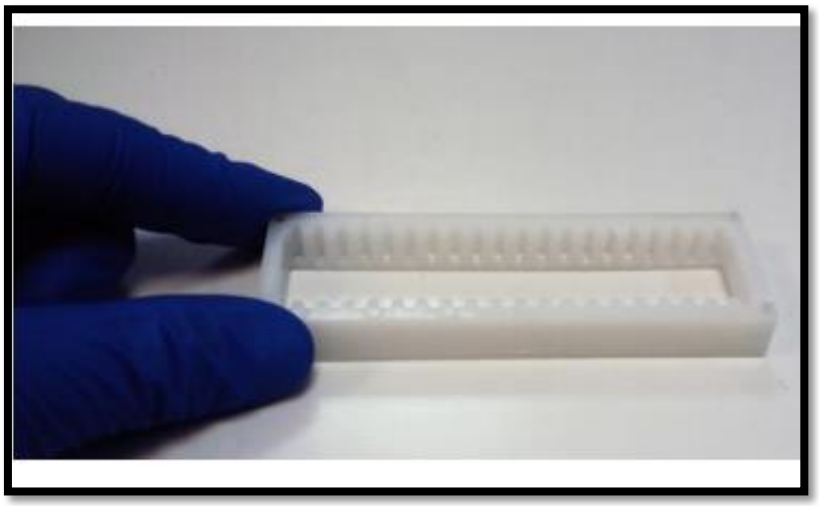


Figure 70 Glass holder



Figure 71 Soap Cleaning process

- Second step: The holder is submerged in acetone in a different 1000ml beaker. The beaker is again put in an ultrasonic bath at room temperature for 10 minutes

- Third step: The holder is taken out of the acetone and submerged in isopropanol (2-propanol, IPA) in a 1000ml beaker which is then put in a last ultrasonic bath again at room temperature for 10 minutes. The substrates are then transferred from the holder to a Petri dish with the glass side facing up.

- Fourth step: The Petri dish is placed in an oven at 120^{o}C for 15 minutes for the substrates to dry.



Figure 72 Ultrasonic bath



Figure 73 Dry in the oven

.

4.7 Alkaline Piranha Solution Preparation for glass substrates cleaning

Base piranha solution is 3:1 mixture of ammonia solution 25% with hydrogen peroxide. The solution should be heated to 60^{O}C before reaction takes off.

1. Put on a full-face mask, goggles, and apron
2. Fill two large rinsing beakers with DI water
3. Place magnetic stirrer in bottom of third beaker
4. Place beaker on hot plate/stirrer
5. 3:1 Ammonia solution 25%: DI water
6. Pour ammonia solution into beaker, enough to cover the top of wafer/samples in Teflon dipper completely when immersed (Do not put wafer/samples in yet)
7. For 125mm crystallization dish use 75ml ammonia solution
8. Heat solution to 60^{O}C
9. Measure hydrogen peroxide with graduated cylinder so that its 1/5 the volume of ammonia (15ml)
10. Very slowly add hydrogen peroxide to ammonia

11. Solution is bubbling

12. Allow the solution to cool down and turn on stirrer

13. Heat at 100-110 ^{O}C-Vigorous bubbling is observed

14. Keep solution to this temperature until cleaning process ends

15. Immerse samples in piranha solution for 10 minutes.

16. Immerse samples in the second beaker with DI water for 5 minutes

17. Dry samples with nitrogen gas.

18. Store piranha for future use and refresh it using hydrogen peroxide in next use.

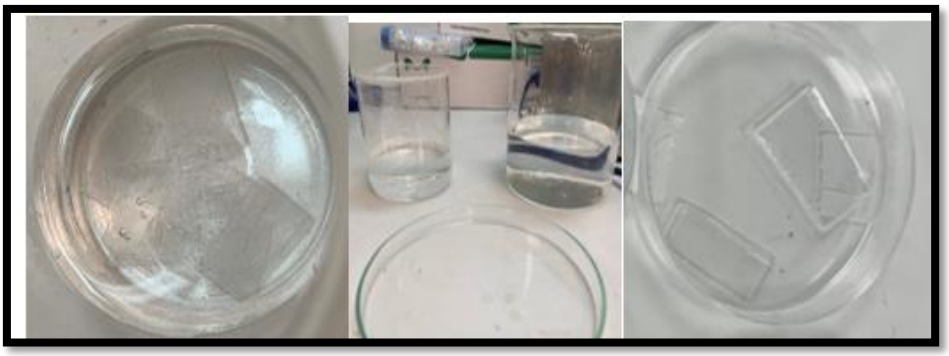


Figure 74 Piranha solution preparation

4.8 Thin film Preparation of the Materials using Spray Gun

For the thin film preparation, spray gun deposition was used. The materials used, GO, rGO and GO-Ag, were dispersed in ultra-pure water (dispersions' preparation is described in Chapter 4), centrifugated at 9000rpm for 30 min and the supernatant was sprayed on glass substrate. Substrate was firstly pretreated using basic piranha solution, which makes the surface hydrophilic, thus aiding deposition of the aqueous dispersions and sets a standard film thickness.

Solid thin films were prepared by spray coating GO (H_2O), GO-Ag (H_2O), rGO (H_2O) with a standard concentration of 1mg/ml for each sample. Substrates were placed on a hotplate at 65^{O}C to enhance the evaporation of liquid solution.

Thin films were prepared by using a commercial airbrush (by Graphotech) as shown in Figure 76 Materials' solutions were transferred to the barrel of the air brush, which was connected to an air compressor set at 2mbar. The compressor enables the formation of tiny droplets and atomizes the solution. Each dispersion was sprayed onto a preprepared glass substrate. The pressurized solution is sprayed through spay gun's nozzle of 0.3mm diameter to produce aerosol deposition on glass substrate.

When this aerosol is deposited on the substrate, on the heat from the hot plate evaporates the solvent, and the material remains on the substrate as a thin solid film (GO, rGO, GO-Ag). The distance between the substrate and the spray gun is set to ~20cm and the repetition rate was 1 spray cycle per 40seconds.

This was repeated until a total of 9ml of each sample was deposited onto a substrate. The deposited thin films were heated at 65^{O}C for 1 h in ambient air to get pure GO, rGO and GO-Ag thin films.

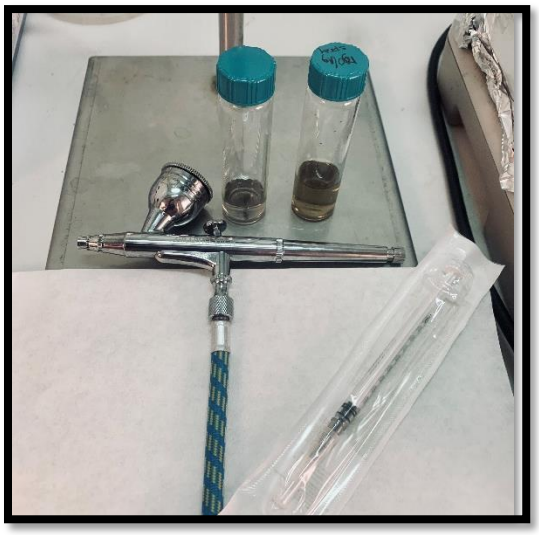


Figure 75 Commercial airbrush and rGO, GO-Ag materials' dispersions

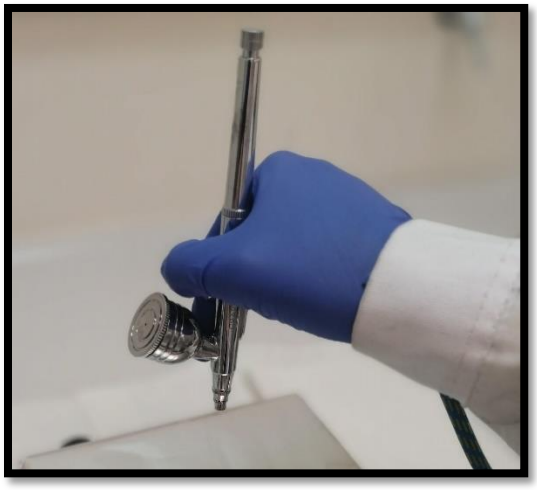


Figure 76 Commercial airbrush used for the preparation of solid thin films



Figure 77 Sprayed samples on glass substrates. 9ml of each material (GO, rGO and GO-Ag) was sprayed on each substrate.

Thin films were used for the further characterizations of the materials, namely XRD, Raman, FT-IR, Contact Angle, Absorbance, Sheet Resistance, which will be discussed in the next Chapter.

Drop casting



Figure 78 Drop Casting of 1mg/ml GO-Ag

Drops of prepared materials' solution is dropped in the clean substrate and wait until the solvent evaporates. Film thickness depends on the volume of dispersion used and the particle concentration. Materials used for the drop casting, were GO, rGO and GO-Ag with concentration 1mg/ml each.

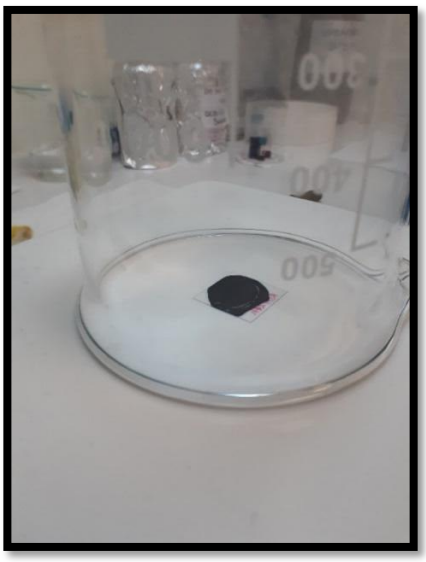


Figure 79 Let dry of the drop casting

.

4.9 Antimicrobial Protocol

For the antimicrobial evaluation of GO, rGO and GO-Ag, a three-day experiment should be carried out in order to prepare the microbial cultures, the surfaces of prepared materials and the characterization results. For the purpose of this master thesis, Escherichia coli strain 25922 and Pseudomonas Aeruginosa strain 27853 were used to test the antimicrobial activity of my materials. To determine whether the materials are antimicrobial or not, qualification and quantification experiments were carried out. The whole procedure is described in steps below.

Qualification

Day 1:

- Using a sterile inoculating loop, bacteria were transferred from the stock culture to the slant culture medium. 5 ml of cultures Escherichia Coli and Pseudomonas Aeruginosa were inoculated in Luria Bertani (LB) broth for 12-16h.

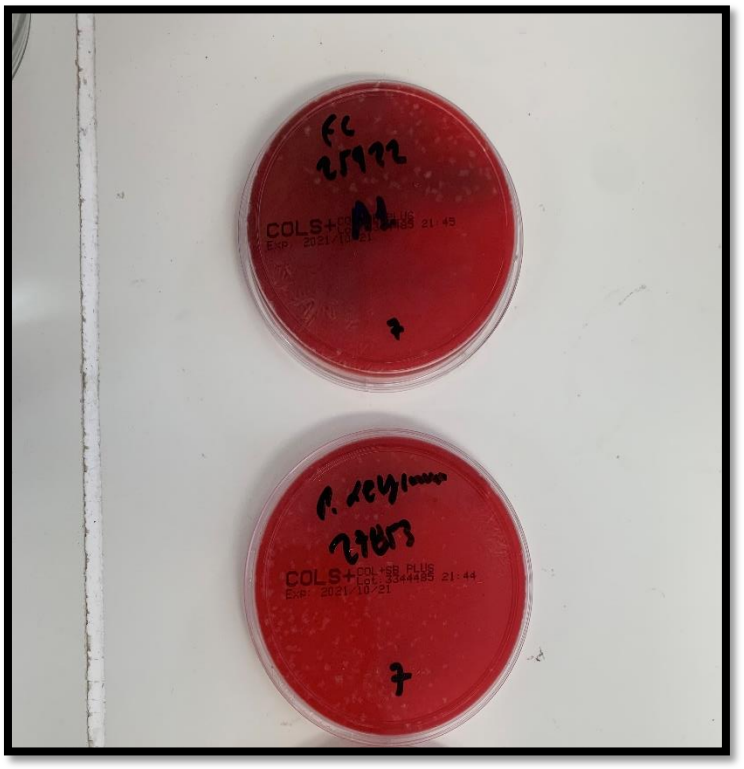


Figure 80 Stock Cultures of E. Coli and P. Aeruginosa

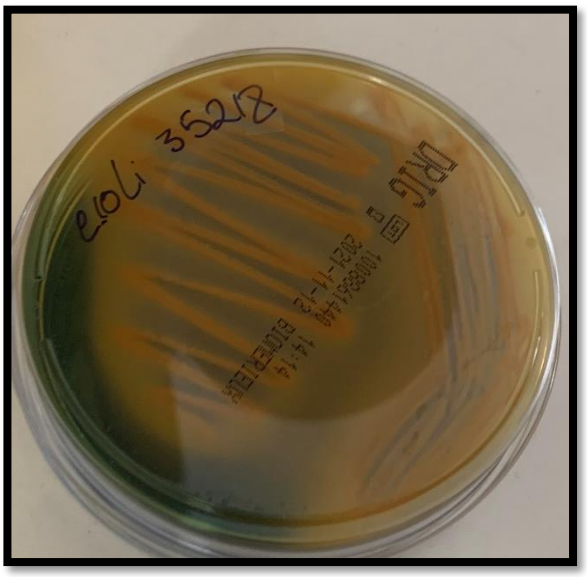


Figure 81 Pre-culture of bacteria using a sterile inoculating loop to transfer bacteria from the stock culture to the slant culture medium.

Day 2:

- Cultures were diluted from 2,5x10^5 cells /ml to 10x10^5 cells /ml (optimum) using 1/500 LB.

- In order to determine how many bacteria cells, exist in the culture, optical density (OD) needed to be measured. OD_{600} was measured in a plastic cuvette, aiming to get an absorbance below 1 in order to obtain a linear correlation between O.D and colony-forming unit (CFU), which are the main parameters in the cell-calculation equation.

Cell-calculation equation:

CFU=Reading X ($8X10^8$) X Dilution.

For O.D.=1 we assume we have 8X108 bacterial cells.

- When best dilution was obtained, the coated surfaces were placed on a 48 well plate and were covered by 400μl of the diluted culture. The materials were then placed in an incubator for 24h at 37ºC.

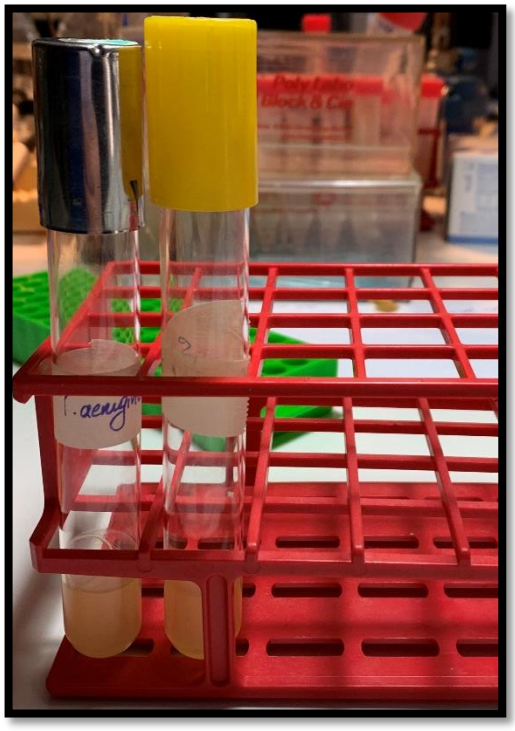


Figure 82 Diluted E. Coli & P. Aeruginosa cultures

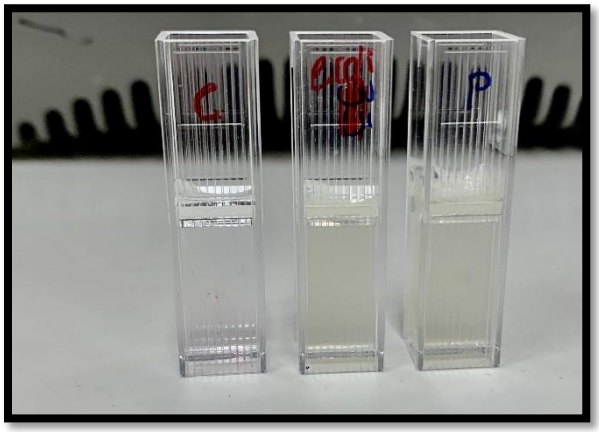


Figure 83 Samples for spectrophotometry OD_{600} in plastic cuvettes, as seen from left to right, control sample LB diluted to 1/500, E. Coli & P. Aeruginosa



Figure 84 BIO-RAID SmartSpec™ Plus Spectrophotometer to measure OD_{600}



Figure 85 Material placement on a 24 well plate and were covered by 400μl of the diluted culture

Day 3:

- After the 24h incubation, supernatant was removed and surfaces of the materials were washed very gently with 1ml of the diluted LB broth in order to remove the untouched cells.

For the Imaging protocol:

For the imaging of the samples, Hoechst 33342 dye was used. Hoechst dyes are cell membrane-permeant, minor groove-binding blue fluorescent DNA stains. Hoechst dyes are widely used in cell cycle and apoptosis studies as nuclear counterstains.

- Hoechst 33342 was diluted to 1:1000 medium and 300μl of the solution was placed in each well. The cultures were stained for 30-40 min.
- Then, solution was removed and washed with the Diluted Broth.
- Surfaces were transferred on slides (with coated surface facing down) using Vector shield and cover slips.
- Control round glass coverslips were used to cover the materials in order to attach Hoechst 33342 to the bacterial DNA.



Figure 86 Surfaces on slides with coated surfaces facing down

For the quantification protocol:

- Enumerate bacteria by performing 10X fold serial dilutions on the 1/500 diluted LB Broth.
- Place 1 ml of 1/500LB supplemented with 0.7% Triton X final concentration on the well and pipette gently up and down. This is Dilution 0.
- Then take 100μl from Dilution 0 and add it in 900μl of 1/500LB broth. This is Dilution 1.
- Then take 100μl of Dilution 1 and place it in 900μl of 1/500 LB broth. From every Dilution take 50μl of the bacterial suspension and spot it in a LB plate.
- You can add up to 8 spots in a plate and you can spot it in duplicates for accuracy. Incubate for 24h and then count the colonies

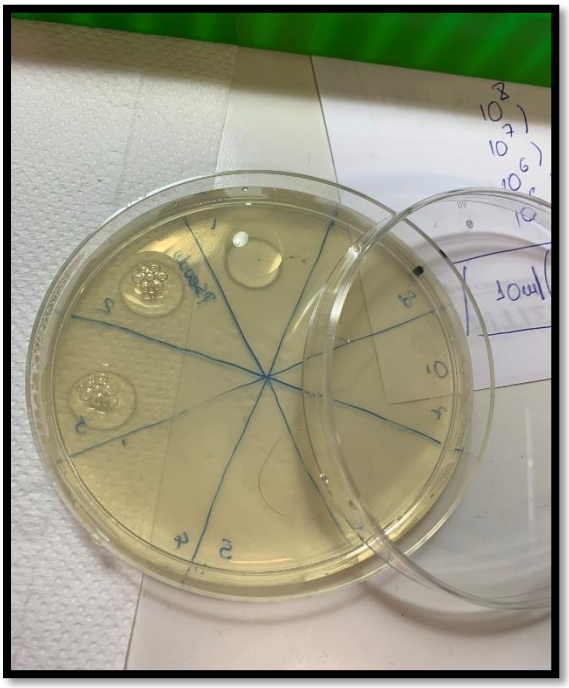


Figure 87 LB plate with bacterial suspension spots

Chapter 5: Characterizations, Results and Discussion

5.1 UV-Vis Absorption Measurements

UV-Vis spectroscopy is an analytical technique that measures the amount of discrete wavelengths of UV or visible light that are absorbed by or transmitted through a sample in comparison to a reference or blank sample. This property is influenced by the sample composition, potentially providing information on what is in the sample and at what concentration. Since this spectroscopy technique relies on the use of light, let's first consider the properties of light. Light has a certain amount of energy which is inversely proportional to its wavelength. Thus, shorter wavelengths of light carry more energy and longer wavelengths carry less energy. A specific amount of energy is needed to promote electrons in a substance to a higher energy state which we can detect as absorption. Electrons in different bonding environments in a substance require a different specific amount of energy to promote the electrons to a higher energy state. This is why the absorption of light occurs for different wavelengths in different substances. Humans are able to see a spectrum of visible light, from approximately 380 nm, which is seen as violet, to 780 nm, which is seen as red. UV light has wavelengths shorter than that of visible light to approximately 100 nm. Therefore, light can be described by its wavelength, which can be useful in UV-Vis spectroscopy to analyze or identify different substances by locating the specific wavelengths corresponding to maximum absorbance.

To accurately determine the decoration of GO with Ag, the maximum absorbance in the UV-Vis spectrum was measured.

According to the Beer-Lambert law, $A = \alpha c l$, the absorption coefficient of GO, rGO and GO-Ag can be determined by preparing a series of dispersions at different given concentrations. To determine the concentration of each dispersion, absorption measurements were carried out in the UV and visible light regions using a Shimadzu UV-2401PC spectrophotometer. The obtained

spectra are featured below. It should be noted that the absorbance is displayed in arbitrary units.

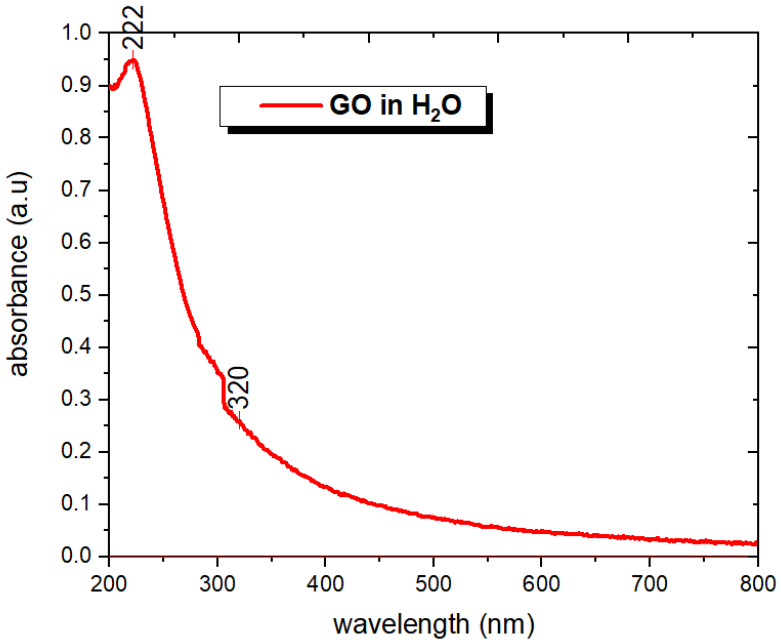


Figure 88 UV-Vis Spectrum of GO/H_2O 1mg/ml

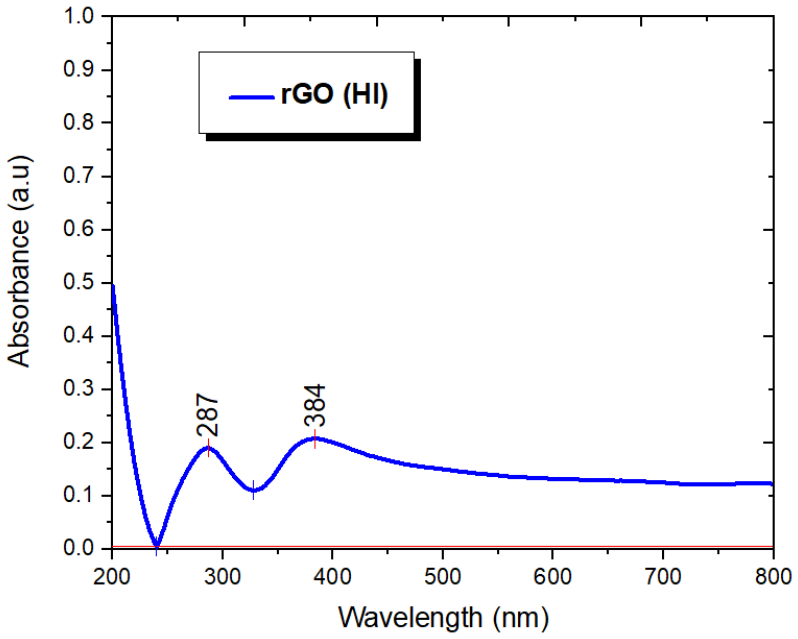


Figure 89 UV-Vis Spectrum of rGO/H_2O 1mg/ml

The two absorption peaks (seen in Figure 88) centered at 222 and 320 nm, are attributed to GO and can be. These peaks seem decay gradually with the reduction of GO and new peaks appeared at 287 and 384 nm attributed to the rGO (Figure 85).

.

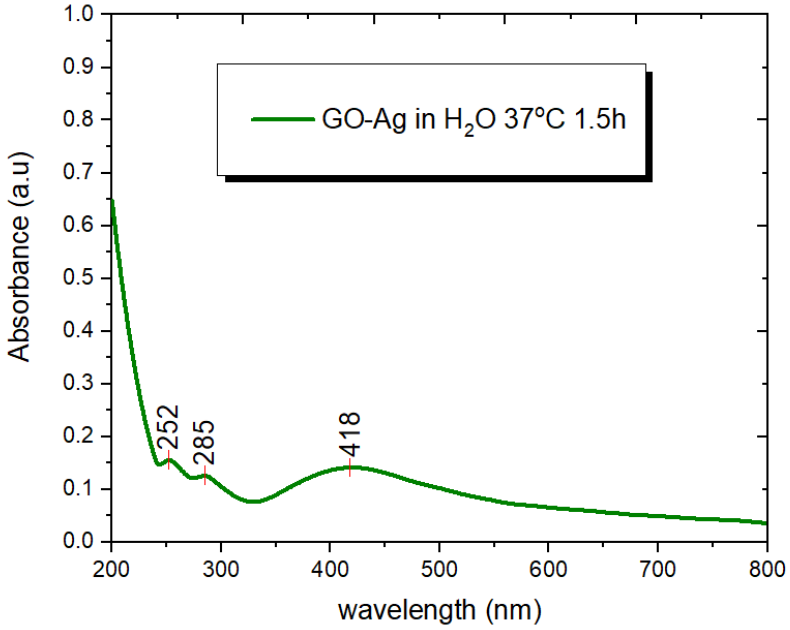


Figure 90 UV-VIs spectrum of GO-Ag 1mg/ml in H_2O

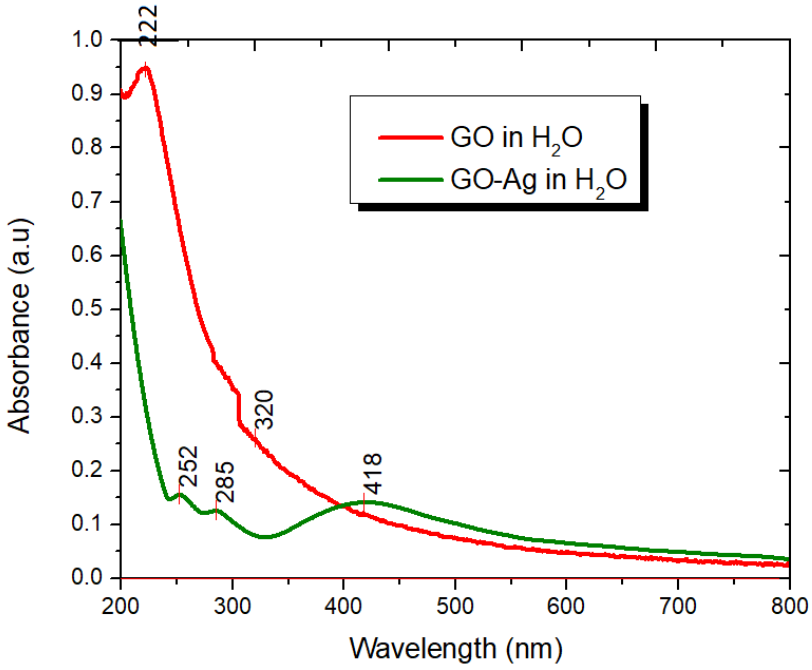


Figure 91 UV-Vis spectra of GO, GO-Ag 1mg/ml in H_2O

In the UV-Vis spectrum of GO-Ag three peaks can be observed, which lead to the identification of the material. Firstly, the peak at 220nm, attributed to the GO has been red shifted to 252nm and has lower intensity, rGO peak also of lower intensity can be seen at 285nm. Due to the co-existence of GO-rGO

peaks, it can be concluded that GO has been reduced to a small rate. Also, the peak at 418nm is attributed to the Ag Nanoparticles, leading to the assumption that GO has been decorated with Ag NPs. In Figure 90, there is the UV-Vis spectrum of GO-Ag and in Figure 91 there is the spectra of both GO and GO-Ag for comparison.

5.2 Sheet-Resistance, Resistivity, Conductivity

In order to choose suitable applications for the prepared material, certain characterizations should be performed. For the material to be used in energy applications, such as electrodes, Sheet Resistance, Resistivity and Conductivity should be calculated.

To calculate Resistivity-Conductivity of a material, the measured sheet resistance is converted to resistance and then resistivity. Resistivity, ρ, is quantitatively equal to the resistance R of a specimen, multiplied by its cross-sectional area A, and divided by its length. The unit of resistance is the ohm (Ω). The area is calculated in square metres, thus the unit of resistivity is ohm-metre. If lengths are measured in centimetres, resistivity may be expressed in units of ohm-centimetre.

$$Rs = Sheet\ Resistance\ \left(\frac{\Omega}{\blacksquare}\right) \times Area\ (cm^2)$$

$$\rho = \frac{Rs\ (\frac{\Omega}{\blacksquare})}{length\ (cm)} \times Thickness\ (cm)$$

$$Conductivity = \frac{1}{\rho}\left(\frac{S}{cm}\right)$$

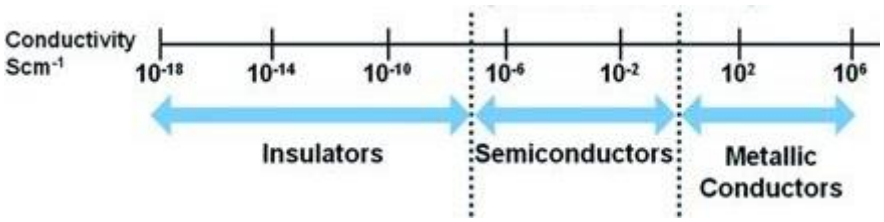


Figure 92 Conductivity scale (S/cm) for insulators, semi-conductors and metallic conductors reference taken by (109)

Sample	Sheet Res(Ω/sq)	Area (cm2)	Resistivity (Ω/cm)	Conductivity (S/cm)
GO	$1.1*10^{9}$	$308*10^{-6}$	$5*10^{-6}$	**$1.55*10^{-8}$**
rGO	$4.321*10^{6}$	$308*10^{-6}$	$8.5*10^{-3}$	**$1.1*10^{-5}$**
GO-Ag	$4.761*10^{7}$	$308*10^{-6}$	$3.1*10^{-4}$	**$0.32*10^{-6}$**

Table 3 Sheet Resistance, Area, Resistivity and Conductivity values as calculated by Kalotina Poulla

According to the data presented in Table 3 and reference Figure 92, GO is found to be an insulator with a conductivity value of $1.55*10^{-8}$ s/cm, whereas rGO and GO-Ag are considered to be a semiconductors with conductivity values of $1.1*10^{-5}$ and $0.32*10^{-6}$ respectively.

5.3 Contact Angle (CA):

In order to determine whether a surface is hydrophilic or hydrophobic, oleophilic or oleophobic, contact angle measurement is necessary. Contact angle is measured when a liquid droplet meets a solid surface. Qualitatively, a contact angle is the macroscopic representation of microscopic phenomena. Microscopic characteristics such as surface roughness, surface energies of the materials involved, and surface coatings play a role in the wettability of a material for a given fluid. Quantitatively, a contact angle is the interior angle formed by the substrate being used and the tangent to the drop interface at the apparent intersection of all three interfaces.

In order for a material to be characterized as hydrophilic, the average angle measured should be below 90o. Anything above 90o is characterized as hydrophobic. Average CAs as measured at ossila θ metrisis are layed out below.

For the determination of the suitable solvent of the prepared materials, in order to be used in different coatings, hydrophilicity of the materials should be investigated. For the purpose of this diploma thesis, the investigated GO-Ag material is of great importance to be dissolved in H_2O, due to its wide variety of applications. The hydrophilicity of GO, rGO and GO-Ag was evaluated

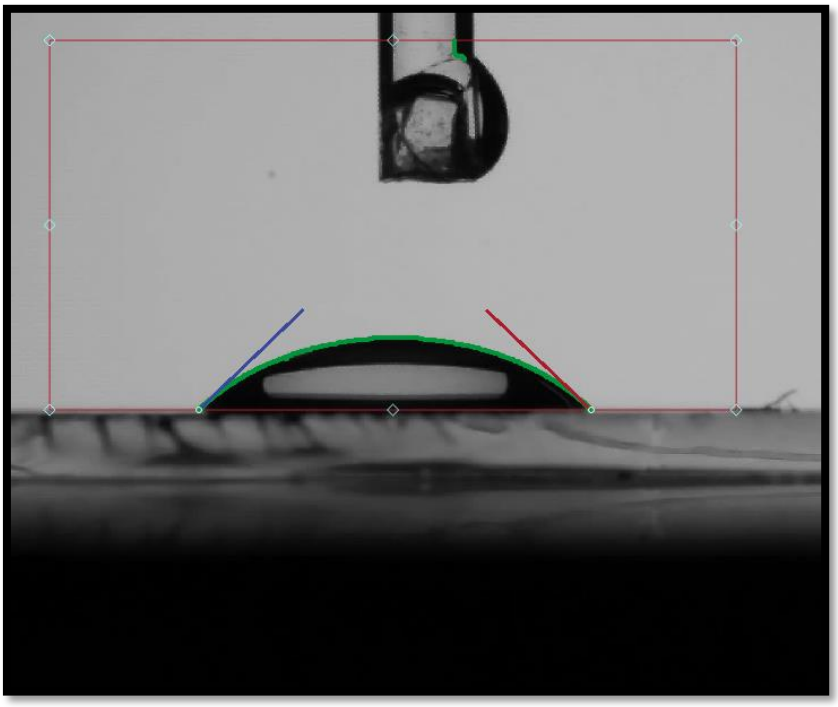


Figure 93 Example of Contact angle measurement. Sample tested: GO-Ag 1mg/ml deposited on borosilicate glass

- Average Contact angle for reference **borosilicate glass** was measured to be: 17º
- Average Contact angle for **GO** sample was measured to be: **29º**
- Average Contact angle for **rGO** sample was measured to be: **95º**

- Average Contact angle for **GO-Ag** sample was measured to be: **38º**

From what is stated above, it can be concluded that GO and GO-Ag are characterized as hydrophilic materials, whereas rGO is characterized to be hydrophobic material. This is attributed to the reduction of GO to rGO which reduces the number of oxygen containing groups, which give hydrophilicity to the material.

5.4 X-ray Powder Diffraction (XRD)

X-ray diffraction analysis (XRD) is a technique used to determine the crystallin structure of the materials studied. In this technique, the material is irradiated through X-Rays and then intensities and scattering angles of the X-rays that leave the material are measured.

Due to a problem concerning the measuring device, the XRD patterns obtained was of bad quality. GO-Ag pattern is seen in Figure 94. However, XRD peaks obtained were in accordance with bibliography as it is described below. Reference XRD can be seen in Figure 95

In GO pattern, a strong peak seen at 2θ = 10.19° value that corresponds to the plane (001), a smaller peak at 2θ = 20.93° was observed, attributed to the (002) plane. In GO, due to the addition of oxygen containing groups, the interlayer spacing is increased compared to the graphite. This is observed due to the oxidation of graphite.

In AgNPs pattern there is a peak located at 2θ value of 38.152° representing the (111) plane and lower intensity peaks at 45o,65o and 78o, representing the (200), (220) and (311) planes respectively (110).

In GO-Ag pattern we can detect peaks attributed to GO, at 10º and 20º and peaks attributed to AgNPs at 38°,45º,65º and 78º. with a slight shift in the peak position toward lower 2θ value confirm the intercalation of AgNPs within GO sheets, as shown in reference XRD patterns as described in

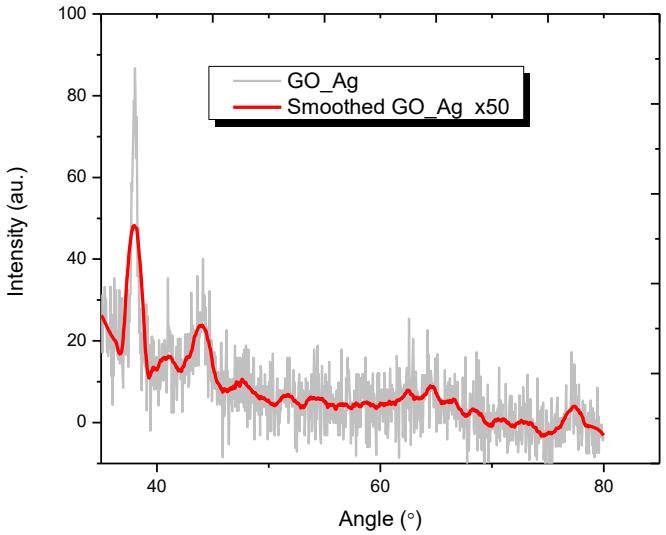


Figure 94 XRD pattern of GO-Ag

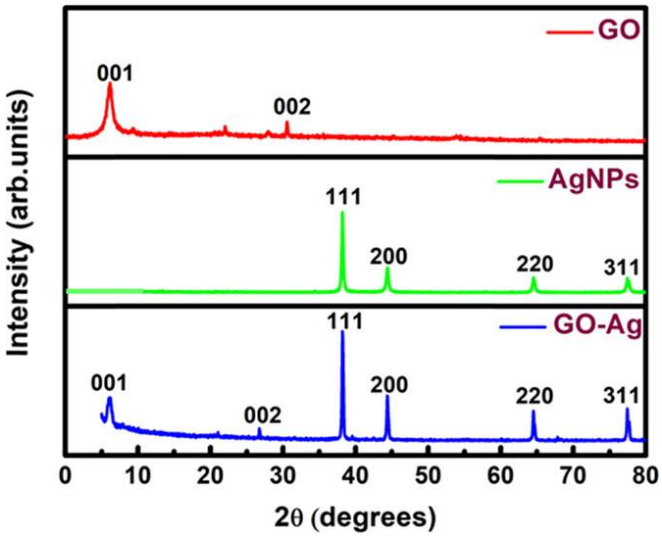


Figure 95 reference XRD patterns as described in (111)

In order to determine the crystallinity of GO-Ag material, the quotient of area of crystalline peaks to area of all peaks, multiplied by 100 needs to be calculated as seen below:

$$Crystallinity = \frac{Area\ of\ crystalline\ peaks}{Area\ of\ all\ peaks} \times 100 = \frac{155.7697}{340.52} = 45\%$$

5.5 FT-IR Spectroscopy:

Fourier-transform infrared spectroscopy (FTIR) is a technique used to obtain an infrared spectrum of absorption or emission of a solid, liquid or gas. An FT-IR spectrometer simultaneously collects high-resolution spectral data over a wide spectral range. The main goal of this spectroscopy is to measure how much light a sample absorbs at each wavelength. The most straight forward way to do this, the "dispersive spectroscopy" technique, is to shine a monochromatic light beam at a sample, measure how much of the light is absorbed, and repeat for each different wavelength. FTIR is an extremely useful technique for confirming the identity of pure compounds but has limited value if used for mixtures of compounds. The technique is based upon the identification of functional groups within molecules where such groups vibrate (either through stretching or bending in various ways) when irradiated with specific wavelengths of light. These vibrations and their intensity (% transmission) are plotted against the frequency of light (cm^{-1}) to which the sample is exposed to produce an FT-IR spectrum. Portions of the FTIR spectrum are unique to the compound under test (this is called the fingerprint region).

FT-IR spectroscopy is one of the methods used for graphene oxide characterization. The oxygen functional groups which are present in graphite oxide, namely, hydroxyl, carbonyl, carboxyl groups and epoxide rings are active in the IR region and can thus be detected using FT-IR spectroscopy. By extension, FT-IR Spectroscopy can be an indicator for the level of oxidation of graphite and the level of reduction of graphite oxide.

For the present work, attenuated total reflectance (ATR) infrared absorbance spectra were obtained with a Bruker Vertex 70v FT-IR vacuum spectrometer equipped with a A225/Q Platinum ATR unit with single reflection diamond crystal, which allows the infrared analysis of unevenly shaped solid samples

and liquids through total reflection measurements, in a spectral range of 7500 - 350 cm^{-1}.

When interpreting the FT-IR spectrum of graphite oxide obtained in this experiment, the peak at 1033cm^{-1} is attributed to the C-O bond of the epoxy group and the peak at 1163cm^{-1} is assigned to the stretching vibrations of the C-OH bonds of the hydroxyl groups. The peak at 1616cm^{-1} is attributed to the skeletal vibrations of the remaining graphitic domains after oxidation, whereas the stretching vibrations modes of the C=O bonds in carbonyl and carboxyl groups is responsible for the peak at 1716cm^{-1}.

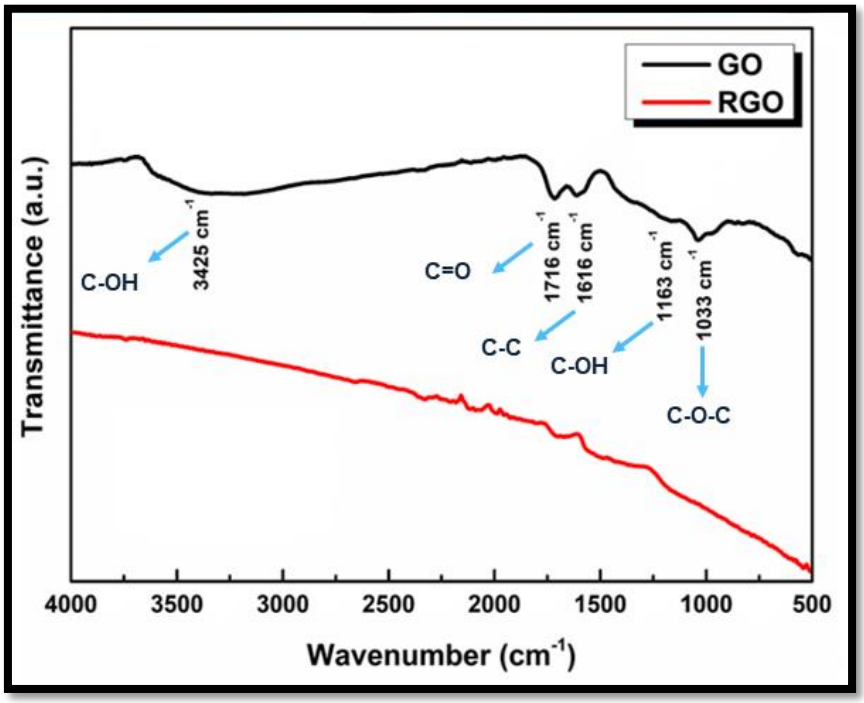


Figure 96 FT-IR spectrum of chemically prepared graphite oxide and reduced graphite oxide (21)

Finally, the large shoulder which appears at 3000cm^{-1} to 3500cm^{-1} is due to C-OH groups stretching vibrations and/or water molecules. Peaks that appear at 3280-3340 cm^{-1} and 3000-3100 cm^{-1} are generally attributed to -C-H and =C-H bonds respectively. Therefore, it is evident that the vibration of these bonds of graphite oxide contribute to the shoulder observed at 3000-3500 cm^{-1} in the obtained spectrum. It is obvious that in the spectrum of reduced graphite oxide does not display these characteristic peaks, indicating that the respective

oxygen functional groups have been reduced during HI/AcOH treatment. The C-C vibrational peak has also decreased. It is estimated that this is due to the breaking of C-C bond and creation of holes in the graphitic lattice.

The FTIR spectra of GO and the GO-Ag nanocomposite obtained from the work of Ai. Anagnostou (21) and can be seen in Figure 97. The whole spectrum is between 4000 and 400 cm^{-1}. As seen, GO absorbs at 3675 cm^{-1}, absorbance attributed to the intermolecular H-bonding, something that disappears in the GO-Ag nanocomposite. Also, other bands appear at 2979, 1392, and 1046 cm^{-1}, corresponding to C–H, C=O, and C–O, respectively. A decrease in intensity of C=O and −OH band reflect intercalation of AgNPs on the GO surface can be seen after Ag decoration of GO.

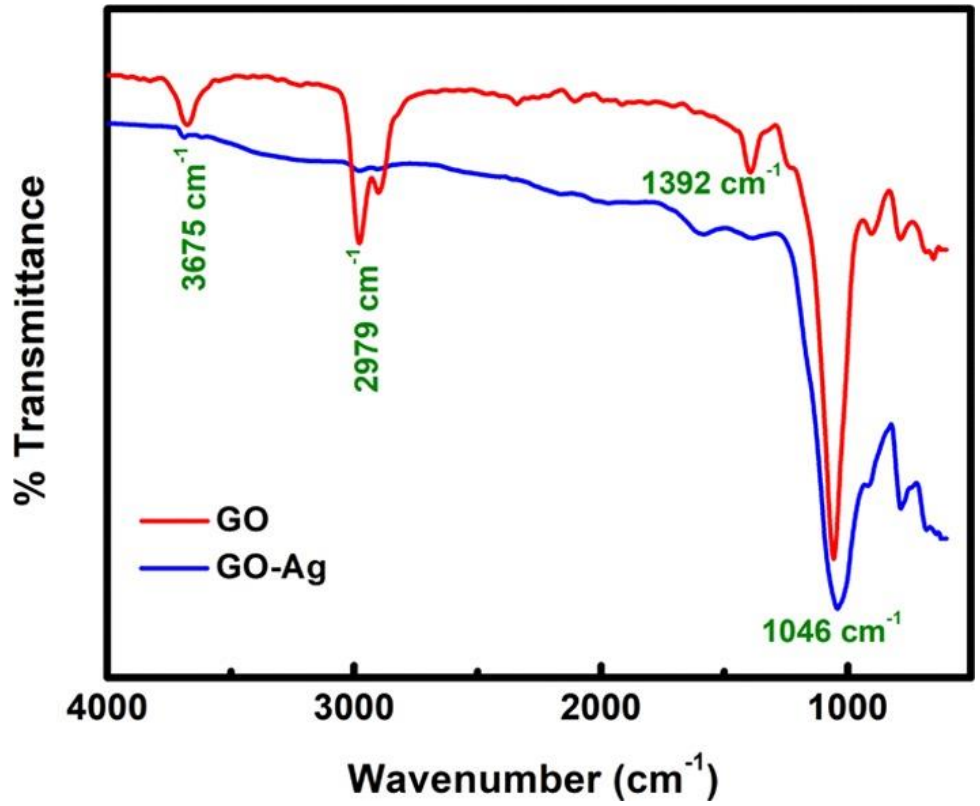


Figure 97 FT-IR spectrum of GO, GO-Ag

5.6 Raman Spectroscopy

Raman spectroscopy is a powerful, non-invasive tool for the characterization of graphene and its derivatives. The Raman spectrum of a graphene related material offers information on disorder, edge and grain boundaries, thickness, doping, strain, and thermal conductivity. Raman spectroscopy uses a monochromatic laser of suitable energy to interact with molecular vibrational modes and phonons in a sample, shifting the laser energy down (Stokes) or up (anti-Stokes) through inelastic scattering (112).

5.6.1. Raman Spectroscopy for Graphene:

In graphene, the Stokes phonon energy shift caused by laser excitation creates two main peaks in the Raman spectrum: The G peak (at 1580 cm^{-1} for a 532 nm laser), which is the primary in-plane vibrational mode of the sp2 carbon atoms, and 2D peak at 2690 cm-1, a second-order overtone of a different in-plane vibration which represents the stacking order. There exists a secondary peak at 1350 cm^{-1} for a 532 nm laser known as the D peak. (113) Theoretically, pristine graphene does not display a D peak since the lattice contains no defects or structural imperfections. This band is correlated with defects in the graphitic lattice, and it is known as the “disorder” or “defect” band It represents a ring breathing mode of vibration of the sp_2 carbon rings that are adjacent to the graphene lattice edge or a defect. The G peak corresponds to the E_2g phonon at the Brillouin zone centre. The D peak is due to the breathing modes of six-atom rings and requires a defect for its activation. It comes from transverse optical phonons around the K or K’ points in the first Brillouin zone (114). The D peak is generally representative of the defects in the graphitic lattice. These defects are anything that disrupts the planar sp_2 conjugated system of graphene and may be the presence of hetero atoms such as oxygen groups in the case GO or RGO, or holes in the lattice created by the removal of carbon atoms.

Because of the additional forces from the Van der Waals interactions between the layers of stacked graphene, as the number of graphene layers increases, the spectrum will change. For few-layer graphene the intensity of the 2D peak decreases as the number of layers increases Figure 98. As the number of layers increases further moving toward multi-layer graphene and graphite, the 2D peak splits into an increasing number of modes that can combine to give a wider, shorter, higher frequency peak. (115) The G peak also experiences a small red shift as the number of layers increases. This is demonstrated in Figure 99 in which Ferrari et al. used a 514 nm and a 633 nm laser to study the shift of the G peak with the increase of the number of layers, starting from mono-layer graphene and ending in graphite. Taking this information into account, it may be concluded that for stacked graphene, the number of layers can be derived from the ratio of peak intensities, I2D/IG, as well as the position and shape of these peaks (116).

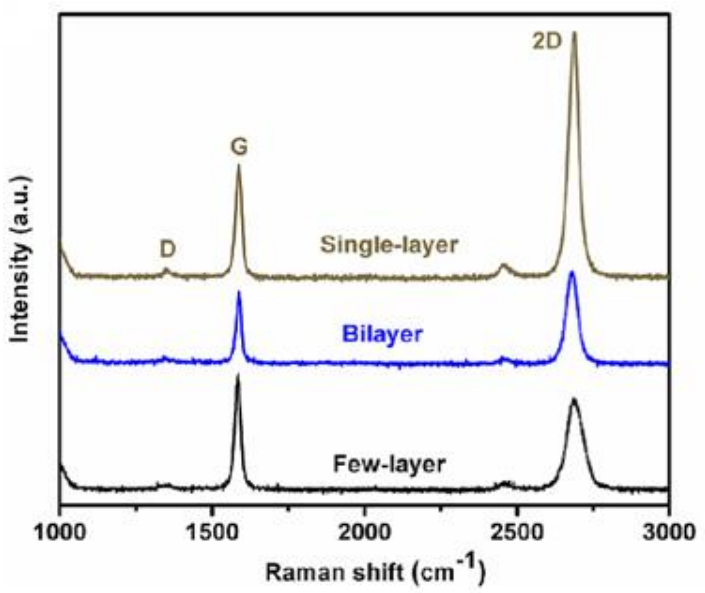


Figure 98 Raman spectra of single layer graphene (grey), bi-layer graphene (blue) and few-layer graphene (black). As the number of layers increases the intensity of the 2D peak decreases. Image source: quantumfrontiers.com

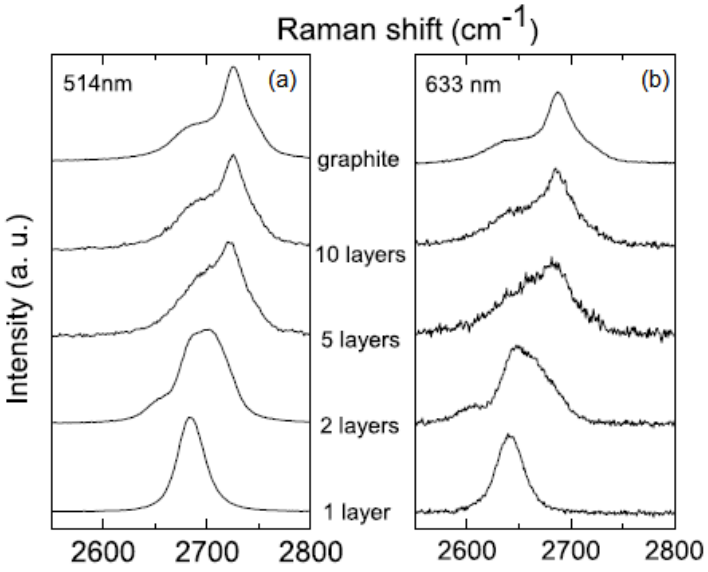


Figure 99Red shift of G peak in graphene Raman spectrum as the number of layers increases from mono-layer to multi-layer (graphite), first using (a) a 514 nm laser and then (b) a 633 nm laser. Image taken from reference (116)

5.6.2. Raman Spectroscopy for Graphite/Graphene Oxide:

When discussing graphene and its derivatives, the ratios of D/G relative intensity (I_D/I_G) and 2D/G relative intensity (I_{2D}/I_G) are used to quantify defects in the graphitic lattice and to qualify the number of stacked graphene layers, respectively.

One can use the ratio of peak intensities I_D/I_G to characterize the level of disorder. As disorder in graphene increases, the I_D/I_G ratio exhibits two different behaviors. There is a system of low defect density where I_D/I_G will increase as a higher defect density creates more elastic scattering. However, for a system of high defect density the reverse effect takes place; the I_D/I_G will begin to decrease as an increasing defect density result in a more amorphous carbon structure, attenuating all Raman peaks. The low defect density system is referred to as “nanocrystalline graphite” and the high defect density structure is referred to as “mainly sp^2 amorphous carbon” (117).

With the oxidation of graphite and the subsequent reduction of graphite oxide, the G and D peaks are affected allowing for the distinction between these three materials through the studying of their Raman spectra. As mentioned earlier,

the presence of oxygen groups in graphitic derivatives, which are considered defects, can be represented by the D peak. When graphite is oxidised, the D peak is notably increased due to the disruption of the sp^2 conjugated system of the graphene layers. When graphite oxide is then reduced, a decrease in the D peak is observed as a few oxygen groups are removed and the sp^2 system is partially restored.

However, it should be noted that although oxygen atoms are removed there may be other defects in the graphitic plane that can attenuate the D peak such as holes in the lattice due to removal of carbon in atoms in the form of CO_2 gases. Therefore, although the I_D/I_G ratio is a good indicator for the extent of defects in the lattice, it is not a reliable indicator for the extent of oxidation or reduction of the graphene species at hand.

5.6.3. Raman Spectroscopy for Graphene Reduced Graphite/ Graphene Oxide:

When graphite oxide or graphene oxide is reduced, the Raman spectrum of the resulting material reveals the appearance of the 2D peak, which corresponds to the graphene region formation. This 2D peak becomes more prominent as the reduction of GO progresses.

Another important change is the intensity ratio of the D and G peaks (I_D/I_G). Through reduction, the sp^2 conjugated system is restored and the G peak becomes more prominent. Conversely, as oxygen atoms are removed, the defects generally decrease resulting in the decrease in the D peak intensity. The result of this is that the I_D/I_G decreases. This is a general indication that the structure and atomic consistency of GO is altered and can be taken as a sign of successful reduction.

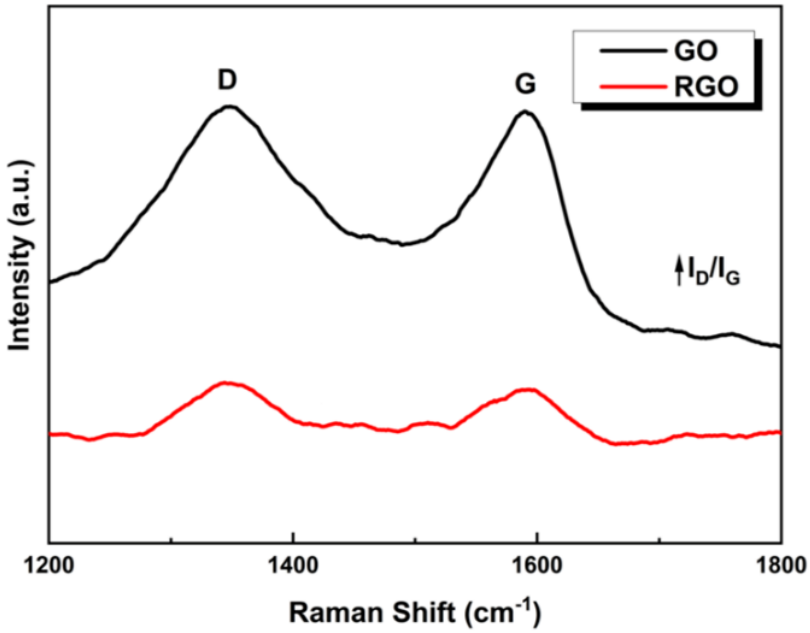


Figure 100 Raman spectrum of graphite oxide prepared via modified Hummers' method.

The Raman spectra for graphite oxide and reduced graphite oxide synthesised for this experiment are presented in Figure 100. Raman measurements were taken at room temperature through a Horiba Lab RAM HR Evolution confocal micro-spectrometer, in backscattering geometry (180°), equipped with an air-cooled solid-state laser operating at 532 nm with 100 mW output power. The laser beam was focused on the samples using a 10 x Olympus microscope objective (numerical aperture of 0.25), providing a ~55mW power on each sample.

It should be mentioned that in the obtained Raman spectra, the 2D peak at ~2690 cm^{-1} is not featured. This is because the spectrometer used only measures from 0 to 2500cm^{-1}. Nevertheless, sufficient information can be derived from the obtained spectra by studying the D and G bands and their intensity ratios.

The G and D peaks for graphite oxide appear at 1597 cm^{-1} and 1361 cm^{-1} respectively. After reduction, these peaks shift to lower wavenumbers and appear at 1594 cm^{-1} and 1307 cm^{-1} respectively.

The I_D/I_G can be used as a typical measure for the number of defects and disorder introduced with the reduction of graphite oxide using HI and AcOH. The I_D/I_G ratio for graphite oxide was measured at 0.83 whereas for reduced graphite oxide I_D/I_G the ratio was 0.15, which means that the intensity ratio of the D and G bands was decreased by about 5.5 times with chemical reduction.

5.6.4. Raman Spectroscopy for Silver decorated Graphene oxide (GO-Ag):

As seen in Figure 101, GO and GO-Ag nanocomposite exhibit their peaks from 0-3000cm^{-1}. For the GO D and G bands appear at 1347 and 1583 cm^{-1}, respectively, while in GO-Ag nanocomposite D and G bands appeared at 1353 and 1592 cm^{-1}, respectively. The D band was assigned to the breathing mode of k-point phonons with A_{1g} symmetry, and the G band was ascribed to E_{2g} phonon of sp^2 carbon atoms. (118) After decoration, the D and G band values increase due to intercalation of AgNPs on the GO surface.

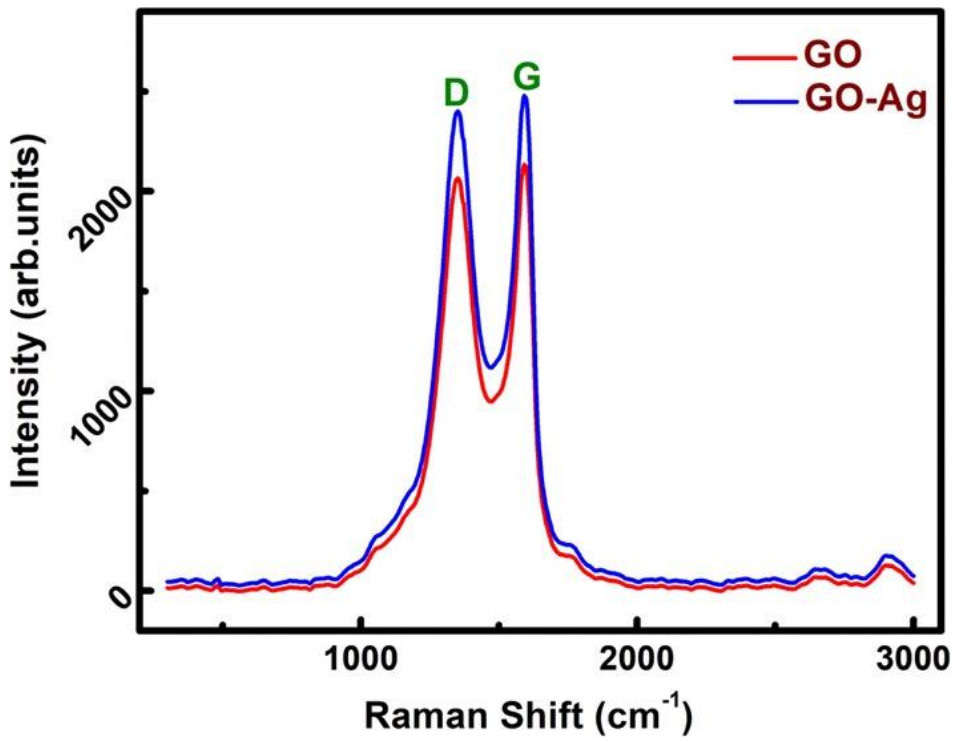


Figure 101 Raman shift of GO, GO-Ag

5.7 Atomic Force Microscopy: AFM

Topography of the samples was obtained using Atomic Force Microscopy as seen in Figure 102, Figure 103 and Figure 104 which depict GO, GO-Ag and rGO respectively. AFM analysis was performed using GO, GO-Ag and rGO bucky papers. (Preparation of the AFM samples is described in Chapter 4 “Synthesis of bucky papers”). The AFM images revealed that, compared to GO, GO-Ag has a predominantly hill-valley-structured surface of nanoscale topography. Ag NPs and some of their aggregates are distributed randomly and attached to the GO sheets. The RMS (average roughness), which mirrors the uniformity of the films, was estimated to be 152nm for GO, 172nm for GO-Ag and 0.55μm for rGO, Roughness is also a parameter which affects the antimicrobial activity of the materials, since it could penetrate the membranes of the bacteria, leading to instant death. As seen, rGO roughness is higher than GO and exhibits better antimicrobial results as it will be discussed below. Roughness also controls the bacterial adhesion and can avoid biofilms’ creation on material surface. Also, it is found that nanoscale surface roughness can play an important role in restraining formation of microcolonies.

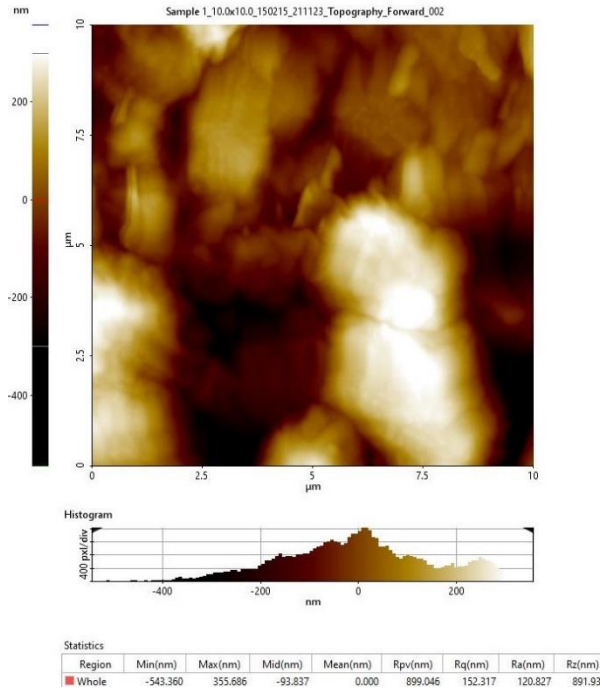


Figure 102 Atomic Force Microscopy for Graphene Oxide

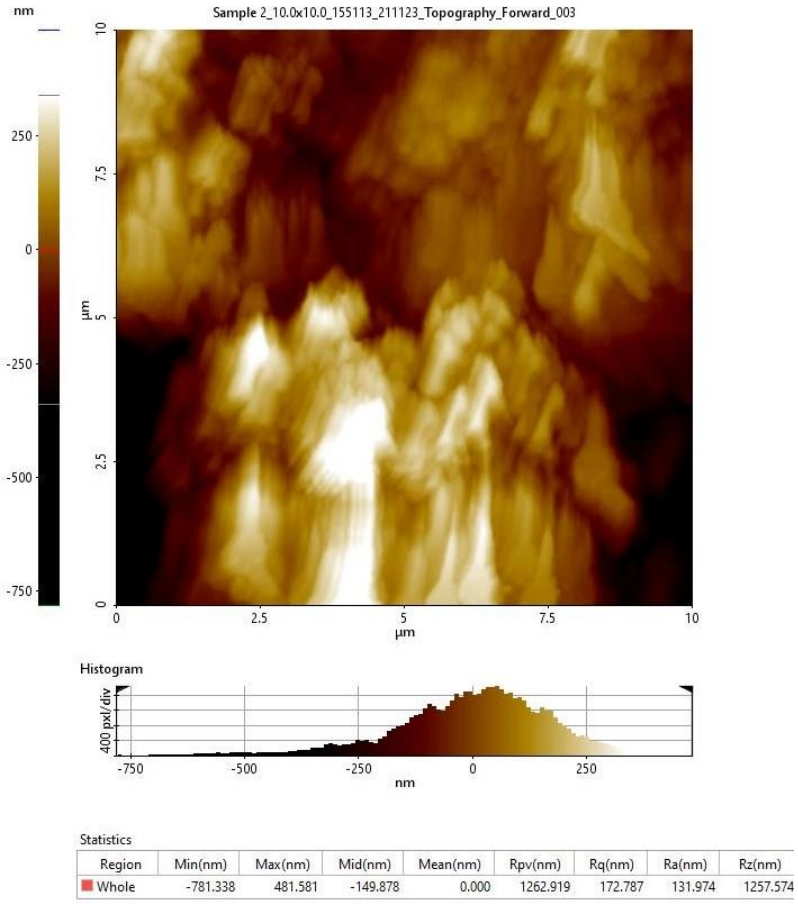


Figure 103 Atomic Force Microscopy for GO-Ag

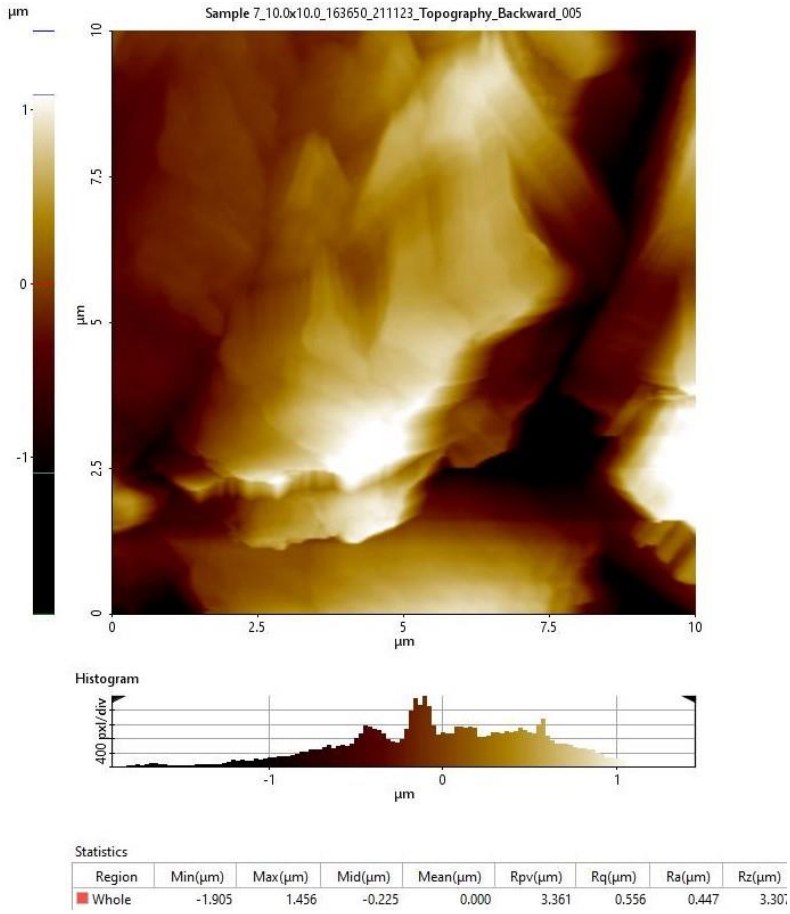


Figure 104 Atomic Force Microscopy for rGO

5.10 Antimicrobial assays

Imaging

Presented in the pictures below (Figure 105 Figure 106 Figure 107 Figure 108 Figure 109 Figure 110 Figure 111 Figure 112)are the images taken by the Optical Spectrometer used for the qualitative antimicrobial evaluation of GO, rGO and GO-Ag materials. The whiter spots on the blue background depict the micro-organisms on the material. As a reference material borosilicate cover glass was used. All materials used prepared as described in the experimental section and in particular: “Bucky papers preparation”.

5.10.1 Pseudomonas Aeruginosa qualitative antimicrobial assays

In the figure below P. Aeruginosa growth on glass is depicted, which is used as reference. The whiter areas are the areas where P. aeruginosa starts to form biofilms.

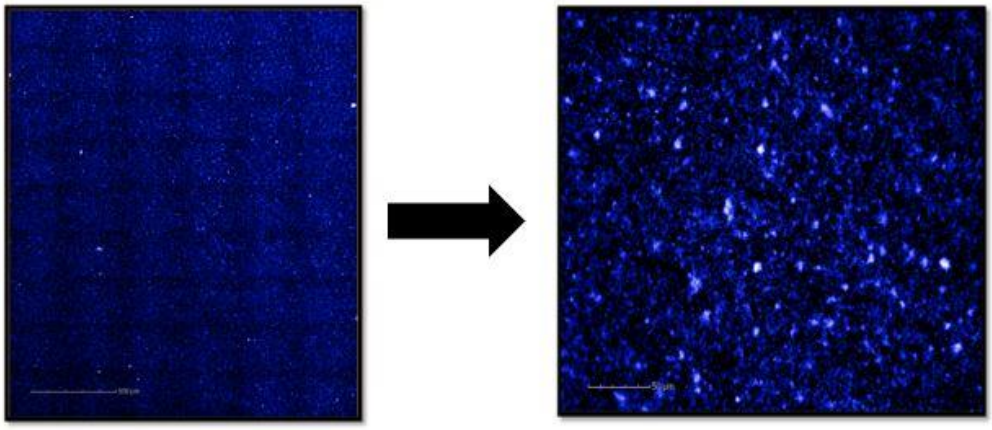


Figure 105 Reference glass- P. Aeruginosa growth on the material. Left 54 different pictures of microbial activity can be seen which can be summed up in one (right) after montage.

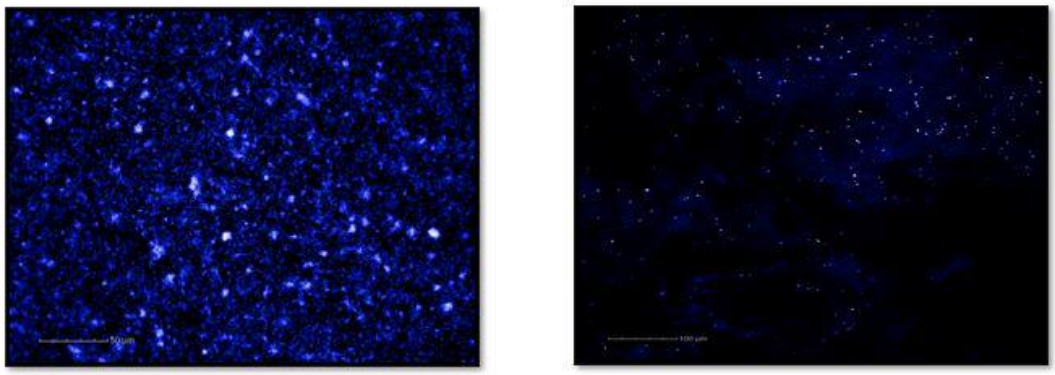


Figure 106 Reference glass with P. Aeruginosa (left) and P. Aeruginosa on GO-Ag (right)

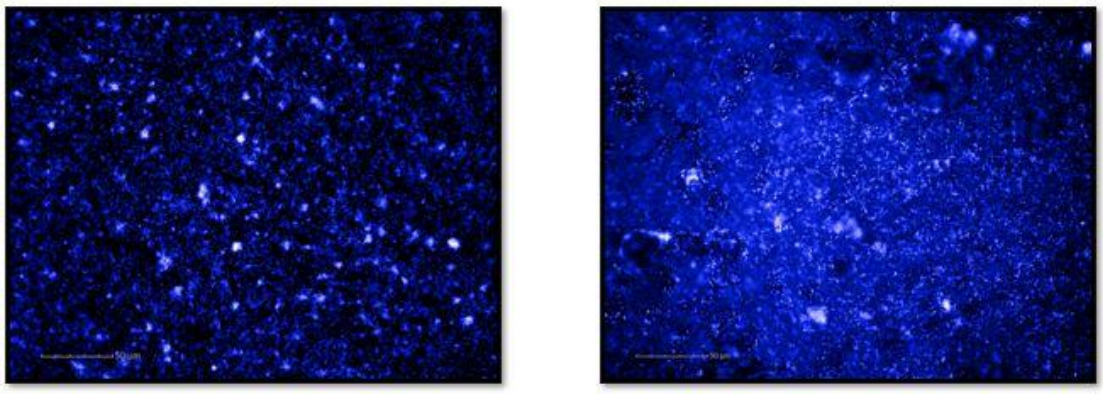


Figure 107 Reference glass with P. Aeruginosa (left) and P. Aeruginosa on GO (right)

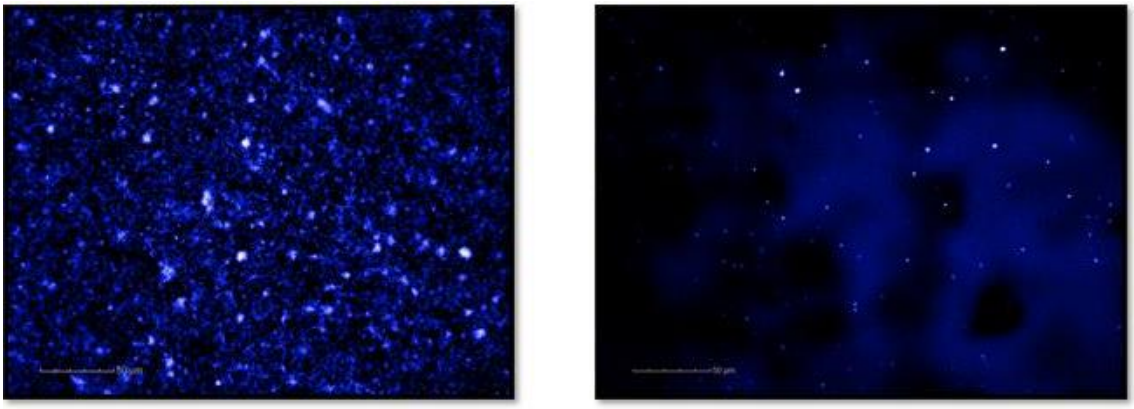


Figure 108 Reference glass with P. Aeruginosa (left) and P. Aeruginosa on rGO (right)

As seen in the figures above, GO-Ag and rGO exhibit good antimicrobial activity at P. Aeruginosa, comparing materials' images with the reference glass. As seen in the figures, GO show lower antimicrobial activity. For a more precise study, qualification through dead/alive assay will show the percentage of antimicrobial activity success.

5.10.2 Escherichia Coli qualitative antimicrobial assays

In the figure below E. Coli growth on glass is depicted, which is used as reference. The whiter areas are the areas where E. Coli starts to form biofilms.

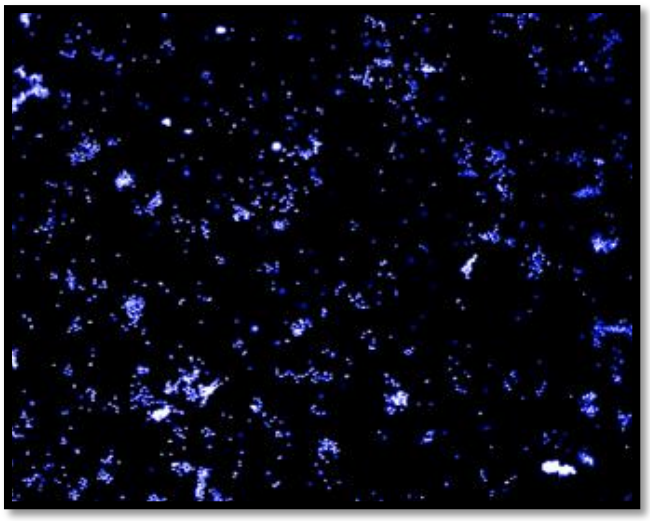


Figure 109 Reference glass of E. Coli

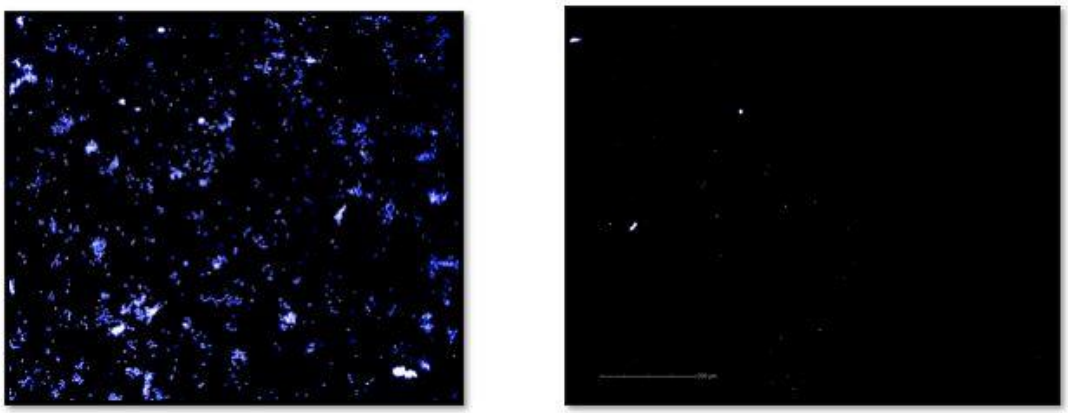


Figure 110 Reference glass with E. Coli (left) and E. Coli on GO-Ag (right)

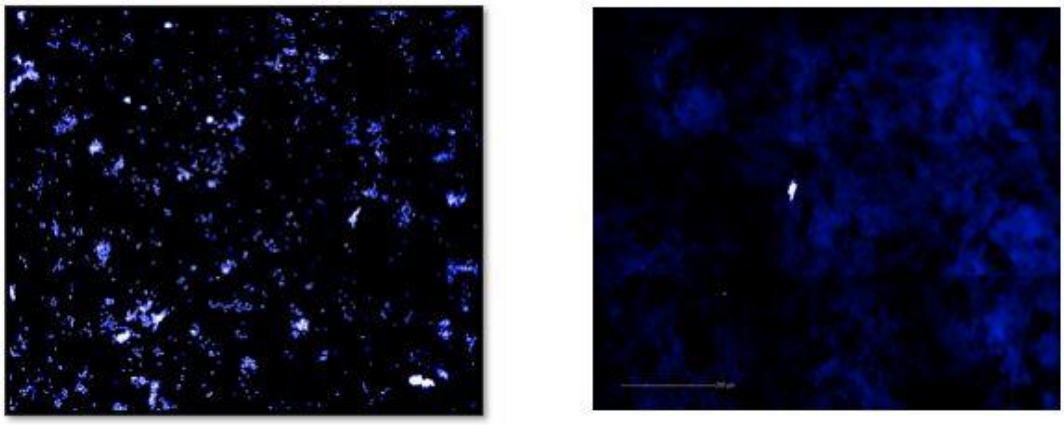


Figure 111 Reference glass with E. Coli (left) and E. Coli on GO (right)

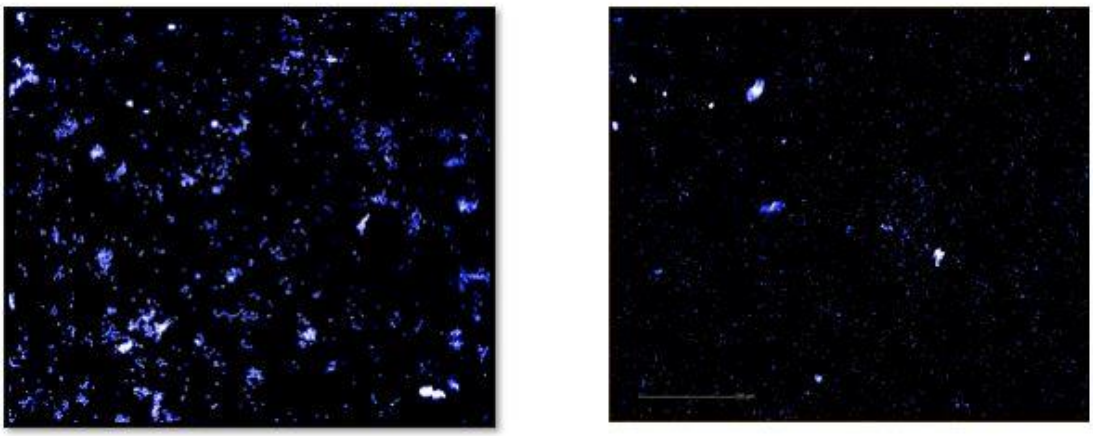


Figure 112 Reference glass with E. Coli (left) and E. Coli on rGO (right)

As seen in the figures above, all materials exhibit good antimicrobial activity at E. Coli, comparing materials' images with the reference glass. For a more precise study, qualification through dead/alive assay will show the percentage of antimicrobial activity success. The studied mechanism of action of the GO-Ag complex are further analysed below.

5.11 Pseudomonas Aeruginosa quantitative antimicrobial assays

Table 4 Qualitative Results of P. Aeruginosa

	Count 1	Count 2
Control	200,000/mL	200,000/mL
GO	4,000/mL	4,000/mL
rGO	1,000/mL	1,000/mL
GO-Ag	200/mL	200/mL

As seen in Table 4, the colonies' number was 200,000/mL at the control sample, for Pseudomonas Aeruginosa. For GO, there is a decrease in the number of colonies, 4,000/mL which means that only the 20% of the initial microorganisms survived on the material surface. Better results were obtained for the rGO, on the surface of which only 1,000/mL colonies could be seen, resulting in 5% viability compared to the initial population. Best results, were obtained by GO-Ag, on the surface of which only 200/mL colonies could be seen which corresponds to 1% viability of the initial number of colonies. Consequently, the prepared materials exhibit antimicrobial activity on P. Aeruginosa.

5.12 Escherichia Coli quantitative antimicrobial assays

Table 5 Qualitative Results of E. Coli

	Count 1	Count 2
Control	4,000/mL	4,000/mL
GO	0/mL	0/mL
rGO	20/mL	0/mL
GO-Ag	0/mL	0/mL

As seen in Table 5, the colonies' number was 4,000/mL at the control sample, for E. Coli. For all the samples, there is an elimination of the number of colonies to zero, which means that the material had 100% success in antimicrobial activity against E. Coli. In case of rGO, on the count 1, there is a number of 20/mL colonies, which corresponds to 0,5% of bacteria viability, which could happen due to contamination in measurement. However, in every case all three materials exhibit an excellent antimicrobial activity against E. Coli and can be used in biomedical applications.

5.13 Discussion of Antimicrobial mechanisms

One of the most important functions of the cell wall and membrane is to protect the microorganism against the threats and to maintain homeostasis while transporting nutrients inside the cell. There are two types of bacteria, the gram positive and gram negative, which have different types of cell wall. Gram negative bacteria are most likely to be eliminated by GO-Ag, because they have thinner wall and less peptidoglycan. Peptidoglycan layer, made of glycan strands cross-linked by short peptides and anionic glycopolymers called teichoic acid, creates a natural barrier which prevents penetration of the nanoparticles and thus protects bacteria. This type of wall can be mostly found in gram positive bacteria. Both microorganisms used for the purpose of this diploma thesis, were Gram negative bacteria, which means that their membrane and cell wall could be easier penetrated. Depending on the degree of membrane damage, AgNPs can penetrate inside the cell and affect the functions of the cell's interactions with proteins and DNA. The silver release from GO-Ag composite, can have an adverse effect on both DNA and proteins, by either transforming DNA or damage vital proteins of the cell, limiting its replication ability.

Another vital mechanism for the cell, is reactive oxygen species (ROS) which are oxygen containing molecules that exhibit strong redox potential. Under normal circumstances, ROS act as antioxidant in order to keep the cell balanced. However, in the case of imbalance between the antioxidant mechanism and excessive production of ROS, the redox balance of the cell favours oxidation, leading to oxidative stress. Although, oxidative stress assists in many aspects of cellular signalling, excessive oxidative stress can be harmful. GO-Ag complex triggers cellular oxidative stress leading to apoptosis of the bacteria. ROS generation mediated by silver ions, it is also reported that it can affect bacterial electron transport chain and proton motive force because of inhibition of enzymes involved in the reactions. Breakdown of membrane

functions by GO-Ag can also lead to protein leakage by increasing the membrane permeability, which result in cell death.

6.0 Conclusions

Taking inspiration from previous literature which investigates the antimicrobial activity of GO, rGO and GO-Ag, this thesis serves to further examine the antimicrobial activity of these three graphene-based materials in Pseudomonas Aeruginosa and Escherichia coli. By implementing a modified Hummer's method for GO preparation, HI/AcOH assisted chemical reduction for rGO preparation and the increased sheer force of an ultrasonic probe for their liquid phase exfoliation, high concentrations of GO and rGO dispersions were achieved. Various synthesis methods were used, including rGO decoration and GO decoration. However, GO decoration was more appealing due to the potentials given by the dispersibility of the material in water. This is because GO-Ag materials exhibit hydrophilicity and can be easily disperse in water. The GO silver decoration methods used included $AgNO_3$, NH_3, NaOH & $NaBH_4$ in order to prepare silver decorated graphene oxide. Bucky papers and thin films were prepared from dispersions of each material. The bucky papers were used to carry out the antimicrobial assays, while thin films were used for other characterizations of the prepared materials. Thin films were prepared using spray gun and drop casting deposition methods on borosilicate glass. For the characterization of the materials prepared several methods were used, namely: UV-Vis spectroscopy to determine the absorbance, Sheet-Resistance to calculate Resistivity and Conductivity, Contact Angle to define the hydrophilic/hydrophobic nature of the materials, X-ray Powder Diffraction, FT-IR Spectroscopy and Raman Spectroscopy to determine the chemical composition of the materials, Atomic Force Microscopy: AFM, Transmittance Electron Microscopy (TEM) and Scanning Electron Microscopy (SEM) to determine the morphology of the prepared samples. Finally, antimicrobial assays included qualification of materials through spectrophotometry imaging and quantification of dead/alive micro-organisms through dead/alive assay.

Beyond any doubt, GO-Ag, GO and rGO exhibit good antimicrobial activity against both P. Aeruginosa and E. Coli. It is of great significance the fact that E. Coli was 100% eliminated in all three materials, as it has occurred by quantification assays. Also, the prepared GO-Ag, GO materials showed good hydrophilicity, in comparison with rGO which is hydrophobic, which means that they can be used to be dissolved in water, alcohol solvents in order to prepare eco-friendly and easy to use coatings for biomedical purposes. The electrical measurements of the materials showed that they have potential to be used in energy applications, such as electrodes, for future purposes such as enhanced antimicrobial activity of materials for new generation coatings.

7.0 Future Work

As demonstrated throughout this thesis, there exist some reports on the antimicrobial behavior of graphene and its derivatives, such as graphite, GO and RGO. These studies aim to identify the most suitable materials and methods with which to successfully to prepare antimicrobial coatings of the afore-mentioned graphene-based materials. However, these investigations must be extended and improved upon before these materials to prepare more efficient materials with enhanced antimicrobial activity. During the realization of this thesis, several suggestions for future improvement of this work were recognized.

Firstly, when studying the preparation of metal-ion-decorated GO, GO and RGO, it is important to acknowledge that GO and RGO samples differ in terms of structure and oxygen content depending on the preferred preparation method, resulting in different dispersion behaviors and thus different coatings. Different oxidation and reduction methods yield different GO and RGO samples, respectively. The resulting products vary in structure, oxygen content

and sp^2 hybridized carbon regions. These characteristics immediately affect the properties of the synthesized products. As a result, different preparation methods yield different GO and RGO samples in terms of properties, such as conductivity, and immediately affect their potential to be used in various applications of enhanced antimicrobial activity (e.g, electrodes). For this reason, the present work does not cover all types of GO and RGO samples. Similar studies should be conducted on GO and RGO samples prepared with different methods with varying structural characteristics.

Another crucial factor on the antimicrobial activity of the materials described above, is the concentration and the size distribution of the silver nanoparticles. Ultrasonic frequencies in the form of a bath or, in the case of this thesis, an ultrasonic probe, have been utilized for exfoliation of graphite oxide and reduced graphite oxide in the liquid phase. These methods may be expanded upon and optimized to achieve higher dispersion concentrations and more uniform or, ideally, monodisperse GO and RGO suspensions. The ultrasonication method can be expanded upon in terms of changing the ultrasonic frequency and the exfoliation time.

Also, the way steps followed in the silver decoration preparation can affect the size distribution of the silver nanoparticles. For example, if $AgNO_3$ has been added in NaOH and NH_3 solution, a partial reduction of $AgNO_3$ could happen which leads to big silver particles, creating a material with structural defects.

Moreover, the prepared material can be used additionally as electrode for enhanced antimicrobial activity in coatings to optimize the antimicrobial results.

Lastly, more metal ions can be used in order to find the most efficient, low cost and eco-friendly material to be used as antimicrobial coatings in a wider variety of applications in the future.

References

1. *Organic Chemistry.* **McMurry, John.** 9th edition.

2. *Elemental carbon in the sp1 hybridization.* **Banhart, Florian.** 3, s.l. : ChemTexts, 2020.

3. *Adsorption of potassium and oxygen on graphite: A theoretical study.* **Lamoen Bo, Persson Dirk.** s.l. : The Journal of Chemical Physics, 1998.

4. *Chapter 1 - Discovery of graphene and beyond.* **Pattammattel, Challa Vijaya, Kumar Ajith.** s.l. : Chemical and Biochemical Applications, 2017.

5. ***Yeop, Majlis Azlan Hamzah Reena Sri Selvarajan Burhanuddin.*** *s.l. : Graphene for Biomedical Applications: A Review, 2017.*

6. Electronic Properties of Fullerenes : Proceedings of the International Winterschool on Electronic Properties of Novel Materials. ***H. Kuzmany, J. Fink, M. Mehring, S. Roth.*** *s.l. : Springer, 1993.*

7. Fullerene C60 with cytoprotective and cytotoxic potential: prospects as a novel treatment agent in Dermatology? ***Angelique Rondags, Wing Yan Yuen,Marcel F. Jonkman,Barbara Horváth.*** *s.l. : Experimental Dermatology, 2016.*

8. Strength of carbon nanotubes depends on their chemical structures. ***Akira Takakura, Ko Beppu, Taishi Nishihara, Akihito Fukui, Takahiro Kozeki, Takahiro Namazu.*** *s.l. : Nature communications, 2019.*

9. Incorporation of carbon nanotubes in photoactive layer of organic solar cells. ***Khan, Danish Khan Zahid Ali Danyal Asif Manoj Kumar Panjwani Idris.*** *s.l. : Ain Shams Engineering Journal, 2020.*

10. Carbon nanotubes added to the SIN List as a nanomaterial of Very High Concern. ***Steffen Foss Hansen, Anna Lennquist.*** *s.l. : Nature Nanotechnology, 2020.*

11. Grouping all carbon nanotubes into a single substance category is scientifcally unjustifed. ***Kostas Kostarelos, Bengt Fadeel.*** *s.l. : Nature Nanotechnology, 2020.*

12. The band theory of graphite. ***PR., Wallace.*** *s.l. : Physics Review, 1947.*

13. Electric Field Effect in Atomically Thin Carbon Films. ***al, Novoselov et.*** *s.l. : Science, 2004.*

14. Two-dimensional gas of massless Dirac fermions in graphene. ***Novoselov, Geim.*** *s.l. : Nature, 2005.*

15. Low-temperature plasma exfoliated n-doped graphene for symmetrical electrode supercapacitors. ***K. Wang, M. Xu, Y. Gu, et al.*** *s.l. : Nano Energy, 2017.*

16. Structure and Properties of Graphene. ***Zhen Zhen, Hongwei Zhu.*** *s.l. : Elsevier, 2018.*

17. ***Young-Woo Son, Marvin L. Cohen, Steven G. Louie.*** *s.l. : Energy Gaps in Graphene Nanoribbons, 2006.*

18. Edge states in quantum Hall effect in graphene (Review Article). ***valery gusynin, V Miransky, Sergei Sharapov.*** *s.l. : Low Temperature physics, 2008.*

19. Highly ordered graphene for two dimensional electronics. ***J. Hass, R. Feng et al.*** *s.l. : Applied Physics Letters, 2006.*

20. Reviewing computational studies of defect formation and behaviors in carbon fiber structural units. ***Niedziel, Sara B. IsbillAshleyE. Shields Delis Mattei-Lopez Roger. Kapsimalis J.L.*** *s.l. : Computational Material Science, 2021.*

21. An Extensive Case Study on the Dispersibility Parameters of HIAssisted Reduced Graphene Oxide and its Graphene Oxide Precursor. ***Anagnostou, Aikaterini.*** *Heraklion : HMU Library, 2020.*

22. Large-scale pattern growth of graphene films for stretchable transparent electrodes. ***Keun Soo Kim, Yue Zhao, Houk Jang, Sang Yoon Lee, Jong Min Kim, Kwang S. Kim, Jong-Hyun Ahn, Philip Kim, Jae-Young Choi.*** *s.l. : Nature, 2009.*

*23. —.****Zhao, Keun Soo Kim Yue.*** *s.l. : Nature, 2009.*

24. ***Young-Woo Son, Marvin L. Cohen & Steven G. Louie.*** *Half-metallic graphene nanoribbons. Nature. 2006.*

25. Control of Graphene's Properties by Reversible Hydrogenation: Evidence for Graphane. ***D.C. Elias, R.R Nair, T.M. Mohiuddin, S.V. Morozov.*** *s.l. : Science, 2009.*

26. Gate-induced insulating state in bilayer graphene devices. ***Jeroen B. Oostinga, Hubert B. Heersche, Xinglan Liu, Alberto F. Morpurgo.*** *s.l. : Nature Materials, 2008.*

27. Superior Thermal Conductivity of Single-Layer Graphene. ***A. Balandin, Suchismita Ghosh, Wenzhong Bao, Irene Calizo.*** *s.l. : Nano Letters, 2008.*

28. Graphene-Based Ultracapacitors. ***Meryl D stoller, Sungjin Park, Yanwu Zhu.*** *s.l. : Nano Letters, 2008.*

29. Detection of individual gas molecules adsorbed on graphene. ***F. Schedin, A. K. Geim, S. V. Morozov, E. W. Hill, P. Blake, M. I. Katsnelson.*** *s.l. : Nature Materials, 2007.*

30. Scanning tunneling microscopy characterization of the electrical properties of wrinkles in exfoliated grahene monolayers. ***Xu K, Cao P, Heath JR.*** *s.l. : Nano Letters, 2009.*

31. Wrinkled, rippled and crumpled graphene: an overview of formation mechanism, electronic properties, and applications. ***Deng S, Berry V.*** *s.l. : matter today, 2016.*

32. Topological defects in graphene: dislocations and grain boundaries. ***Yazyev OV, Louie SG.*** *s.l. : Physics reviews, 2010.*

33. Properties of fluorinated graphene films. ***Robinson JT, Burgess JS, Junkermeier CE, et al.*** *s.l. : Nano Letters, 2010.*

34. Photochemical chlorination of Graphene. ***Li B, Zhou L, Wu D, et al.*** *s.l. : ACS Nano, 2011.*

35. Hydrogen on graphene: electronic structure, total energy, structural distortions and magnetism from first-principles calculations. ***Boukhvalov DW, Katsnelson MI, Lichtenstein AI.*** *s.l. : Physics Reviews, 2008.*

36. Graphene at the edge: stability and dynamics. ***Meyer JC, Kisielowski C, Erni R, et al.*** *s.l. : Nano Letters, 2008.*

37. Embedding transition-metal atoms in graphene:structure, bonding, and magnetism. ***Krasheninnikov AV, Lehtinen PO, Foster AS, et al.*** *s.l. : Physics review letters, 2009.*

38. A chemical route to carbon nanoscrolls. ***M. Viculis, J. J. Mack, and R. B. Kaner,.*** *s.l. : Science, 2003.*

39. Electric field effect in atomically thin carbon films. ***K. S. Novoselov, A. K. Geim, S. V. Morozov, D. Jiang, Y. Zhang,.*** *s.l. : Science, 2004.*

40. Graphene made easy: high quality large-area samples. ***A. Shukla, R. Kumar, J. Mazher, and A. Balan.*** *s.l. : Solid State Communications, 2009.*

41. Stable aqueous dispersions of graphitic nanoplates via the reduction of exfoliated graphite oxide in the presence of poly(sodium -styrenesulfonate). ***S. Stankovich, R. D. Piner, X. Chen, N. Wu, S. T. Nguyen.*** *s.l. : Material Chemistry, 2006.*

42. Environmental Synthesis of Few Layers Graphene Sheets Using Ultrasonic Exfoliation with Enhanced Electrical and Thermal Properties. ***Monir Noroozi, Azmi Zakaria.*** *s.l. : Plos, 2016.*

43. Towards high quality CVD graphene growth and transfer. ***al, G.Deokar.Avila Razado-Colambo et.*** *s.l. : Carbon, 2015.*

44. Graphene CVD growth on copper and nickel: role of hydrogen in kinetics and structure. ***Maria Losurdo, Maria Michela Giangregorio , Pio Capezzuto and Giovanni Bruno.*** *s.l. : Royal Society of Chemistry, 2011.*

45. Introduction to CVD technique. ***Website, ACS Suppliers.***

46. Epitaxial growth of single-domain graphene on hexagonal boron nitride. ***Wei Yang, Guorui Chen, Zhiwen Shi, Cheng-Cheng Liu et al.*** *s.l. : Nature Materials, 2013.*

47. Graphene sheets via microwave chemical vapor deposition. ***al, G.D Yuan W.J. Zhang Y.Yang et.*** *s.l. : Chemical Physics Letters, 2009.*

48. Synthesis of graphene sheets with high electrical conductivity and good thermal stability by hydrogen arc discharge exfoliation. ***Gao, Zhong-Shuai Wu Wencai Libo.*** *s.l. : ACS Nano, 2009.*

49. ***Z. Goknur Cambaz, Gleb Yushin, Sebastian Osswald, Vadym Mochalin, Yury Gogotsi.*** *Noncatalytic Synthesis Of Carbon Nanotubes, Graphene And Graphite On SiC. Crystallography Reports. 2011.*

50. Gram-scale production of graphene based on solvothermal synthesis and sonication,. ***M. Choucair, P. Thordarson, and J. A. Stride.*** *s.l. : Nature Nanotechnology, 2009.*

51. Synthesis, characterization, structural, optical properties and catalytic activity of reduced graphene oxide/copper nanocomposites. ***M. Nasrollahzadeh, F. Babaei, P. Fakhric, B. Jaleh.*** *s.l. : RSC Advanced, 2015.*

52. Synthesis of Graphene Oxide using Modified Hummers Method: Solvent Influence. ***. I. Zaabaa, K. L. Fooa, U. Hashima, S. J. Tan, W. W. Liua, C. H. Voona.*** *s.l. : Procedia Engineering, 2017.*

53. The Chemistry of Graphene Oxide. ***D. R. Dreyer, S. Park, C. W. Bielawski, R. S. Ruoff.*** *s.l. : Chemistry Society Reviews, 2010.*

54. On the Atomic Weight of Graphite. ***Brodie, B. C.*** *s.l. : Philos. Trans. R. Soc. London, 2009.*

55. Verfahren zur Darstellung der Graphitsaure. ***Staudenmaier, 5 L.*** *s.l. : Ber. Dtsch. Chem. Ges, 1898.*

56. The Role of Oxidative Debris on Graphene Oxide Films. ***L. D. David, V. Mercedes, S. Maria.*** *s.l. : ChemPhysChem, 2013.*

57. Chemistry with Graphene and Graphene Oxide-Challenges for Synthetic Chemists. ***Hirsch, S. Eigler and A.*** *s.l. : Angew. Chem. Int. Ed, 2014.*

58. Fast and facile preparation of graphene oxide and reduced graphene oxide nanoplatelets. ***al, Shen et.*** *s.l. : Chem. Mater, 2009.*

59. An Investigation on 4-Aminobenzoic acid Modified Polyvinyl chloride/Graphene Oxide and PVC/Graphene Oxide based Nanocomposite Membranes. ***Ahmad, Nafees.*** *s.l. : Journal of Plastic Film and Sheeting, 2015.*

60. Chemistry and Structure of Graphene Oxide. ***al, Shreya H. Dave et.*** *s.l. : ACS Nano, 2016.*

61. Field Electron Emission Characteristics and Physical Mechanism of Individual Single-Layer Graphene. ***Xiao, Zhiming.*** *s.l. : ACS Nano, 2010.*

62. Solution processed reduced graphene oxide electrodes for organic photovoltaics. ***E. Kymakis, E. Stratakis et al.*** *s.l. : Royal Society of Chemistry, 2016.*

63. Thermally modulated multilayered graphene oxide for hydrogen storage. ***Byung Hoon Kim.*** *s.l. : Physical chemistry chemical physics, 2012.*

64. Synthesis and applications of graphene oxide aerogels in bone tissue regeneration: a review. ***al, M.E.Berrio et.*** *s.l. : Materials today chemistry, 2021.*

65. Recent advances in graphene-based biosensor technology with applications in life sciences. ***Peña-Bahamonde, J.*** *s.l. : Nanotechnology, 2018.*

66. Graphene and graphene oxide: biofunctionalization and applications in biotechnology. ***Wang.*** *s.l. : Trends in Biotechnology, 2011.*

67. The renaissance of fluorescence resonance energy transfer. ***Selvin.*** *s.l. : Nature Structural Biology, 2000.*

68. PEGylated Nanographene Oxide for Delivery of Water-Insoluble Cancer Drugs. ***Z. Liu, J. T. Robinson, X. Sun, Ho. Dai.*** *s.l. : Am. Chem. Soc., 2008.*

69. Fluorescence and Sensing Applications of Graphene Oxide and Graphene Quantum Dots: A Review. ***Peng Zheng, Prof. Nianqiang Wu.*** *s.l. : Chem Asian J, 2018.*

70. Graphene in biomedicine: opportunities and challenges. ***Liu, L. Feng Z.*** *s.l. : Nanomedicine, 2011.*

71. Advancement of the Emerging Field of RNA Nanotechnology. ***Guo, D. Jasinski F. Haque D. W. Binzel P.*** *s.l. : ACS Nano, 2017.*

72. Graphene-based 3D scaffolds in tissue engineering: fabrication, applications, and future scope in liver tissue engineering. ***Hilal-Alnaqbi, R. G. Bai K. Muthoosamy S. Manickam A.*** *s.l. : International Journal of Nanomedicine, 2019.*

73. Preparation, characterization and biological test of 3D-scaffolds based on chitosan, fibroin and hydroxyapatite for bone tissue engineering. ***Almeida, P. A. L. Lima C. X. Resende G. D.de Almeida Soares K. Anselme L.E.*** *s.l. : Mater Sci Eng C, 2013.*

74. The effect of cyclic stretch on maturation and 3D tissue formation of human embryonic stem cell-derived cardiomyocytes. ***Miyagi, A. Mihic J. Li Y.*** *s.l. : Biomaterials, 2014.*

75. Graphene based scaffolds on bone tissue engineering. ***Khalilzadeh, N. Shadjou M. Hasanzadeh B.*** *s.l. : Bioengineered, 2018.*

76. A graded graphene oxide-hydroxyapatite/silk fibroin biomimetic scaffold for bone tissue engineering. ***Qi, Q. Wang Y. Chu J. He W. Shao Y. Zhou K.*** *s.l. : Mater. Sci. Eng. C Mater. Biol. Appl., 2017.*

77. Electrically conductive graphene/polyacrylamide hydrogels produced by mild chemical reduction for enhanced myoblast growth and differentiation. ***Park, H. Jo M. Sim S. Kim S. Yang Y. Yoo J.-H.*** *s.l. : Acta Biomater, 2017.*

78. The effect of cyclic stretch on maturation and 3D tissue formation of human embryonic stem cell-derived cardiomyocytes. ***Miyagi, A. Mihic J. Li Y.*** *s.l. : Biomaterials, 2014.*

79. Postnatal human dental pulp stem cells (DPSCs) in vitro and in vivo. ***Shi, S. Gronthos M. Mankani J. Brahim P. G.Robey S.*** *s.l. : Proc. Natl. Acad. Sci, 2000.*

80. Comparison of human dental pulp and bone marrow stromal stem cells by cDNA microarray analysis. ***Gronthos, S. Shi P. G. Robey S.*** *s.l. : Bone, 2011.*

81. Graphene oxide-based substrate: Physical and surface characterization, cytocompatibility and differentiation potential of dental pulp stem cells. ***Rajan, N. Dubey T. T. Madanagopal S. S.*** *s.l. : Dent. Mater., 2016.*

82. Interaction with teichoic acids contributes to highly effective antibacterial activity of graphene oxide on Gram-positive bacteria. ***Li, Meizhen Wang Zhangqiang.*** *2021.*

83. Antimicrobial Activity, DFT Calculations, and Molecular Docking of Dialdehyde Cellulose/Graphene Oxide Film Against Covid-19. ***Sawsan, Dacrory.*** *2021.*

84. Synthesis of graphene-based nanosheets via chemical reduction of exfoliated graphite oxide. ***al, Stankovich et.*** *s.l. : ACS Nano, 2007.*

85. Temperature dependence of graphene oxide reduced by hydrazine hydrate. ***Li, Peng-Gang Ren Ding-Xiang Yan Xu Ji Tao Chen Zhong-Ming.*** *s.l. : Elsevier, 2010.*

86. Creation of Conductive Graphene Materials by Bacterial Reduction Using Shewanella Oneidensis. ***Stan, Benjamin A E Lehner Vera A E C Janssen Ewa M Spiesz Dominik Benz.*** *s.l. : Elsevier, 2019.*

87. Pulsed laser assisted reduction of graphene oxide. ***Shi, Lei Huang Yang Liu Le-Chun Ji Yi-Qun Xie Tao Wang Wang-Zhou.*** *2011.*

88. Tuning the sub-processes in laser reduction of graphene oxide by adjusting the power and scanning speed of laser. ***Wan, Zhengfen.*** *s.l. : Elsevier, 2019.*

89. Electrochemical Biosensing of Dopamine Neurotransmitter: A Review. ***Pavel, Sophie Lakard Ileana-Alexandra.*** *s.l. : Biosensors (Basel), 2021.*

90. Terms of endearment: Bacteria meet graphene nanosurfaces. ***Katsogridaki, Evangelia Tegou Maria Magana Alexandra Eleni.*** *s.l. : Biomaterials, 2016.*

91. Study of antibacterial mechanism of graphene oxide using Raman spectroscopy. ***Sekhar, Nanda Sitansu.*** *s.l. : Scientific reports, 2016.*

92. Antimicrobial Properties of Graphene Oxide Nanosheets: Why Size Matters. ***François Perreault, Andreia Fonseca de Faria, Siamak Nejati, and Menachem Elimelech.*** *s.l. : ACS Nano, 2015.*

93. Facile synthesis of graphene oxide–silver nanocomposite for decontamination of water from multiple pollutants by adsorption, catalysis and antibacterial activity. ***Hina, Naeem.*** *s.l. : Journal of Environmental Management, 2019.*

94. Synthesis and antibacterial activity of graphene oxide decorated by silver and copper oxide nanoparticles. ***Menazea, Ahmed.*** *s.l. : Journal of Molecular Structure, 2020.*

95. Multifunctional oil-produced reduced graphene oxide – Silver oxide composites with photocatalytic, antioxidant, and antibacterial activities. ***G.S.Lekshmi.*** *s.l. : Journal of Colloid and Interface Science, 2022.*

96. Bio-Reduced Graphene Oxide as a Nanoscale Antimicrobial Coating for Medical Devices. ***Choudhary, Priyadarshani.*** *s.l. : ACS Omega, 2019.*

97. Promising antimicrobial and antibiofilm activities of reduced graphene oxide-metal oxide (RGO-NiO, RGO-AgO, and RGO-ZnO) nanocomposites. ***Elbasuney, Sherif.*** *s.l. : Royal Society of Chemistry, 2021.*

98. Biocide mechanism of highly efficient and stable antimicrobial surfaces based on zinc oxide–reduced graphene oxide photocatalytic coating. ***Valenzuela, Laura.*** *s.l. : Journal of Material Chemistry, 2020.*

99. ***PubChem.*** *National Library of Medicine. [Online] [Cited: 11 25, 2021.] www.pubchem.ncbi.nlm.nih.gov/element/Silver.*

100. Invasive fungal infections: a review of epidemiology and management options. ***Enoch, D. A.*** *s.l. : Journal of Medical microbiology , 2006.*

101. Silver nanoparticles inhibit hepatitis B virus replication. ***L, Lu.*** *s.l. : Scopus, 2008.*

102. Silver nanoparticles: A new view on mechanistic aspects on antimicrobial activity. ***Durán, Nelson.*** *s.l. : Nanomedicine, 2016.*

103. Antimicrobial activity of. ***Kailasa.*** *s.l. : Nanoparticles in Pharmacotherapy, 2019.*

104. Silver nanoparticles: mechanism of antimicrobial action, synthesis, medical applications, and toxicity effects. ***Prabhu, Sukumaran.*** *s.l. : ACS Nano, 2012.*

105. Key parameters to enhance the antibacterial effect of graphene oxide in solution. ***Grecia Guadalupe Montes-Duarte.*** *s.l. : RCS Advances, 2021.*

106. Anti-adhesion and antibacterial activity of silver nanoparticles and graphene oxide silver nanoparticles composites. ***Savaria, Sandra Gabriela Gomez de.*** *s.l. : Revistamateria, 2020.*

107. Facile synthesis of graphene oxide–silver nanocomposite and its modified electrode for enhanced electrochemical detection of nitrite ions. ***Ikhsan, Nurul Izrini.*** *s.l. : Talanta, 2015.*

108. An extensive case study on the dispersion parameters of HI-assisted reduced graphene oxide and its graphene oxide precursor. ***Kymakis, Katerina Anagnostou Minas M.Stylianakisa Grigoris Atsalakis Dimitrios M.Kosmidis Athanasios Skouras Ioannis J.Stavroucd KonstantinosPetridise Emmanuel.*** *s.l. : Journal of Colloid and Interface Science, 2020.*

109. Polymer composites for tribological applications. ***K.Friedrich.*** *s.l. : Advanced Industrial and Engineering Polymer Research, 2018.*

110. Synthesis and surface chemistry of nano silver particles. ***Rao, Revathi Janardhanan Murugan Karuppaiah Neha Hebalkar Tata Narsinga.*** *s.l. : Polyhedron, 2009.*

111. A Novel Synthesis of the Graphene Oxide-Silver (GO-Ag) Nanocomposite for Unique Physiochemical Applications. ***al, Sujata Kumari et.*** *s.l. : ACS Omega, 2020.*

112. Raman spectroscopy of graphene and carbon nanotubes. ***R. Saito, M. Hofmann , G. Dresselhaus , A. Jorio & M. S. Dresselhaus.*** *s.l. : Advances in Physics, 2011.*

113. Negatively curved cubic carbon crystals with octahedral symmetry. ***al, Makoto Tagami et.*** *s.l. : Carbon, 2014.*

114. Quantifying Defects in Graphene via Raman Spectroscopy at Different Excitation Energies. ***L. G. Cancado, A. Jorio, E. H. Martins Ferreira, F. Stavale et al.*** *s.l. : Nano Letters, 2011.*

115. Characteristics of Graphene Oxide Films Reduced by Using an Atmospheric Plasma System. ***C. R. Yang, S. F. Tseng, Y. T. Chen.*** *s.l. : Nanomaterials, 2018.*

116. Raman Spectrum of Graphene and Graphene Layers. ***A. C. Ferrari, J. C. Meyer, V. Scardaci, C. Casiraghi, M. Lazzeri, F. Mauri, S. Piscanec, D. Jiang, K. S. Novoselov, S. Roth, and A. K. Geim.*** *s.l. : Phys. Rev. Lett., 2006.*

117. Raman Spectroscopy of Graphene and Related Materials. ***Childres, L. A. Jauregui, W. Park, H. Cao, Y. P. Chen.*** *2013 : New Developments in Photon and Materials Research.*

118. Noble metal (Pd, Ru, Rh, Pt, Au, Ag) doped graphene hybrids for electrocatalysis. ***M., Giovanni, et al.*** *s.l. : Nanoscale, 2011.*

119. Graphene-Based Nanomaterials for Tissue Engineering in the Dental Field. ***R. Guazzo, C. Gardin, G. Bellin, L. Sbricoli et al.*** *s.l. : Nanomaterials, 2018.*

120. ***Diodes, Reduced Graphene Oxide Inserted into PEDOT:PSS Layer to Enhance the Electrical Behaviour of Light-Emitting.*** *Fernando Rodríguez-Mas . Nanomaterials . 2021.*